Boillot, G., Winterer, E. L., et al., 1988
Proceedings of the Ocean Drilling Program, Scientific Results, Vol. 103

8. LIMESTONE DIAGENESIS AND DOLOMITIZATION OF TITHONIAN CARBONATES AT ODP SITE 639 (ATLANTIC OCEAN, WEST OF SPAIN)[1]

Jean-Paul Loreau,[2] Laboratoire de Géologie du Museum National d'Histoire Naturelle, Paris, France
and
Pierre Cros, Laboratoire de Stratigraphie de l'Université Pierre et Marie Curie, Paris, France

ABSTRACT

A Tithonian sequence of shallow-water limestones, intercalated with siliciclastics and overlain by dolomite, was recovered during drilling at ODP Site 639 on the edge of a tilted fault block. The carbonates were strongly affected by fracturing, dolomitization, dedolomitization, and compaction. The chronology and nature of the fractures, fracture infilling, and diagenesis of the host rock are established and correlated for both the limestone and the dolomite.

A first phase of dolomitization affected limestone that was already, at least partially, indurated. In the limestone unit, fractures were filled by calcite and dolomite; most of the dolomite was recrystallized into calcite, except for the upper part. In the dolomitic unit, the first-formed dolomite was progressively recrystallized into saddle dolomite, as fractures were simultaneously activated. The dolomitic textures become less magnesian (the molar ratio $^{m}Mg/^{m}Ca$ goes from 1.04–0.98 to 0.80), and the $\delta^{18}O$ (PDB) ranges from $-10‰$ to $-8‰$. The varying pores and fissures are either cemented by a calcic saddle dolomite ($^{m}Mg/^{m}Ca$ ranging from 0.95 to 0.80) or filled with diverse internal sediments of detrital calcic dolomite, consisting of detrital dolomite silt ($\delta^{18}O$ from $-9‰$ to $-7‰$) and laminated yellow filling (with different $\delta^{18}O$ values that range from $-4‰$ to $+3‰$). These internal sediments clearly contain elements of the host rock and fragments of saddle crystals. They are covered by marls with calpionellids of early Valanginian age, which permits dating of most of the diagenetic phases as pre-Valanginian.

The dolomitization appears to be related to fracturing resulting from extensional tectonics; it is also partially related to an erosional episode. Two models of dolomitization can be proposed from the petrographic characteristics and isotopic data. Early replacement of aragonite bioclasts by sparite, dissolution linked to dolomitization, and negative $\delta^{18}O$ values of dolomite suggest a freshwater influence and "mixing zone" model. On the other hand, the significant presence of saddle dolomite and repeated negative $\delta^{18}O$ values suggest a temperature effect; because we can dismiss deep burial, hydrothermal formation of dolomite would be the most probable model. For both of these hypotheses, the vadose filling of cavities and fractures by silt suggests emersion, and the different, and even positive, $\delta^{18}O$ values of the last-formed yellow internal sediment could suggest dolomitization of the top of the sequence under saline to hypersaline conditions.

Fracturing resulting in the reopening of porosity and the draining of dolomitizing fluids was linked to extensional tectonics prior to the tilting of the block. These features indicate an earlier beginning to the rifting of the Iberian margin than previously known. Dolomitization, emersion, and erosion correspond to eustatic sea-level lowering at the Berriasian/Valanginian boundary. Diagenesis, rather than sedimentation, seems to mark this global event and to provide a record of the regional tectonic history.

INTRODUCTION

Six holes were drilled at Ocean Drilling Program (ODP) Site 639 on the western Iberian continental margin off Galicia (Fig. 1A). The holes are along the steeper edge of one of the tilted fault blocks formed during the Early Cretaceous phase of rifting (Fig. 1B). Drilling results document a Tithonian sequence of shallow-water limestone deposits with intercalated siliciclastics. Dolomite of unknown thickness overlies this sequence and is, in turn, overlain by a Valanginian calpionellid marl. We suggest that the depositional environment of the Tithonian carbonates corresponds to the middle part of a ramp (see Moullade et al., this volume), indicative of a relatively quiet tectonic regime, as would be expected during the pre-rift stage of margin evolution. However, the carbonates have been affected since their deposition by fracturing, dolomitization, dedolomitization, and compaction. The characteristics of these transformations, the number of phases, the chronology, and the relationships with tectonics remain under debate.

The main objective of this study was to establish the timing, nature, and environment of the different diagenetic transformations of these shallow-marine, infratidal limestones. We first investigated the evidence of synsedimentary diagenesis, and then attempted to establish the sequence of early to late diagenesis by studying the chronology and nature of the fracture infilling and the transformation of the host rock and the interrelationship of fracturing, fissure filling, and host rock diagenesis within the same facies. Finally, we compared these interrelationships observed in the limestone recovered in Hole 639D with the dolomite recovered in Hole 639A.

Internal sediments of detrital dolomite in fractures and cavities within the dolomite are sealed by marly limestone containing Valanginian calpionellids, providing a means of precisely dating one stage of the diagenetic history of these deposits. Consequently, aside from late stylolitization, we were able to date most of the diagenetic features.

Based on the Mg/Ca, $^{18}O/^{16}O$, and $^{13}C/^{12}C$ ratios in the different dolomite crystalline textures, we discuss the nature of the dolomitizing fluids, which may provide information on the environment(s) of diagenesis. Finally, we discuss evidence for the possible emersion of these carbonates (or the top of the sequence of these carbonates) before the Valanginian major environmental change.

[1] Boillot, G., Winterer, E. L., et al., 1988. *Proc. ODP, Sci. Results*, 103: College Station, TX (Ocean Drilling Program).

[2] Present address: Centre des Sciences de la Terre de l'Université de Bourgogne et UA 157 CNRS, Dijon, France.

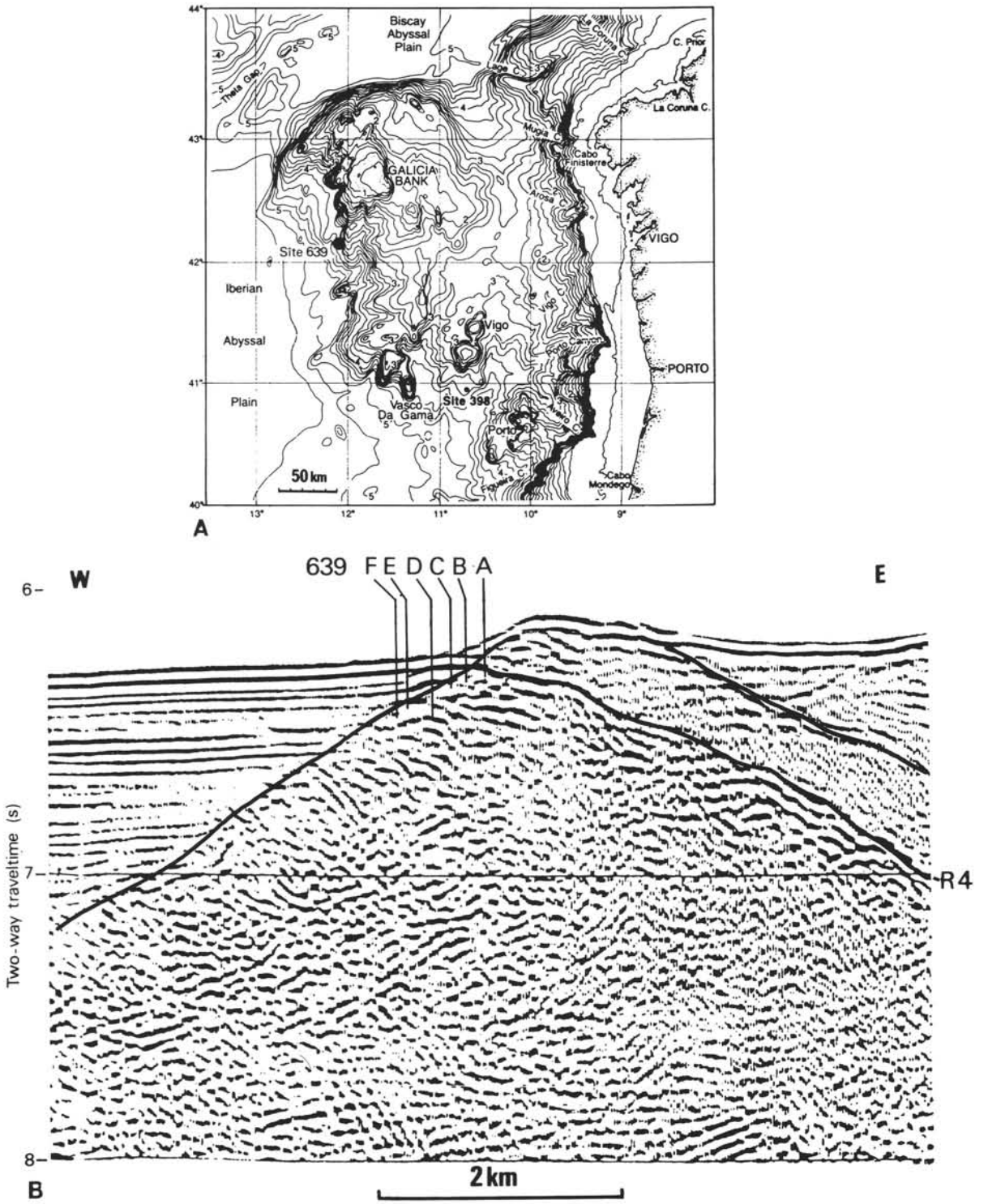

Figure 1. **A.** Galicia margin, with location of ODP Site 639 and DSDP Site 398. **B.** Section of Institut Français du Pétrole seismic line GP-101 (courtesy of L. Montadert) showing the projected positions of Holes 639A through 639F. R4 = seismic reflector correlated with the top of the dolomite.

MATERIALS AND METHODS

The carbonates proved difficult to drill at Site 639, and technical problems prevented recovery of a continuous sequence of cores. At Hole 639A, after coring easily through Neogene and Lower Cretaceous rocks, drilling conditions in the underlying dolomite became impossible. As stated in the Leg 103 *Initial Reports* (Boillot, Winterer, et al., 1987, p. 448), the dolomite is apparently too fractured to maintain a firm hole, causing sticking of the pipe, plugging of the bit, and other problems. These obstacles eventually led to the drilling of an additional five holes (Holes 639B through 639F), located progressively farther west, in an attempt to sample the entire section. The stratigraphic section pieced together in this manner was incompletely cored, and recovery of each core was partial (cf. Fig. 2), especially within the dolomitic section. Consequently, some facies may be unrepresented in the recovered material, and thus, some aspects of the sedimentary and syndiagenetic history un-

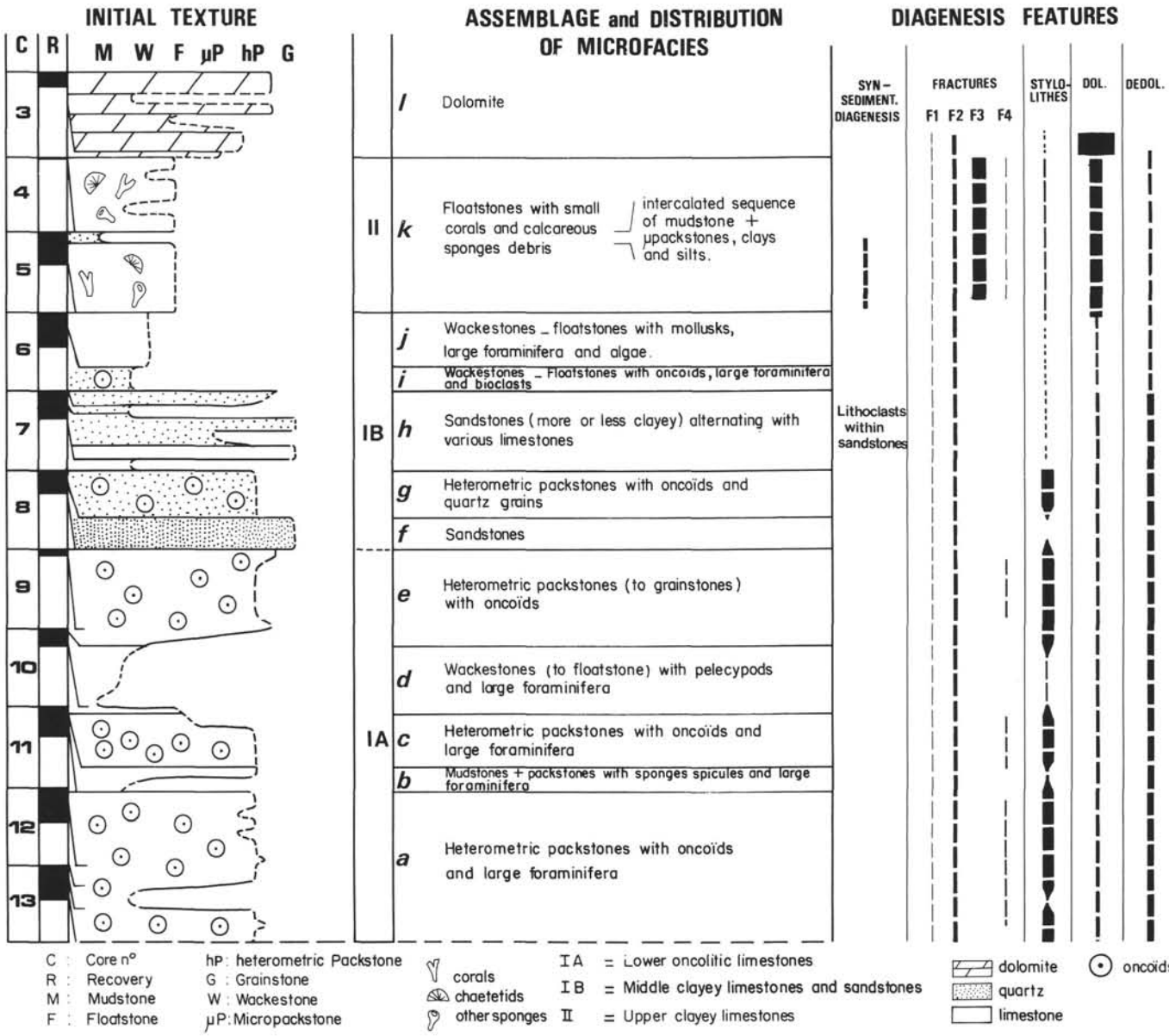

Figure 2. Initial textures and diagenetic features of Hole 639D limestones. The textural, compositional, and diagenetic columns are not to scale with the core recovery; dotted lines in graphic descriptions express unknown thickness. The thickness of silty marl and mudstone sheet within Core 5 is to scale, as inferred from logging data. See Moullade et al. (this volume) for further discussion of microfacies assemblages and distribution.

revealed. However, the diagenesis observed in a single bed may reflect various events occurring through time on a larger scale than the bed itself. For instance, all of the dolomite samples exhibit the entire sequence of crystalline textures described in Hole 639A. Both the chronology of diagenesis and paleoenvironmental interpretations are derived only from observations of the recovered rock samples, without making inferences about potentially nonrepresented facies that could bias interpretation. To this end, more than 300 thin sections were studied.

Classical methods of investigation, such as use of the polarizing microscope and staining of samples (by mixing alizarin + potassium ferricyanide), were complemented by other techniques, including the following:

1. Photographic enlargement of all nonhomogenous thin sections. Enlargements were used to study textural variations, to make semiquantitative evaluation of the constituents (see Moullade et al., this volume), to determine the relationships between fractures, voids, fillings, and the host rock, and to recognize the diagenetic facies. They also served as useful "guidelines" during microprobe analysis of the thin sections.

2. Cathodoluminescence. This method permitted us to identify the various crystalline structures and to determine their chronology by providing a better view of the stages of crystalline growth within the crystals that appeared homogeneous under natural light. Phantoms of earlier structures and crystals, including inherited zonation, and differences between fracture sets were revealed. Color and intensity of luminescence were used to describe the pictures. In the carbonates, two colors are dominant: rose-red and orange (Pierson, 1981; Amieux, 1982). Bright yellow is an accessory color. Intensity is described here as light, dull, and nil (black).

3. Analysis of crystalline phases and diagenetic textures by microprobe. Dolomites were analyzed to determine the molar ratio $^{m}Mg/^{m}Ca$ and the concentrations of Fe, Mn, and Sr. In addition to the cations utilized for this study, Na, Si, Al, and S were also analyzed in order to determine the presence or absence of impurities or inclusions. The margin of error for the Mg/Ca ratio is about 2%. The conditions used for carbonate analysis were 15-kV high voltage, 12-nA intensity, and 12-μm probe diameter.

4. Stable isotope analysis of carbon and oxygen. Fifteen samples of crystalline dolomites and five samples of micrite matrices in limestones

were separated by microdrilling with a dentist's drill for carbon and oxygen stable isotope analysis. The powders were placed in 100% H_3PO_4 at 25°C for 3 days, and the carbon and oxygen isotope values were determined by mass spectrometry within the derived CO_2. An argon test revealed the absence of atmospheric pollution. Errors in $\delta^{13}C$ and $\delta^{18}O$ (PDB standard) determinations are on the order of 0.1‰.

Friedman's (1965) nomenclature was used to describe crystals and crystalline textures. Other terms used are as follows:

Phantom: Textural trace of an inorganic grain, bioclast, or crystal that is conserved or outlined by impurities after its replacement by another mineral and crystalline structure.

Pseudomorph: The conserved shape of a former crystal after replacement by another mineral.

Relic: The morphology and mineralogy of any texture, grain, or crystal entirely or partially conserved inside a subsequently developed mineralogy.

Baroque dolomite: Transparent clean overgrowth of "dirty" crystals, showing undulating extinction between crossed polarizers.

Saddle dolomite: Subhedral crystals with slightly curved faces through anhedral crystals with more curved faces, curved cleavages, saddlelike and spearlike forms, showing systematic sweeping extinction between crossed polarizers (Radke and Mathis, 1980).

Compromise boundary: Geometric locus in fissure filling where the crystals growing from one edge (or from the roof) and crystals growing from the other edge (or from the floor) make contact.

Wall: Border of the host rock, along the fissure.

PETROGRAPHY OF LIMESTONES (CORES 103-639D-4R THROUGH 103-639D-13R)

Sedimentary Textures and Types of Matrix

The original textures of the Site 639 limestones are dominantly wackestones, floatstones, and heterometric packstones (Fig. 2), representing sediments with a high mud content and little space for cement. There are three types of matrix: (1) a micritic matrix with varying abundances of small recrystallized bioclastic debris (Fig.3); (2) a matrix with a micropackstone texture composed of pellets and/or very small bioclastic debris smaller than 100 μm closely packed within an interstitial micrite (Fig. 4) (the association of both floating and closely packed allochems with the micropackstone matrix gives the sediment a heterometric packstone texture—see Moullade et al., this volume); and (3) a matrix with clotted structure that consists of micrite in imprecise "islets" surrounded by microspar (Pl. 1, Fig. 2).

Bioturbation is common and causes abrupt variations in texture. The variations are somewhat amplified by differential diagenesis in the same microfacies (Fig. 4).

Synsedimentary Diagenesis Features

Only weak evidence for synsedimentary diagenesis is seen in the Hole 639D limestones. Synsedimentary diagenetic features are most noticeable in the wackestones and floatstones at the top of the limestone unit, as opposed to the underlying section containing oncoids (Unit II vs. Subunit IA; Fig. 2).

Genesis of Firm Ground

Sample 103-639D-5R-3, 42–44 cm, exhibits synsedimentary diagenetic structures (Fig. 5A). The primary sediment is a wackestone with a dark aspect in transmitted light. The wackestone contains open burrows filled with internal geotropic sediment of lighter micrite (Fig. 5B). These two sediments are dissected by a clear and irregular boundary that profiles microcliffs and suggests an erosional surface (Fig. 5A). The hollows are filled with a packstone of even lighter transparency. These features clearly suggest the development of a firm ground (Fürsich, 1979; Juignet and Kennedy, 1974).

Figure 3. Micrite matrix rich in small recrystallized bioclastic debris and coral section showing micritic filling and very fine details of the calcitized skeleton. Sample 103-639D-4R-2, 97–99 cm; natural light.

Lithification of Siliceous Sponges

Some examples of dull, micritic "encrustations" are rich in elongated and reniform spicules of sponges (Fig. 6). Such structures, called tuberoids (Fritz, 1958; Gaillard, 1982), result from the *in-situ* decomposition of lithistid sponges and their induration by syngenetic precipitation of carbonate, which prevents dispersal and compaction of the spicules. This phenomenon causes partial induration of the sediment.

Significance of Clasts within Intercalated Sandstones

Flat micritic lithoclasts with an elongated morphology and crumbled edges occur in the intercalated sandstones (Fig. 2). Quartz grains are embedded in the surface of the lithoclasts (*a* in Fig. 7), suggesting "mud pebbles" reworked from a firm ground. Other elongated lithoclasts with a micrograinstone structure and rounded edges (*b* in Fig. 7) indicate increased lithification prior to the deposition of the sandstone.

Early through Late Diagenesis

Diagenesis of the Matrix

The matrix in several parts of the Hole 639D limestones shows evidence of dolomitization and later calcitization. This is inferred from specific characteristics of the resultant fine crystalline mosaics:

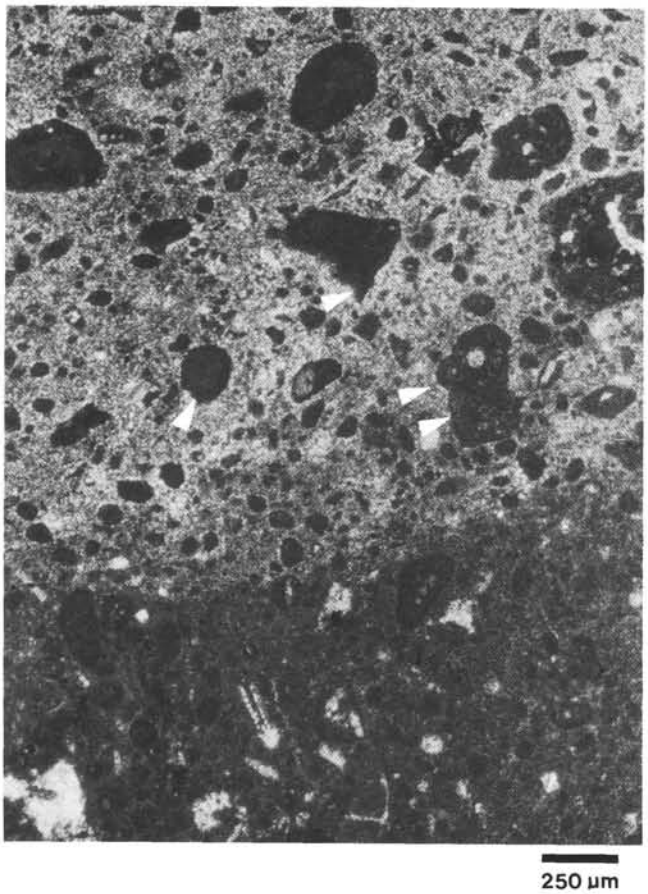

Figure 4. Micropackstone matrix composed of fine bioclasts and pellets closely packed in micrite, passing to recrystallized microspar with relic pellets and bioclasts. Some grains are polygonal and exhibit serrated edges (arrows). See also Plate 1, Figures 1 and 2. Sample 103-639D-13R-1, 77–80 cm; natural light.

1. In the heterometric packstones containing oncoids in a micropackstone matrix, the micrite embedding very small bioclasts and pellets evolves into a microsparite (Pl. 1, Fig. 1). The microsparite consists of anhedral to subhedral, limpid crystals 10–30 µm in diameter and contains mono- or polycrystalline rhombohedral pseudomorphs (Pl. 1, Fig. 2). Staining clearly distinguishes the calcite (pink) and the rare relics (uncolored) of dominantly anhedral dolomite, with some occurrences in the form of rhombs.

Under cathodoluminescence, the microsparitic mosaics are often lighter than the untransformed micrite and reveal phantoms of zoned rhombs with dull centers and discontinuous light borders (Pl. 1, Fig. 3). Correlatively, the micropellets have polyhedral edges derived from the ancestral limits of the crystals penetrating the pellet-surrounding micrite boundary (Pl. 1, Fig. 2).

2. In the wackestones and a mudstone (Sample 103-639D-5R-1, 55–57 cm), cathodoluminescence of the clotted structure shows a mosaic with phantoms of rhombohedrons, most of them with dull centers (Pl. 1, Fig. 4). The xenotopic microsparite textures in these limestones are not drusy, which suggests that they are not cement but have resulted from replacement. The dolomite relics and the rhombohedral pseudomorphs are evidence of an early phase of dolomitization of the matrix, which was followed by a late (and poorly dated) phase of dedolomitization (i.e., recrystallization into calcite from dolomite).

Diagenesis of the Bioclasts: Comparison with the Original Void Cements

In the wackestones and floatstones of the upper unit (microfacies assemblage *k*; Fig. 2), aragonitic bioclasts observed under transmitted light seem to be classically recrystallized into calcite. The texture is xenotopic sparite (Pl. 2, Fig. 2). The calcite filling the rare voids is similar; however, the cements within the voids possess a drusy structure (Pl. 2, Fig. 4; Pl. 3, Figs. 1 and 2), and the crystals increase in size toward the center and present mostly enfacial junctions (Bathurst, 1975).

Under cathodoluminescence, aragonite-calcite replacement and calcite cements are not as classic as expected. Calcite replacing skeletal aragonite and drusy calcite infilling voids exhibit common characteristics; the cathodoluminescent response is relatively dull and somewhat zoned, with black patches having straight boundaries (Pl. 2, Figs. 1 and 4; Pl. 3, Fig. 1). On the other hand, peculiar cathodoluminescence characteristics occur along the borders of some of the drusy mosaic (Pl. 3, Fig. 1 and cf. Fig. 2) and within some areas of calcite replacing aragonite (Pl. 2, Fig. 1). The cathodoluminescence reveals bright yellow and slightly zoned rhombohedral pseudomorphs; some of the phantoms have curved faces. Cathodoluminescence mainly shows large endings of zoned rhombs that have little relation to the crystalline limits of the sparite (Pl. 2, Fig. 3). These bright yellow endings of rhombohedrons and crystals with curved faces strongly suggest the growth limit of an early dolomite. Part of calcite, especially at the inner edges of bioclasts and cemented voids, could be recrystallized, mostly from saddle dolomite.

In the same microfacies, the initial morphology of sponge spicules is outlined by a rim showing the same bright yellow cathodoluminescence, but there are no phantoms of rhombs and crystals with curved faces (Pl. 2, Fig. 1). The similar cathodoluminescence fringing each calcite occurrence could be interpreted in either of two ways. It may be the signature of the same stage for the two calcites, with calcite replacing opal (or precipitating in the voids of dissolved spicules) synchronized with calcite replacing dolomite. Alternatively, it may be the signature of the same stage for calcite replacement of opal and for partial dolomitization of bioclasts and cements; later (undated) calcite replacing dolomite would preserve the zoned cathodoluminescence characters of dolomite.

Another type of calcite that occurs infrequently is a late sparite cement with equant crystals several hundred microns in diameter. Cathodoluminescence response is clear and multizoned (Pl. 3, Figs. 3 and 4).

Five types of calcite were recognized in the bioclasts and the cements: initial calcite of bioclasts, calcite replacing aragonite and calcite replacing opal (probably not contemporaneous), early drusy calcite filling voids, calcite resulting from recrystallization of dolomite, and late, larger and equant sparite in voids.

Calcitic bioclasts (calcareous sponges and fibrous pelecypods) are partially silicified, and the siliceous parts exhibit some euhedral dolomite (Pl. 3, Figs. 1 and 2). A later but poorly dated phase of dolomitization is still present in the form of 200-µm–1-mm subhedral or euhedral crystals cutting across the calcite structures that originated from the replacement of the first dolomitization.

Diagenesis Linked with Fracturing

Fractures and fissures provide evidence of local or regional tectonic events while reflecting the state of the sediment or the rock at the time of their genesis. They help to determine a relative chronology that sometimes can be dated, and they are also important in the reopening of porosity. Fractures and fissures are thus of major interest in any diagenetic study.

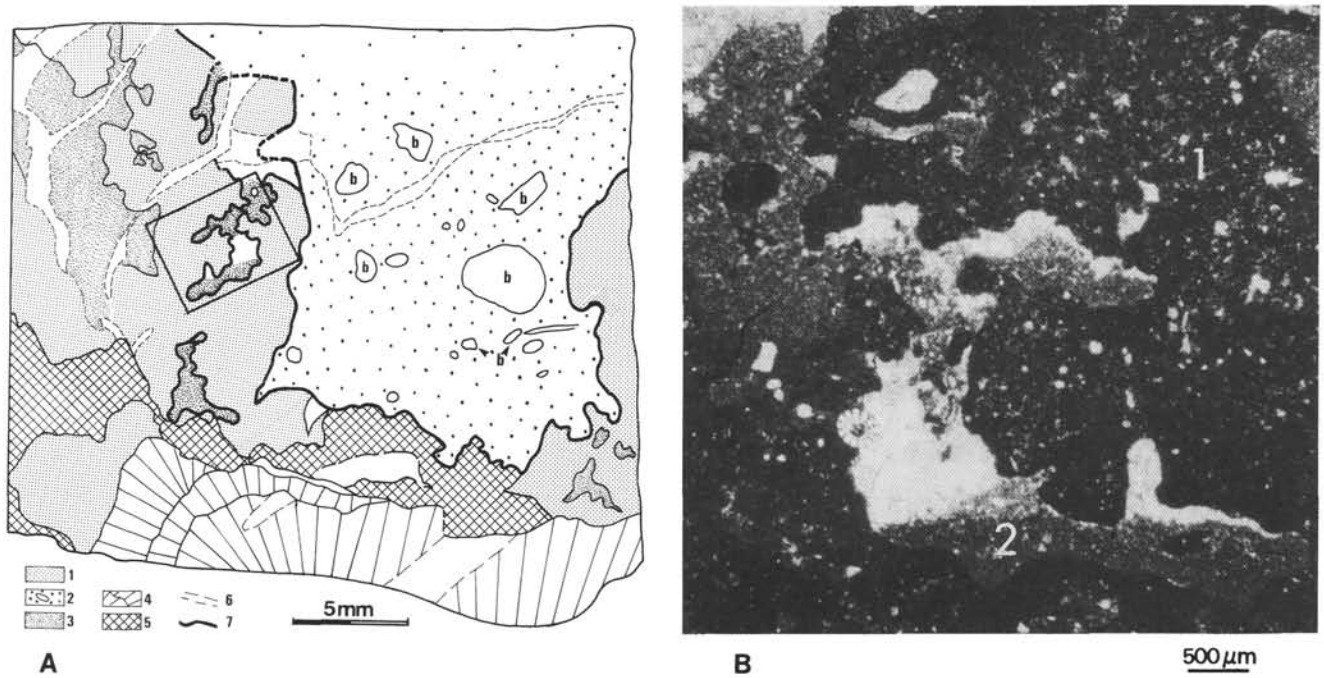

Figure 5. Synsedimentary diagenesis and firm ground in limestone. Sample 103-639D-5R-3, 42–44 cm. **A.** Sketch showing open burrows filled with internal sediment and erosion features that suggest early, minor lithification of the sediment. 1 = wackestone texture with dark micritic matrix rich in sponge spicules; 2 = heterometric packstone texture rich in various bioclasts (b); 3 = clearer micrite filling burrows; 4 = polyphased bindstone texture with *Taumathoporella* and *Chaetetes* and a coral; 5 = recrystallized and altered area; 6 = fissures filled with dolomite; 7 = erosion boundary; b = bioclast; □ = location of Figure 5B. **B.** Detail of dark micrite (1) containing an open burrow filled with clearer micrite (2) and sparry calcite, evidence for a firm or weakly lithified bottom (see Fig. 5A for location). Natural light.

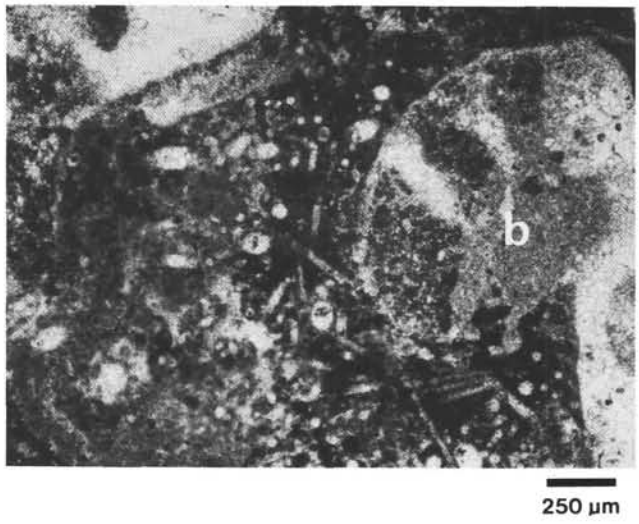

Figure 6. Siliceous lithistid sponge encrusting a bioclast (b). Calcitized spicules are in place within the early diagenetic micrite. Sample 103-639D-5R-2, 94–97 cm; natural light.

In this study, the fractures and fissures have been characterized by their general morphology and filling in the different facies. Chronological order was established in relation to the state of induration of the host rock and in relation to stylolites.

Criteria for Classifying Fissures in Limestones

Fissure outline is used to distinguish two types of fissures: (1) undulating (zig-zagging) fissures, with either serrated or irregular

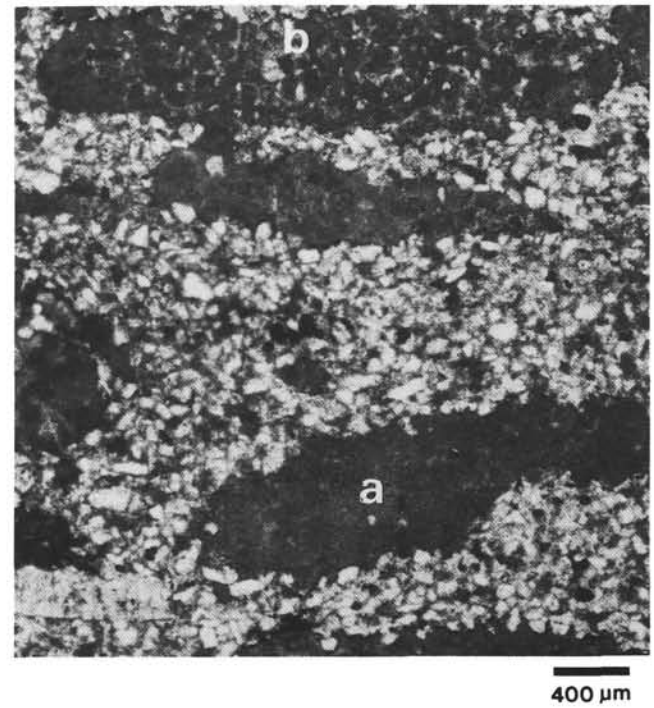

Figure 7. Fine sandstone containing micritic (a) and micrograinstone (b) intraclasts from the underlying limestones. Quartz grains are printed or embedded at the surface of the micritic intraclasts. Such "mud pebbles" and micrograinstone pebbles suggest a pronounced degree of limestone lithification prior to sandstone deposition. Sample 103-639D-7R-1, 48–51 cm; natural light.

edges with no particular geometry; and (2) roughly rectilinear fissures, with either serrated, clean-cut, or irregular (in close-up examination) edges.

The variations are numerous. For example, a conjugate set of fissures gives corner or bayonetlike shapes (see F2c and F2c′ fissures; Fig. 8). A change in direction can vary the width of the fissure in the plane of the thin section. The microfacies sometimes influence the general morphology of the fissures. For instance, in the heterometric packstones with oncoids, the irregular edges of the fissures often circumvent the grains (Fig. 9), in particular the pellets of the micropackstone matrix. The microfissures break apart like branches between the grains. In the wackestones and mudstones, fissures with straight outlines and generally regular edges are more numerous than in the heterometric packstones.

The relative chronology of the fissures, based on observation of their intersections, is not always well defined. This is due to several reasons, including the following:

1. Recrystallization of the intersections can conceal the anterior-posterior relations or even inverse them.
2. The similar nature of the fillings (e.g., late impregnation by ferric hydroxide) can give the impression of one set of conjugate fractures, whereas the morphology indicates that they are different (Pl. 4, Fig. 4).
3. It is not always possible to distinguish a set of fractures arranged in a conjugate synchronous network from fractures belonging to two successive systems.

However, it was possible to establish the relative chronology of most of the fissures observed in the Site 639 samples on the basis of the relationships of outlines, edges, fillings (especially observed under cathodoluminescence), and interpretable intersections. Four main sets of fissures were thus identified in the limestone unit and are indexed F1, F2, F3, and F4.

Fissure Classification in Limestones

Table 1 lists the different fissures within the Hole 639D limestones and summarizes their respective characteristics: outline, edge, morphology, size, direction, and filling. Peculiar aspects of the fillings and of the relationships between the fillings and the host rock in some selected samples are reported in the following.

Type F1a: Undulating fissures, with variable zig-zags and calcite filling (Fig. 8 and Pl. 4). Samples 103-639D-7R-2, 102–105 cm, 103-639D-8R-1, 19–23 cm (Pl. 4, Figs. 1–3), 103-639D-10R-1, 38–41 cm (Fig. 8), and 103-639D-12R-1, 136–139 cm.

Fissures of type F1a have a width varying from 100 μm to several millimeters, a varicose appearance, and variable orientation with respect to the drill hole. The xenotopic filling is composed of anhedral, equigranular, nondrusy sparite or microsparite. It molds the edges of the matrix without cutting the small grains; however, some of the larger grains are cut. This morphology, in conjunction with observed intersections with other fractures (Fig. 8) and the stylolites, shows that the fissures formed very early in a weakly indurated porous sediment.

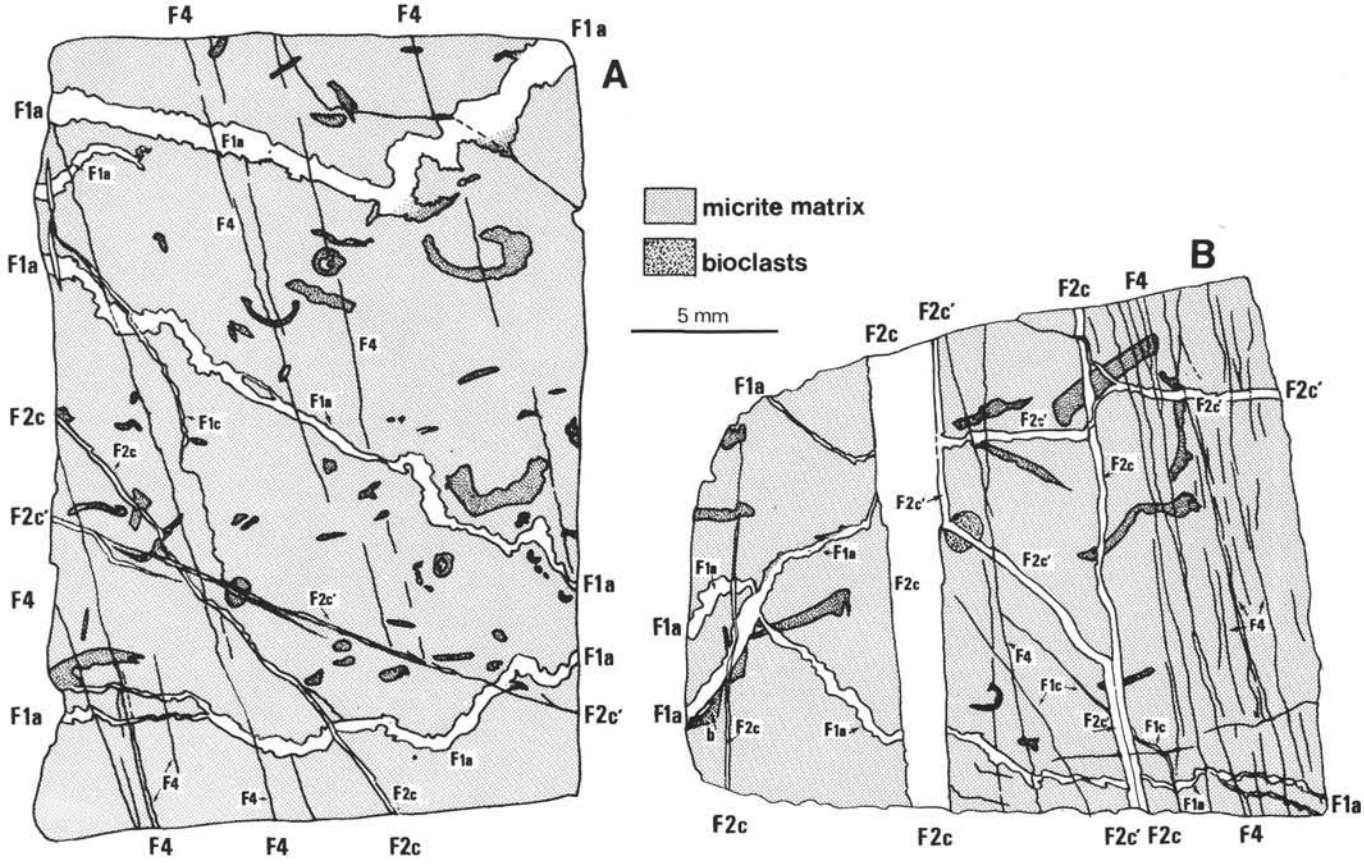

Figure 8. Thin sections showing morphologies and mutual intersections of different fissure sets. (F1a, F1c, F2c, and F4; see Table 1). Note the geometry of the fissures (especially F2c and F2c′ showing reactivation and pull-apart patterns), which suggests an extensional tectonic origin. **A.** Sample 103-639D-10R-1, 38–41 cm. **B.** Sample 103-639D-10R-1, 42–45 cm.

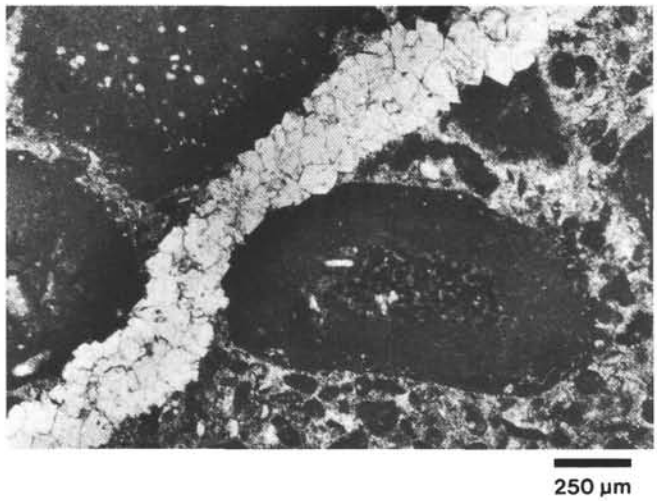

Figure 9. Fissure type F2a showing serrated edges and dolomite filling in limestone. Sample 103-639D-11R-1, 146–149 cm; natural light.

Under cathodoluminescence, the mosaic of the filling is slightly lighter than the surrounding micropackstone matrix, and some areas have a speckled aspect because many of the crystals are partially nonluminescent. This contrast in luminescence causes incomplete crystalline forms to appear against the walls (Pl. 4, Fig. 3). These endings show that centrifugal growth of the original minerals replaced the micropackstone matrix of the wall. In certain cases, the bioclasts are included in this diagenesis mechanism, giving a varicose appearance to the fissure (Pl. 4, Figs. 1 and 2). Staining shows some relics of dolomite (which are not stained), especially near the fissure edges; the replacing calcite appears "lilac" (i.e., ferroan) (e.g., Samples 103-639D-10R-1, 38–41 cm, and 103-639D-8R-1, 19–23 cm).

Type F1b: Fissures of irregular width with calcite filling (Pl. 5, Figs. 3 and 4; Pl. 6, Figs. 2 and 3). Samples 103-639D-5R-2, 63–65 cm (Pl. 5, Figs. 3 and 4), and 103-639D-5R-2, 137–139 cm (Pl. 6).

Fissures of type F1b must have formed relatively early because they are cut by other fissures; however, we are not sure if types F1a and F1b are strictly contemporaneous. Like the F1a fissures, the F1b fissures are of variable width, and their filling is similarly xenotopic and not drusy calcite. They differ by having a straighter general outline (compare Pl. 4, Fig. 1, to Fig. 8A), probably as a function of the microfacies type in which they occur (e.g., the edges are straighter in micritic matrix). In addition, the cathodoluminescence of the calcite filling is darker and mostly homogeneous.

Type F1c: Rectilinear fissures with calcite filling. (Fig. 8 and Pl. 5, Figs. 1 and 2). Samples 103-639D-10R-1, 38–41 cm, 103-639D-10R-1, 42–45 cm, and 103-639D-10R-1, 128–130 cm.

Like the F1a and F1b fissures, the type F1c fissures are cut by the other fissure types. Their edges are somewhat irregular, but they are more rectilinear than type F1a, and they possess a regular width (Pl. 5, Figs. 1 and 2). F1c fissures have a nondrusy filling similar to F1a and F1b fillings; however, their cathodoluminescence is relatively dull and homogeneous (Pl. 5, Fig. 1).

Several morphologies and fillings are found in a second set of fissures (F2), which formed after the F1 fissures.

Type F2a: Undulating or zig-zag fissures, with serrated edges and dolomite fillings (Fig. 9). Samples 103-639D-5R-2, 63–65 cm, 103-639D-5R-3, 39–41 cm, and 103-639D-11R-1, 146–149 cm.

The F2a fissures are typically filled with crystals that outline a serrated edge along the matrix and along the truncated oncoids or bioclastic elements (Fig. 9). The filling texture is hypidiotopic, consisting of anhedral baroque dolosparite with local occurrences of rhombohedral, euhedral crystals or some developed faces adjoining the matrix or grains. Alignments of microcrystals appear under cathodoluminescence with characteristic forms of the dolomite marked on the wall; the contact with the limestone host rock is underlined by a narrow fringe that is alternatively dull and bright (Pl. 5, Fig. 3), indicating that the dolomite crystals grew from the center out at the expense of the host rock along the fissure. The filling is not only a cement but also, at least in part, a replacement of the wall by syntaxial growth, with the original nuclei originating in the fissure. Dedolomitization islets of calcite occur in the core of this dolomite.

Type F2b: Rectilinear fissures, with serrated edges and dolomite filling.

Type F2b is a variant of type F2a, with a rectilinear morphology. These fissures are of essentially capillary size (50–400 µm).

Type F2c: Rectilinear fissures, with straight edges and calcite filling. Samples 103-639D-10R-1, 38–41 cm, and 103-639D-10R-1, 42–45 cm (Fig. 8), 103-639D-10R-1, 128–130 cm (Pl. 5, Figs. 1 and 2), 103-639D-11R-1, 142–144 cm, and 103-639D-11R-2, 23–25 cm (Fig. 10).

Type F2c fissures vary in width from 400–500 µm through 2–3 mm. They are sometimes conjugate and/or reactivated (F2c and F2c′ fissures; Fig. 8), and their geometric pattern strongly suggests origin by extensional tectonics. They are filled with large crystals (up to 300 µm), some of which are twinned (Pl. 5, Fig. 2). The sparite is generally xenotopic with a nondrusy texture. Under cathodoluminescence, phantoms are found with curved boundaries and blurred zonation that are unrelated to crystalline morphology (Pl. 5, Fig. 1). These characteristics indicate that the calcite recrystallized from subhedral or baroque dolomite. Elsewhere, anhedral relics of dolomite are detected by the absence of color in stained sections (Fig. 10B) and by a lighter and zoned cathodoluminescence (Fig. 10A). Geometric relationships between the calcite and dolomite and the growth direction of the calcite (Fig. 10) show that calcite replaced dolomite.

Type F2d: Rectilinear fissures, with dolomite filling (Fig. 11 and Pl. 6, Figs. 2 and 3). Samples 103-639D-5R-2, 137–139 cm (Pl. 6, Figs. 2 and 3), and 103-639D-5R-3, 39–41 cm (Fig. 11).

Type F2d fissures vary from a few millimeters in width to 20-µm capillary size. They are filled with saddle dolomite and show traces of dedolomitization to calcite. Their cathodoluminescence is relatively light. A fissure may appear as both types F2a and F2d along its length.

Some of the millimeter-size type F2d fissures were reactivated and suggest a subsequent phase of extension. Under cathodoluminescence, such fissures exhibit two stages of filling (Fig. 11C). The first saddle dolomite shows a relatively light luminescence and is present on the edges, corresponding to a first stage of fracture opening and cementation. A second saddle dolomite occurs at the center of the fissure and has a different cathodoluminescence character. The cathodoluminescence alternates dull and light with very uneven zonations. This second dolomite corresponds to the reactivation of the fracture filled with a second stage of dolomite cement.

Type F3: Large fissures filled with large crystals of saddle dolomite and calcite, in association with tectonic breccia (Fig. 11 and Pl. 6, Fig. 1). Samples 103-639D-5R-2, 137–139 cm (Pl. 6, Fig. 1, and Fig. 12), and 103-639D-5R-3, 39–41 cm (Fig. 11A).

Type F3 fissures are large, on a millimeter to centimeter scale width, and have straight edges (Fig. 11A and Pl. 6, Fig. 1). They intersect the F2 fissures but formed prior to the stylolites. The diagenetic fabric resulting from these fissures is complex. The nonfissured rock consists of calcite (mainly micrite matrix and bioclasts), dolomite relics, and dedolomitized calcite. A transi-

Table 1. Fissures in Hole 639D Tithonian limestones.

Fissure type	Outline	Edge morphology	Size (width)	Direction	Fissure filling			
					Dominant mineralogy and structure	Cathodoluminescence[a]	Minor mineralogy	
							Relic	Recrystallization
F1a	Undulating, zig-zag, and varicose appearance; of variable width	Irregular, without cutting small grains, but some cutting the larger ones	100 μm through 2–3 mm	Variable, from vertical or oblique to horizontal	1. Calcite (equigranular anhedral sparite or microsparite), some ferroan	Speckled aspect (see text)	Dolomite (uncolored in stained thin section)	
					2. Calcite + Fe hydroxide	Light, orange to yellow		
F1b	± Rectilinear; ± variable width	± Straight; intersects large grains similar to F1a	100 μm through 2–3 mm		Calcite (equigranular anhedral sparite or microsparite)	Dark, ± homogeneous		
F1c	± Rectilinear	± Straight	50–400 μm		Calcite (similar to F1b)	Dark, homogeneous		
F2a	Undulating and zig-zag	Serrated	100 μm through 1–2 mm	Variable, from vertical or oblique to horizontal	Anhedral saddle dolomite + some rhombs	Dark, narrow fringe		Calcite (dedolomitized)
F2b	± Rectilinear	± Serrated	50–400 μm		Anhedral saddle dolomite			
F2c	± Rectilinear; some are reactivated	± Straight	400–500 μm through 2–3 mm	and conjugate sets	Calcite (sparite, some twinned and cleaved)	Dark but not homogeneous + phantoms with blurred zonation	Dolomite (lighter cathodoluminescence and uncolored in stained thin section	
F2d	Rectilinear; some are reactivated	Straight	20 μm through 2–3 mm	Variable	Saddle dolomite			Calcite (dedolomitized)
					Two stages of saddle dolomite	Light, zoned		
F3	Rectilinear; wide	Straight	Several millimeters through 1 cm	Variable	Calcite (dedolomitized sparite) + saddle dolomite		Dolomite within sparite	
F4	Rectilinear	Straight	Dominantly 10–200 μm	± Vertical	Calcite + Fe hydroxides	Light, orange to yellow		

[a] Color is rose orange unless noted.

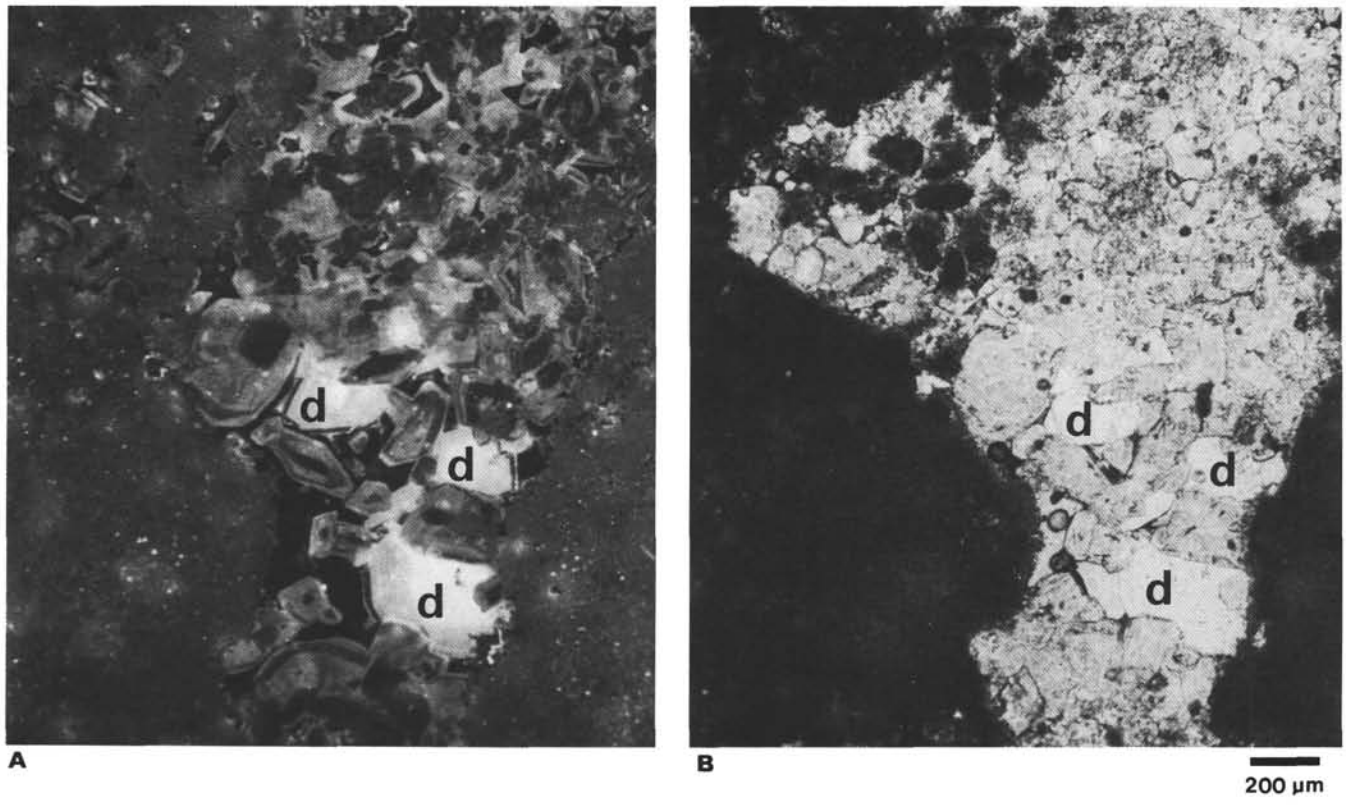

Figure 10. Detail of fissure type F2c and associated pores in limestone showing calcite recrystallized from dolomite and dolomite relics (d). Dolomite relics are not stained and show a clearer cathodoluminescence. In nondrusy sparite, cathodoluminescence reveals zoned phantoms of earlier dolomite. Sample 103-639D-11R-2, 23-25 cm. **A.** Cathodoluminescence. **B.** Natural light; stained thin section.

tional zone of micrite and sparite fragments of host rock, still in place, and pieces of the same, large sparite enclosed by clear, large saddle dolomite (Fig. 12B) with zoned cathodoluminescence (Fig. 12A) occurs in some places between the host rock and the F3 fissure. The fissure is filled with xenotopic saddle dolomite of large, mostly clear, anhedral crystals, with zoned cathodoluminescence.

This fracture-reworked sparite corresponds to significant recrystallization of the host rock. Some relics of both the calcite and dolomite replaced by the sparite are preserved; part of the dedolomitization is associated with or preceded the formation of the type F3 fissures. However, there is no evidence indicating that the range of the previously described dedolomitized calcites is contemporaneous with this dedolomitization phase. In any case, the dolomite filling the F3 fissures represents another phase of dolomitization.

Type F4: Straight, narrow fissures that probably formed after the stylolites. Samples 103-639D-7R-2, 102-105 cm, and 103-639D-10R-1, 38-45 cm (Fig. 8).

Type F4 fissures are found in limestones where F3 fissures are not observed (Cores 103-639D-13R to 103-639D-6R) and consist of a set of fractures that cut both the F2 fissures (Fig. 8 and Pl. 4, Fig. 4) and the stylolites (see the following section). These range from several tens of microns to about 200 µm in width and are filled with calcite without dolomite relics.

Stylolite Relationships with Fissures and the Host Rock

The relative abundance of stylolites observed in the Hole 639D limestones is shown in Figure 2. Dating the timing of formation of these stylolites is difficult, although most of them cut fissures types F1, F2, and F3. This constrains the timing of fissure formation to earlier than the general compaction of the sediments. The F4 fissures seem to cut across the stylolites. Even when the filling of such a fissure is not continuous, the edges of these fissures intersected by the stylolite are in alignment (Sample 103-639D-7R-2, 102-105 cm), and such coincidence is rarely preserved by pressure solution. Therefore, this intersection is interpreted to mean that stylolite formation was followed by the development of the F4 fissures.

The stylolites commonly contain euhedral and rhombohedral crystals of dolomite that range in size from several tens of microns to 200 µm. The presence of dolomite crystals in the stylolites is associated with pressure-solution phenomenon (Wanless, 1981). In addition, iron hydroxides are concentrated in the stylolites. At their boundaries, selected zones of the host rock and different types of fissures are colored by these hydroxides, similar to that of a chromatographic process. This contamination is probably related to the late circulating fluids, which would explain how fissures belonging to different sets could have the same cathodoluminescence (Pl. 4, Fig. 4).

PETROGRAPHY OF THE DOLOMITES OF HOLE 639A

Diagenetic Macrofacies

The dolomites of Hole 639A are heterogeneous, crystalline (in contrast to microcrystalline) dolomites. A color change from gray to light brown outlines the pattern of the grains and gives the impression of an original packstone, or possibly grainstone, texture. The identifiable organic remains are rare and consist mainly of echinoderm debris, foraminifers, red algae, corals, pelecypods, and gastropods. Echinoderm debris is the most abundant because it is the most resistant to neomorphism and,

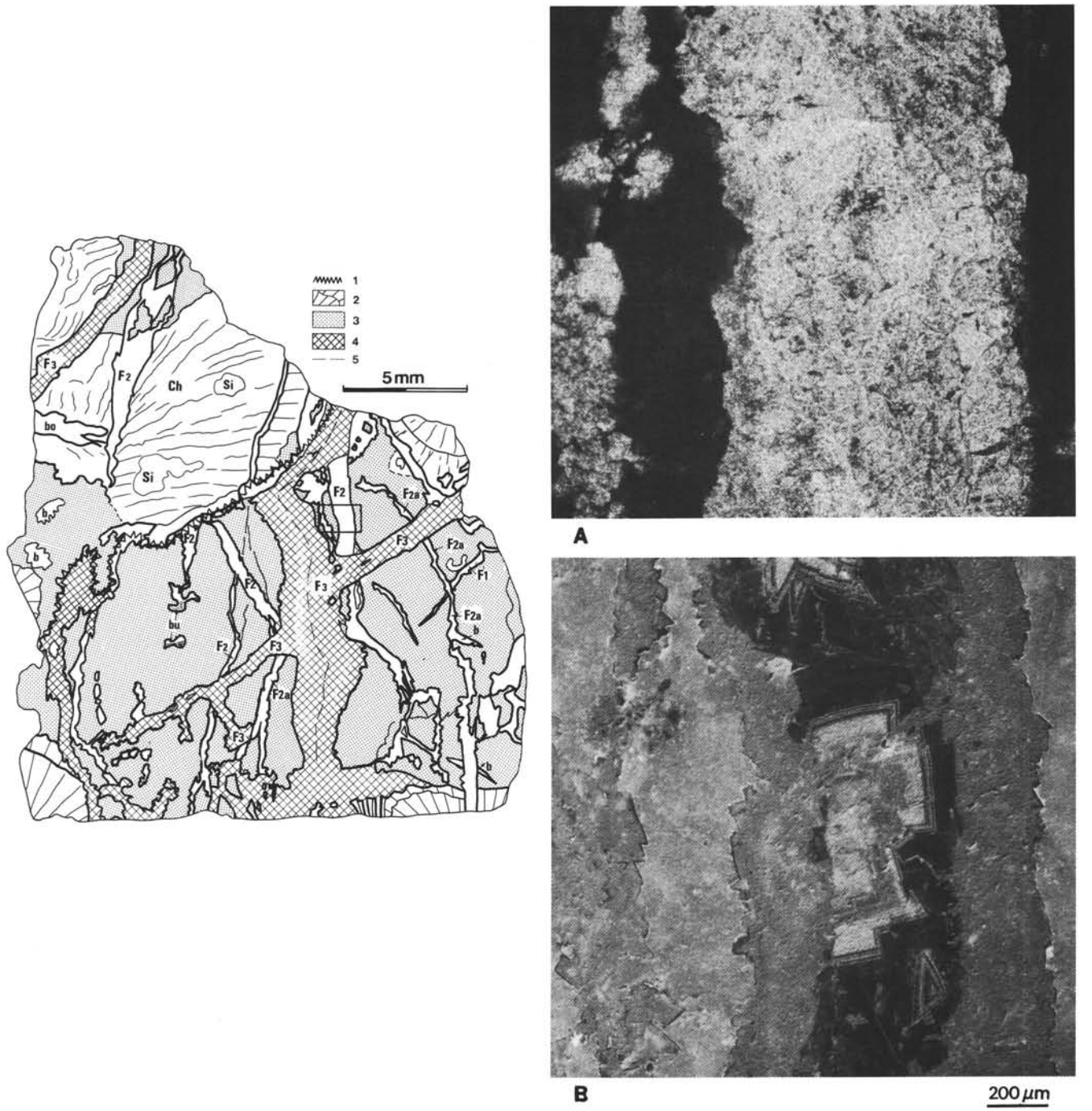

Figure 11. Fissures and tectonic breccia within a floatstone of the upper limestone unit. Sample 103-639D-5R-3, 39–41 cm. **A.** Sketch showing three sets of fissures. 1 = stylolites; 2 and Ch = *Chaetetes*; 3 = micrite; 4 = dominant saddle dolomite and sparite filling the last set of fissures; 5 = compromise boundary; Si = silicification; bu = burrow; b = bioclast; bo = boring; □ = location of Figures 11B and 11C. **B.** Natural light. **C.** Cathodoluminescence. Fissure type F2d. Cathodoluminescence reveals a reactivation of the fissure and two kinds of dolomite fillings not observed in natural light. The inner area is filled with a later, zoned dolomite.

therefore, the best conserved. However, the original sediment was not an entrocal sand.

The dolomite is dissected by a network of fractures and brecciated zones that were sealed by different types of fillings, including silts, cements, and recrystallized zones (e.g., Samples 103-639A-10R-1, 10–19 cm, 103-639A-10R-1, 124–127 cm, etc.). Some pores are partially or totally filled by various sediments, which are either grayish light brown or yellow. Numerous rock fragments are coated with these same sediments. The internal sediments were clearly deposited after fracturing as they are not truncated by fractures.

The dolomites recovered in Hole 639A have a diagenetic macrofacies with three main components: fractures and their fillings, pores and their fillings, and the surrounding (host) rock.

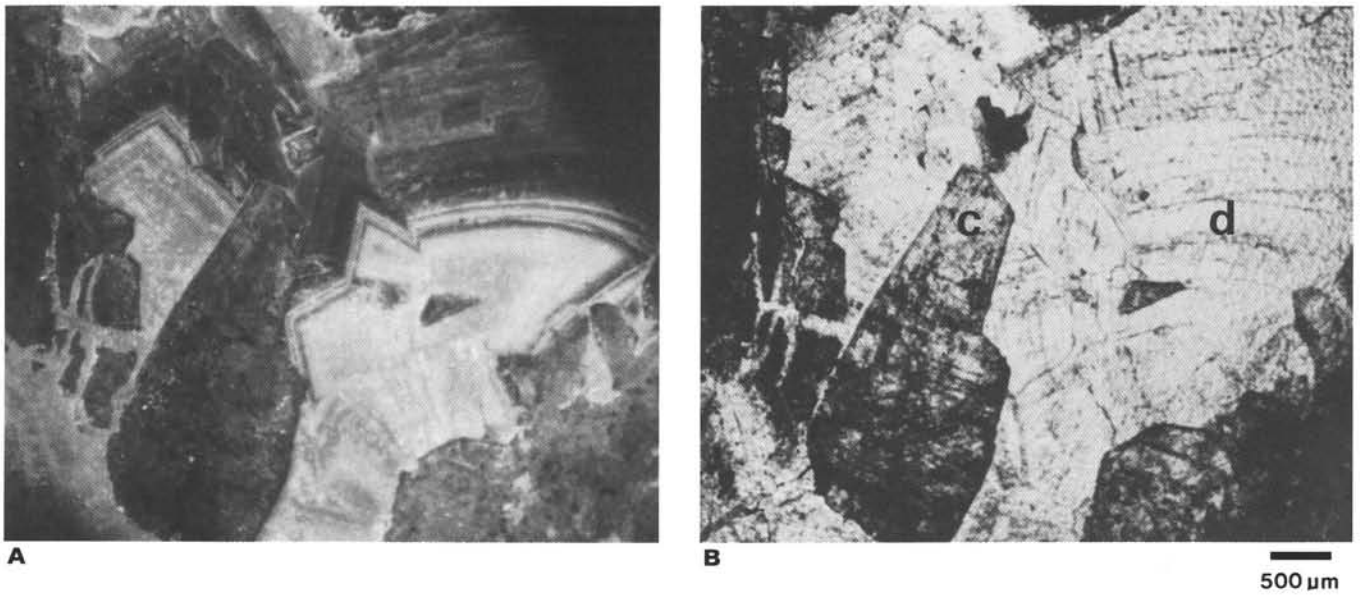

Figure 12. Detail of a type F3 fissure in limestone, filled with large saddle dolomite enclosing coarse sparite. Dolomite is not stained (d) and shows characteristic curved zonation under cathodoluminescence. Calcite (c), stained by alizarin, clearly comes from the wall and an intermediate fissured zone and is cemented by dolomite. Sample 103-639D-5R-2, 137–139 cm. **A.** Cathodoluminescence. **B.** Natural light; stained thin section.

These dolomites have textures that are relatively distant from the original microfacies of the limestone. No relics of calcite were evidenced by staining or detected with X-ray diffraction.

Dolomite Textures

Table 2 summarizes the crystal characteristics of each textural type observed in the Hole 639A dolomites. Four textural types (and their variants) are distinguished: (1) dirty dolomite textures, (2) mostly transparent saddle dolomite textures, (3) tectonic breccia, and (4) resedimented detrital dolomite.

Dirty Dolomite Textures

Texture 1a: Xenotopic dirty texture (Fig. 13)

Zones of darkish irregular anhedral crystals with nonundulating extinction, less than 1 mm in size, are located between the fissures and the pores. The dark impurities are either localized in the center of the crystal or form a band along the edges of skeletal debris (e.g., Samples 103-639A-10R-1, 143–144 cm, and 103-639A-10R-2, 52–56 cm; Fig. 13). The lighter areas may correspond to recrystallized shells, organic cavities, or intergranular spaces. Under cathodoluminescence, the dull zones show a rose color with bright intensity. The more transparent parts are dull.

Texture 1b: Hypidiotopic texture consisting of dirty crystals with clean baroque rims (Fig. 14)

Texture 1b includes varied geometric crystals within the same field and may be locally anhedral. The centers are dark, often crystalline, and subhedral to euhedral, even when the crystals are not. The edges have irregular extensions that are clean and baroque with undulating extinction. Locally, the distribution of the impurities vaguely marks zones of crystalline growth.

Texture 1': Variant texture of textures 1a and 1b with cleaved and fissured crystals (Table 2, Fig. 15, and Pl. 7)

The crystals within textures 1a and 1b may be partially or entirely effected by abundant cleavages and microfissures. These microfissures and cleavages are filled with a clear (without impurities) dolomite that is developed in a syntaxial manner in regard to deformed crystals (Fig. 15).

Together, texture types 1a and 1b consist essentially of crystals of dirty dolomite with a transparent growth zone around the nucleus. This contrast reveals phantoms of the original texture, such as 1–2-mm pellets or grains, pelecypods, gastropods (Fig. 14), foraminifers, and red algae. The distribution of impurities resembles micritized skeletal debris (Bathurst, 1966) or micritic coatings. Echinoderms are easily recognizable due to their straight extinction as opposed to the sweeping extinction of saddle dolomite; under cathodoluminescence, bright yellow traces sometimes underline the initial porous lattice.

These structures are representative of those closest to that of the original sediment. However, there are no mineralogic relics of limestone nor obvious primary rhombs of the first step of dolomitization. For instance, phantoms, as small as foraminifer size, are found in several dolomite crystals, which indicates replacement of the original mineralogy and neomorphism.

Mostly Transparent Saddle Dolomite Textures

Texture 2a: Hypidiotopic texture composed of baroque crystals with rare impurities outlining crystallographic planes (Pl. 7, Figs. 1–3)

In the subhedral crystals of this mosaic, a few dark impurities, including the outlines of bioclastic phantoms (Pl. 7, Fig. 3) or foraminifers (Pl. 7, Fig. 2) are distributed along cleavages and previous growth faces. The crystals have transparent and well-developed edges with sweeping extinction. Compared with texture 1b, the texture 2a crystals tend to be larger (see Table 2), and clean baroque zones are more abundant than in the darker zones.

This texture is interpreted as a second syntaxial growth of the baroque crystal rim observed in texture 1b and/or as a complete replacement of textures 1a and 1b. In coexistence with textures 1a and 1b, the diagenetic evolution represented by texture 2a further impedes the recognition of original sediment types.

Texture 2b: Hypidiotopic cement texture with saddle- and spear-shaped transparent crystals (Pl. 7. Fig. 4)

Table 2. Textures in the Hole 639A dolomite.

	Texture type	Crystal characters: Morphology	Mean size	Under transmitted light (TL) and reflected light	Under cathodoluminescence
Dirty dolomite textures	1a	Anhedral to subhedral	Less than 1 mm	Dirty dolomite with clean growth around the nuclei and nonundulating extinction; dark impurity in the center of crystals or outlining bioclast phantoms	Light rose Dark rose red Light rose
	1b	Anhedral to subhedral	Up to 1 mm	Dirty dolomite, crystals have subhedral to euhedral dark centers; clean and baroque edges (with undulating extinction)	Light rose Dark rose red
	1′ (a and b)	Same as 1a and 1b		Abundant cleavages and microfissures modifying any texture 1; microfissures filled with pure transparent and syntaxial dolomite	 Dark
Mostly transparent saddle dolomite textures	2a	Subhedral	Greater than 1 mm	Distribution of impurities producing crystalline forms; clean and transparent edges; sweeping extinction; bioclast phantoms belonging to several crystals	Light Dark
	2b	Subhedral, saddlelike and spearlike; curved faces	Greater than 1 mm (up to 5–6 mm)	Clean and transparent crystals with well-zoned growth; commonly two parts in crystals: 1. basal part zoned with impurities and ± cleaved (see also 2′) 2. distal part pure and transparent	Dark with ± blurred zonation
	2c	Anhedral; saddlelike; curved faces	Greater than 1 mm	Dominantly transparent and homogenous crystals; maximum of curved faces	Dark or partially blurred zonation
	2′ (a, b, and c)	Same as 2a–2c		Abundant cleavages and microfissures modifying any texture 2	
Tectonic breccia	3			Tectonic breccia composed of dolomitic rocks, crystal fragments, and textures 2c and 2′	Phantom of zoned crystals, evidence of light yellow fissures
Resedimented detrital dolomite	4			Resedimented detritic dolomite, including:	
	4a	Anhedral	30–100 μm (up to 200 μm)	Gray-brown silt, translucent in transmitted light; some jig-saw structures	Dark
	4b	± Fragmented transparent crystals and dolomite rock fragments from 200 μm to several millimeters; in matrix.		Yellow microbreccia; ± gradded bedding	
	4c	Similar composition to 4b		Yellow laminated sediment; two dominant types of laminae: 1. Crystals and lithic debris are closely packed and show transparent overgrowth rim; yellow color matrix is very dark in TL 2. Crystals and lithic debris are ± floating, do not show overgrowth rim; yellow matrix is very dark in TL	 Dark Black Black Black
	4d		Microcrystalline	Yellow very fine sediment, very dark or opaque in TL	Black

This saddle dolomite texture (Radke and Mathis, 1980) is made up of large (>1 mm), clean, transparent crystals with curved faces and pointed tips. Their typical sweeping extinction indicates subcrystal organization into supergroups. This type of texture has various occurrences, including within the 1a, 1b, and 2a textural fields described previously: concentrations in irregular areas, some of which are linked in form a network, with the center of such fields commonly occupied by a residual pore (Pl. 7, Fig. 4); fracture infillings; and fringes around cavities filled with internal sediment. It is either a cement filling vugs and fissures or a product of recrystallization within the host rock.

The crystals are zoned and commonly divided into two parts (Pl. 7, Fig. 4). The basal part is slightly zoned by dark impurities and often cleaved, appearing under cathodoluminescence as orange punctuated with light patches. The distal part is very pure and transparent, appearing under cathodoluminescence as dull rose with blurred zonation.

Texture 2c: Xenotopic saddle dolomite texture (Fig. 16)

Texture 2c is a variation of texture 2b. It is more homogenous and dominantly transparent. Anhedral, relatively isometric crystals exhibit a maximum of curved faces and sweeping extinction (Fig. 16). Texture 2c belongs to the surrounding (host) rock and is interpreted as the final stage of replacement of textures 1a and 1b and 2a.

Texture 2′: Variant texture of textures 2a, 2b, and 2c with cleaved and fissured crystals (Table 2, Pl. 7, Fig. 4, and Fig. 22B)

The texture 2′ crystals are partially or entirely affected by abundant cleavages and microfissures, which appear dirty in saddle transparent dolomite (Pl. 7, Fig. 4, and Fig. 22B).

From the dirty texture 1a, with some faintly observable phantoms of the initial sediment, to the purest crystalline texture, crystal size continuously increases, and the saddle character is increasingly pervasive. The dark, inherited traces decrease, and

Figure 13. Dirty dolomite texture type 1a. Hypidiotopic texture of subhedral dirty crystals is dominant but is always associated with another textural area composed of clearer, baroque crystals (see text). The contrast between the two textures outlines the original grains. Sample 103-639A-10R-1, 143–144 cm; natural light.

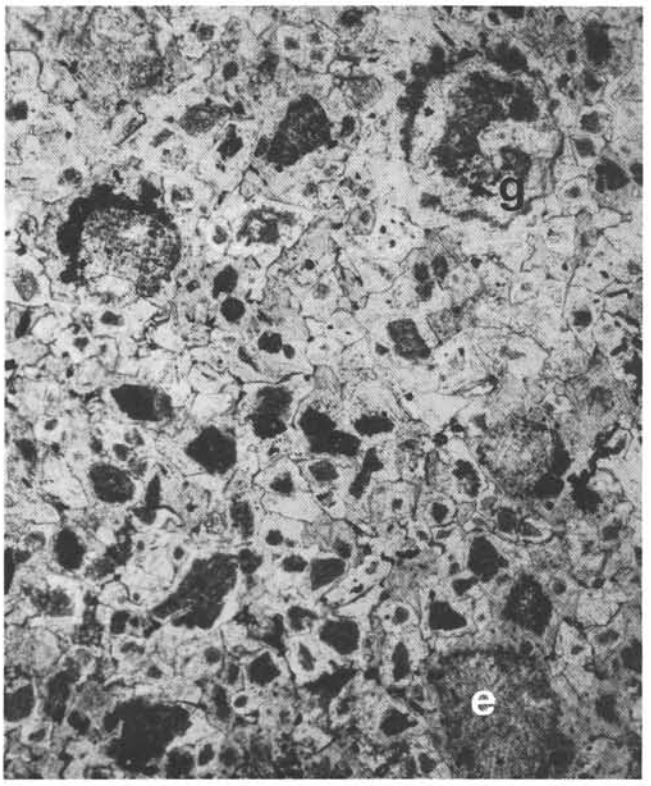

Figure 14. Dirty dolomite texture type 1b. Hypidiotopic texture crystals generally have dirty nuclei showing euhedral morphologies and clean, baroque edges. Elsewhere in the sample, the repartition of impurities reveals phantoms of the original structure and micrite envelopes of gastropods (g) and echinoderm particles (e). Sample 103-639A-10R-2, 52–56 cm; natural light.

their redistribution is progressively linked to the growth of the crystals.

Texture 3: Tectonic breccia dolomite

Some fragments of host rock and crystals are included in the tectonic breccia of texture 3. The coarse, clear saddle dolomite commonly is the result of the infilling of successive fracture sets. Only cathodoluminescence reveals that the host rock was completely replaced (Pl. 10, Figs. 1 and 2).

Texture 4: Resedimented detrital dolomite (Pls. 8 and 9 and Figs. 23 and 24)

Reworked elements of the dolomite rocks and mostly fragmented crystals, ranging from silt to rudite size, are sediments infilling the fractures or cavities.

Study of Fracturing: Morphology and Filling of Fissures

The scarcity of compaction structures does not allow distinction of pre- and post-stylolite fissures in the dolomites, as is possible for the Hole 639D limestones. Moreover, dolomite recrystallization homogenizes the fillings into a saddle texture, complicating the interpretation of the fissure crossings. However, the general morphology of the fissures, the aspects of the edges, the presence of several fillings, and some pronounced intersections characterize several sets of fractures and suggest a relative chronology.

Table 3 lists fissure types F(a) through F(g) and summarizes their characteristics.

Type F(a): Mostly undulating, meandering fissures, well outlined by dark impurities. Samples 103-639A-9R-1, 94–98 cm, (Fig. 17) and 103-639A-10R-2, 108–112 cm (Fig. 18)

Fissure type F(a) appears as a phantom. It is transparent and well defined on each side by a dark border. The saddle crystals of the texture as a whole are not related to the extent of the fissure and traverse the two edges (Figs. 17A and 17B), a sign that the fracture preceded the baroque or saddle-shaped crystal growth. Some intersections show that the fissure set is cut by all of the other fissures. Their formation prior to the other fissures and other similarities suggest that this set of fissures is equivalent to the F1 fissures in the limestones. The development of this fracture type could precede dolomitization.

Type F(b): Undulating to straight fissures, outlined by a serrated repartition of dark impurities. Sample 103-639A-9R-1, 94–98 cm (Fig. 19)

F(b) fissures are also phantoms. In comparison to the F(a) fissures, this type is characterized by straighter fissures (but still undulating) and a repartition of dark impurities in wall crystals outlining euhedral phantoms of rhombs (Fig. 19). It is uncertain as to whether the F(b) type is a simultaneously formed variant of F(a) or if formation was after F(a); the serrated aspect is strongly reminiscent of the F2a fissures in Hole 639D limestones. These rhomb phantoms, well aligned along the fissure, suggest that the dolomite crystal growth was linked to fracturing in a dolomitic limestone.

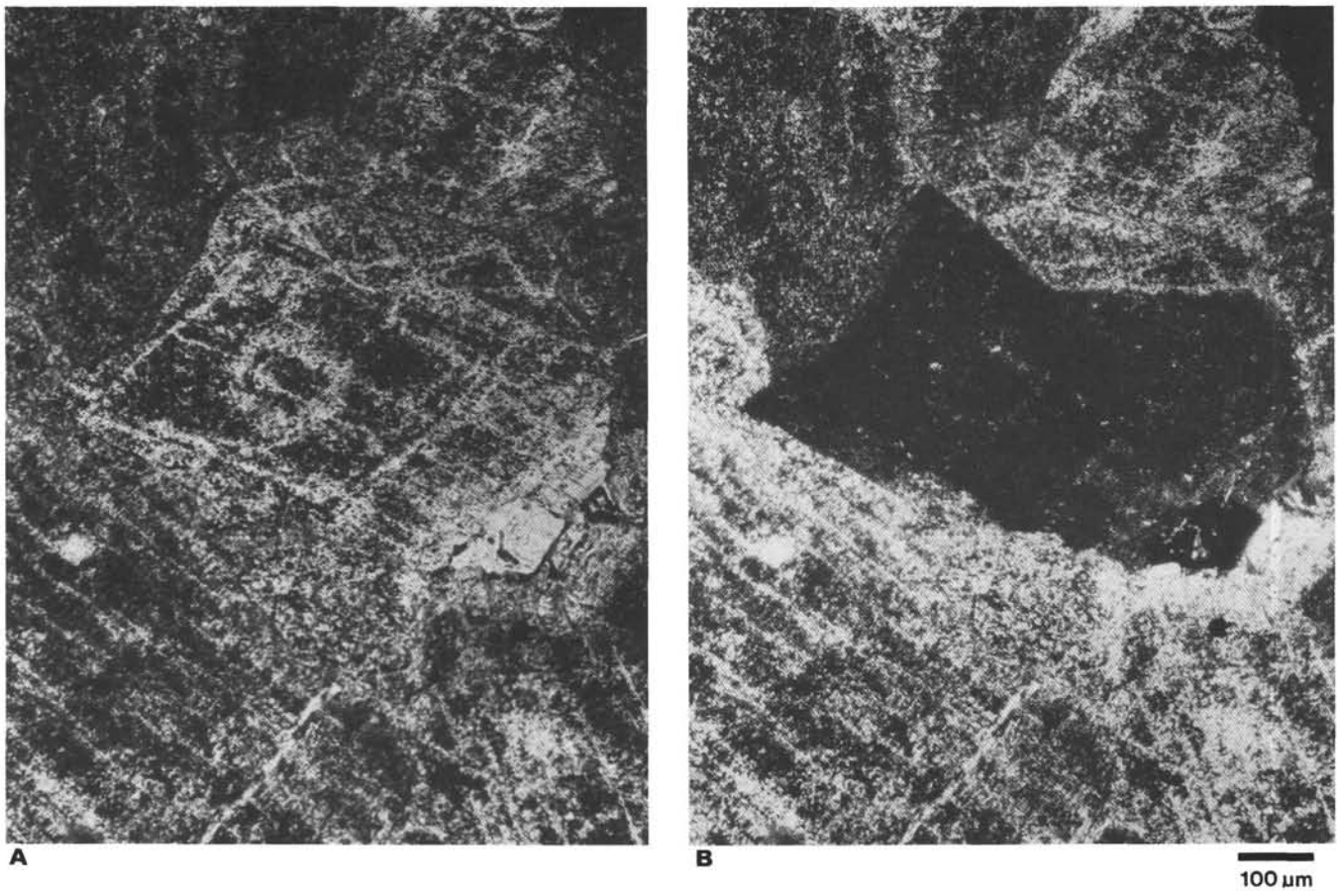

Figure 15. Dolomite texture of type 1′a, variant of texture 1a in which dirty dolomite crystals showing some baroque overgrowth mosaic are cleaved and fissured. Microfissures are filled with clean dolomite in syntaxial growth with the crystal, as seen under polarized analyzed light. Note the transformation step of a euhedral crystal into a saddle-shaped, progressively purer crystal. Sample 103-639A-10R-1, 13–14 cm. **A.** Natural light. **B.** Polarized analyzed light.

Type F(c): Rectilinear fissures with straight edges and without borders marked by impurities. Sample 103-639A-10R-1, 13–14 cm (Fig. 20)

This fissure type is not a phantom and clearly intersects all of the crystalline textures as well as fissure types F(a) and F(b). The F(c) fissures are filled with clean, commonly baroque, dolomite crystals, which are syntaxial with the wall crystals (Fig. 20). A compromise boundary occurs approximately in the middle of the fissures. These fissures formed after saddle crystal neomorphism.

Type F(d): Mostly undulating fissures, millimeter width with saddle dolomite fillings. Sample 103-639A-9R-1, 67–71 cm (Fig. 21)

These wider fissures are filled with large saddle crystals growing from each edge to a compromise boundary at the center of the fissure. Their general pattern is similar to that of the F(c) fissures and suggests extensional tectonics.

Type F(e): Large fissures, generally straight, with polyphased fillings

This type of wide fissure is asymmetrically filled, with multiple dolomite textures (2b, 2′, and 4; Table 2). Some textures are bedded and generally present a geotropic polarity. Sample 103-639A-10R-1, 10–19 cm, is a good example of this type of fissure (Figs. 22A–22C). The irregular, furrowed floor of this fissure is covered by a clean baroque fringe, which is dull under cathodoluminescence. The floor is overlain by a bedded detrital texture that is heterometric and predominantly silty. Recrystallization is significant (Figs. 22B and 22C). The top of the fissure shows a clear, straight boundary between the filling and the host rock. Large transparent crystals hanging from the roof terminate by joining the summit of the inner sediment (Figs. 22B and 22C). In such fissures, the compromise boundary results in an equilibrium between crystalline growth and "inner mechanical sedimentation" (Sander, 1936).

In Sample 103-639A-10R-1, 10–19 cm, the polarity of the fissure fillings does not correspond with the orientation of the core and assumes rotation on the order of 90°. The length of the sample precluded its rotation within the drill pipe. In Sample 103-639A-10R-1, 40–49 cm, the depositional polarity of the internal sediment is in good agreement with the core orientation. Sample 103-639A-10R-1, 10–19 cm, could belong to a transported block of highly fractured and eroded dolomite.

Type F(f): Fissures and margins of samples fringed with saddle cement and filled with microbreccia. Sample 103-639A-10R-1, 80–85 cm (Pl. 8, Figs. 1 and 2)

This type of wide fissure is generally rectilinear, fringed with a saddle rim cement, and filled with a yellow detrital dolomite of type 4b (see Table 2 and Pl. 8, Figs. 1 and 2). Under cathodoluminescence, the edges of the saddle dolomite fringe and the resedimented crystals show a very dark or black final overgrowth (Pl. 8, Fig. 1). The timing of this evidence of postfilling recrystallization is poorly constrained. Many rock piece margins are truncated, fringed by saddle dolomite, and coated by the

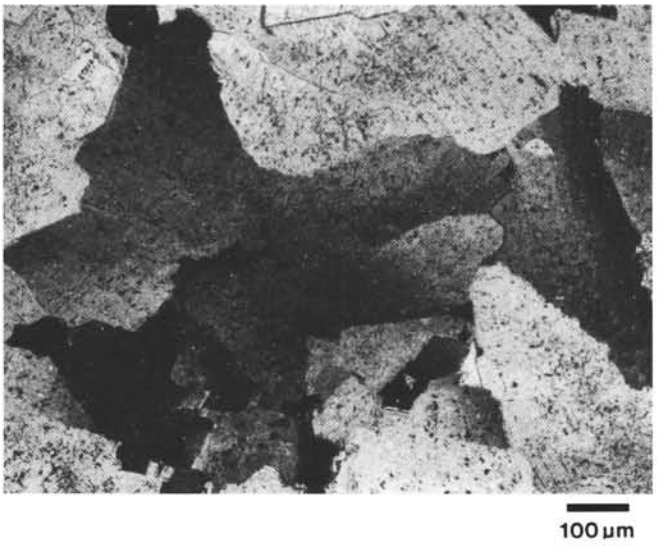

Figure 16. Texture type 2c. Xenotopic saddle dolomite texture with a maximum of curved faces and sweeping extinction. Sample 103-639A-9R-1, 94–98 cm; polarized analyzed light.

same yellow microbreccia. However, these fissures are so large that their recovery was incomplete.

Geotropic polarity is evidenced by locally graded bedding of small fragments and the differential growth of the saddle dolomite at the top and floor of the fissure (Pl. 8, Figs. 1 and 2).

Type F(g): Fissures and margins of samples fringed with saddle cement and filled with bedded sediments

Type F(g) fissures distinctly truncate the host rock. They are bordered by saddle-shaped crystals like the F(f) fissures and filled with type 4c texture detrital dolomite (a yellow heterometric and finer laminated sediment) (see Table 2 and Pl. 8, Fig. 3). This type of fill is common to the internal cavities as well as several sample margins.

Cavities with Internal Sediments

Cavities range in size from millimeter scale to 1 or 2 cm. Many of the cavities were incompletely recovered at the edge of the sample, implying that they are several centimeters or larger in size.

The cavities are completely rimmed by transparent saddle cement (type 2b texture). The host rock has a dominantly type 1 dirty texture and contains abundant fissures of different types. Around the cavities, saddle dolomite of texture type 2c with rare islets of textures 1a and 1b is especially dominant (Fig. 23). This textural variation in relationship to the fissure network strongly suggests the evolution of finely fractured and recrystallized rocks.

A number of the cavities are filled with one or several types of the following varieties of detrital dolomite:

1. Grayish light brownish silt (detrital dolomite texture 4a; Table 2). This dolomite appears translucent in transmitted light. It is composed of 50–100-μm (and some larger) anhedral crystals, with jig-saw structure (Pl. 9, Fig. 2) and highly blurred bedding (Fig. 23 and Pl. 9, Fig. 1). Some of the silt is recrystallized into larger, transparent saddle crystals (Fig. 24 and Pl. 9, Fig. 2), with zoned cathodoluminescence.

2. Yellow laminated sediment with fine matrix (detrital dolomite texture 4c; Table 2). This type of internal sediment is composed of variable size (200 μm to several millimeter), clear crystal debris and parts of the host rock. Under transmitted light, the matrix is opaque. This internal sediment is bedded, and the laminae have differing textural and cathodoluminescence characters (see Table 2 and Pl. 9, Figs. 3 and 4).

3. Yellow very fine sediment (detrital dolomite texture 4d; Table 2). This sediment is microcrystalline, very dark or opaque under transmitted light, very dark to black under cathodoluminescence, and contains rare, fine debris of clear dolomite. This sediment definitely represents the finest fraction of the yellow laminated sediments.

These three sediment types are either isolated in the small fractures and cavities or superimposed in the larger fractures and cavities; however, not all of the types are necessarily present.

As a matter of curiosity, it is interesting to note a fine, opaque, highly ferric sediment in the residual pores. It may be superimposed on one of the yellow inner sediments.

COMPARISON OF DOLOMITES FROM HOLES 639B THROUGH 639D WITH VALANGINIAN DOLOMITIC LIMESTONE FROM HOLE 639A

A comparison of the dolomites from Holes 639A through 639D shows the following differences:

1. The dolomite in Hole 639B consists of a commonly occurring diagenetic facies that is unusual in Hole 639A: a dark grayish brown rock with a dominantly heterogeneous and comparatively finer texture (Sample 103-639A-9R-1, 80–85 cm). The heterogeneity results from patches showing variation in color, crystalline size, and content of crystal impurities. The darkest patches contain many elongated, flat and whitish structures that can be interpreted two ways. Some of these structures are probably bioclasts (pelecypods); others are fissure fillings (Pl. 10, Fig. 3).

2. An important characteristic of the Hole 639B dolomite is the high abundance of the tectonic breccia (texture 3) associated with the highly fissured facies that was recovered (Pl. 10, Figs. 1 and 2). This characteristic strongly suggests the presence of a fault.

3. Some of the rocks in Hole 639B show a complex structure of cemented fractures separating patches of clear baroque dolomite or even "cellular" zones. These structures are similar to the dissolution aspect of cavernous or cellular dolomite and do not retain any sedimentary character. Dolomite of Hole 639B is directly overlain by Tertiary sediments. The significance of this dissolution can be linked to a long submarine exposure of the cliff from the Early Cretaceous tilting of the fault block to the Tertiary sediment deposit.

4. In Holes 639C and 639D, the dominant facies observed in Holes 639A and 639B are mixed. As previously suggested (Boillot, Winterer, et al., 1987), the dolomite of Holes 639C and 639D could be slides and blocks that glidèd from the upper edge of the tilted block during the Cretaceous or early Tertiary. Within the dolomites of Holes 639B and 639D, a great number of the vugs, pores, and fissures are infilled with sediments quite similar to those described for the dolomites of Hole 639A. Most of these dolomites show the same advanced diagenetic structures, thereby confirming the important role of fracturing. An exceptional example of a compacted facies with features resembling stylolites occurs in Sample 103-639D-4R-1, 3–7 cm. However, parts of all of the cores exhibit the less evolved facies characteristic of the recovered dolomites. Dirty type 1 textures are dominant, many fossils and debris are clearly recognizable (corals, echinoderms, calcitic red algae, and calcareous sponges), and type F(a) fissures are numerous. Initial or diagenetic structures inherited from precursor limestones have the best preservation.

5. The calcareous marls with calpionellids of Valanginian age are partially dolomitized. The dolomite has two structures that are quite different from the Tithonian dolomites: (a) iso-

Table 3. Fissures in Hole 639A dolomite.

Fissure type	Outline	Edge morphology	Size (width)	Filling under transmitted light (TL) (specified color under reflected light)	Cathodoluminescence
F(a)	± Undulating and meandering; variable width	± Irregular; well outlined by dark impurities	100 μm through 1 mm	Transparent, some baroque dolomite crystals traversing both edges of the fissure;	Dark
				part of crystals within the cheek is dirty; no compromise line	Light
F(b)	± Undulating to straight; ± variable width	± Irregular; well outlined by a serrated repartition of dark impurities	100 μm through 1–2 mm	Transparent, some baroque dolomite crystals;	Dark
				dirty part of crystals within the cheek outline endings of rhombs	Light
F(c)	Rectilinear	Straight; poorly outlined by dark impurities	100 μm through 1–2 mm	Transparent, some baroque dolomite crystals; compromise line present	Dark
F(d)	± Undulating; wide	± Irregular	1–4 mm	± Transparent baroque dolomite; compromise line present	
F(e)	Rectilinear ± variable width; wide	± Irregular for one edge; fairly straight for the other one	1–6 mm	Asymmetric filling with 2b, 2′ (a and b), 4a textures, geotropic polarity;	
				furrowed floor covered by a fringe of transparent saddle crystals;	Dark + black endings
				inner bedded sediment, predominantly silty (texture 4a);	Light
				large saddle crystals hanging from the roof; compromise line present	Dark
F(f)	Rectilinear; ± variable width; very wide	± Straight; rimmed with saddle dolomite	1 mm through several centimeters	Yellow microbreccia (texture 4b):	
				elements of fractured dolomite and broken crystals;	Light
				yellow matrix, opaque under TL	Dark
				± graded bedding	Black
F(g)	Rectilinear; ± variable width; very wide	± Straight; rimmed with saddle dolomite	1 mm through several centimeters	Yellow laminated sediments (some indurated early; see texture 4c, Table 2)	

[a] Color is rose red unless noted.

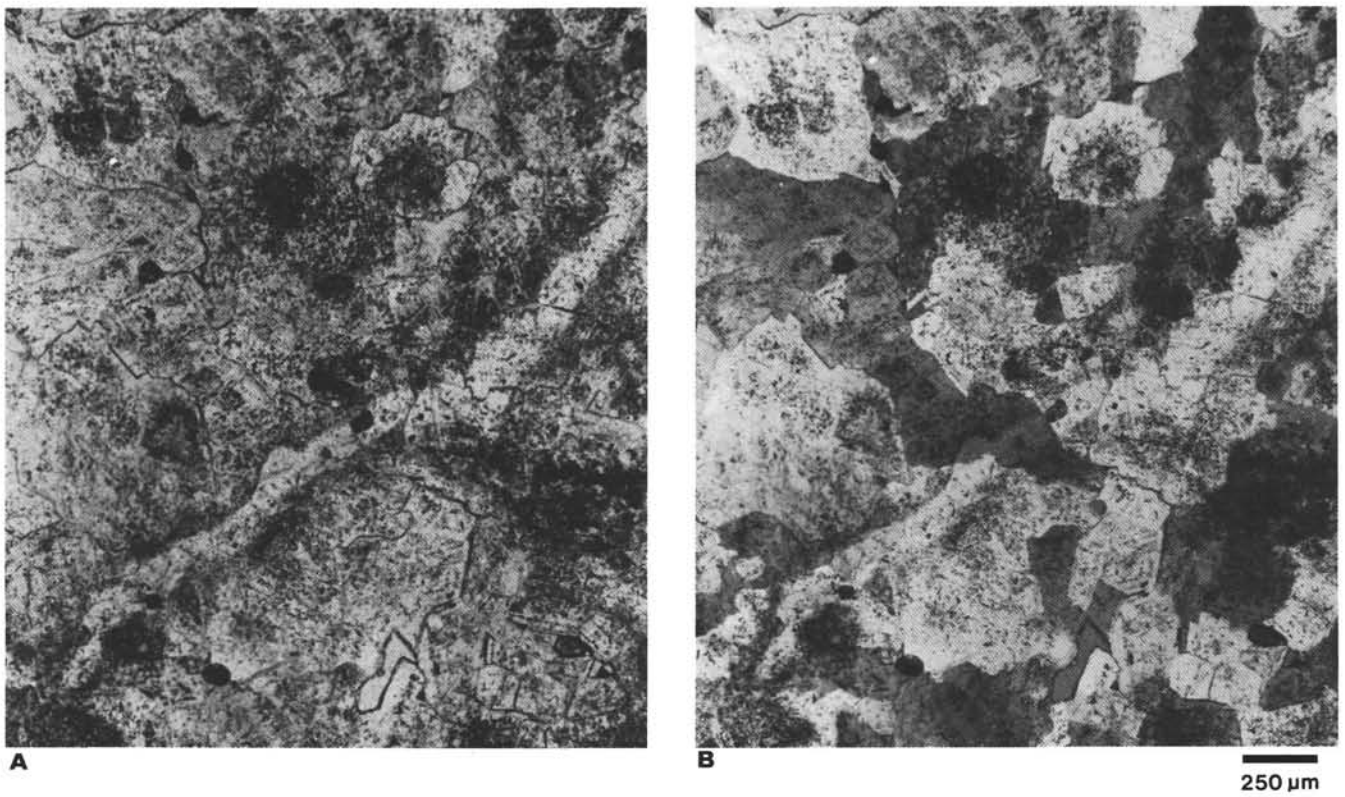

Figure 17. Fissure type F(a) in the dolomite unit is a mostly undulating fissure with edges well defined by dark impurities. Large anhedral crystals, mostly baroque, intersect the whole fissure, which shows that the fissure is a phantom that formed in the host rock before recrystallization. Sample 103-639A-9-1, 94–98 cm. **A.** Natural light. **B.** Polarized analyzed light.

lated rhombs with a dark nucleus, sometimes dissolved, and rich in impurities and iron hydroxides (Pl. 10, Fig. 4) and (b) a microdolosparitic mosaic that becomes less significant upsection. This post-Valanginian dolomitization has not been dated and may have originated either from the usual burial dolomitization of basinal sediments or from burial dolomitization at the contact with the underlying dolomite, from which there is an upward decrease in dolomitization.

PRELIMINARY RESULTS OF CHEMICAL ANALYSIS

Stable Carbon and Oxygen Isotopes

Carbon and oxygen isotopic values from 15 separated samples of crystalline dolomite textures range between +1.55‰ and +3.47‰ for $\delta^{13}C$ and between −10.30‰ and +3.08‰ for $\delta^{18}O$ (Table 4). However, two sets of common values clearly expressed for both $\delta^{13}C$ and $\delta^{18}O$ (Fig. 25) correspond to distinct petrographic textures.

The first value set for $\delta^{18}O$ (I; Fig. 25) includes samples of the host rock (dirty dolomite with crystalline textures 1a, 1b, and 2a), saddle dolomite (cavity and fracture fillings of crystalline texture 2b), and gray, translucent dolomicrospar silts. These $\delta^{18}O$ values are strongly negative, from −10.30‰ to −6.94‰. The second set of $\delta^{18}O$ values (II; Fig. 25) includes samples of yellow microbreccia and laminated internal sediments with both negative and positive values, between −4.16‰ and +3.08‰. Interestingly, dolomite from the top of the Tithonian falls into this second set of values.

Although these two distinguished sets also exist for $\delta^{13}C$, the deviation is less significant than for the $\delta^{18}O$ values.

Five separate micritic matrices that do not show evidence of dolomitization or dedolomitization were analyzed from the underlying limestones. Their carbon and oxygen isotopic values belong to a third set of values that range between +0.99‰ and +1.97‰ for $\delta^{13}C$ and between −0.98‰ and −2.69‰ for $\delta^{18}O$ (Table 5 and III on Fig. 25). The difference within dolomite set I (Fig. 25) does not correspond with what would be expected for cogenetic (or codiagenetic) dolomite and calcite in the same temperature range. For instance, given that the $\delta^{18}O$ of dolomite has a mean value of −9‰, a codiagenetic calcite would have a $\delta^{18}O$ of about −13‰ (see Veizer, 1983), not the −1.5‰ value found.

Microprobe Data

Preliminary results of 1200 microprobe analyses show that the molar ratio $^{m}Mg/^{m}Ca$ of Site 639 dolomites is between 1.07 and 0.70. Fe content varies between 3700 and 440 ppm, rarely falling to 0 (normalized atomic content, i.e., 1.2% FeO or 2% $FeCO_3$). Mn content varies between 900 and 0 ppm. Strontium was not observed.

Interestingly, there are three sets of $^{m}Mg/^{m}Ca$ values which correspond to distinct petrographic textures observed in samples from all of the holes:

1. Dirty dolomite (textures 1a, 1b, and 2a) has a $^{m}Mg/^{m}Ca$ ratio of 1.01 ± 0.05, showing a stoichiometric or very near stoichiometric composition.
2. Saddle dolomite (textures 2b and 2c) has a wider range, from 1.05 to 0.80, but most of the values vary between 0.95 and 0.80. Translucent crystal silt belongs to this value set, with a mean of 0.87 ± 0.05. Saddle dolomite of type F3 fissures in limestones (Samples 103-639D-5R-2, 82–85 cm, and 103-639D-5R-2, 137–139 cm) is less magnesian, with $^{m}Mg/^{m}Ca$ = 0.80 ± 0.04, and shows the highest Fe content (3100 ppm or 1.8 mol% $FeCO_3$). Dolomite rhombs within stylolites have a $^{m}Mg/^{m}Ca$ ratio of 0.82 ± 0.03.

Figure 18. Fissure type F(a) in the dolomite unit is a phantom of an earlier meandering fissure, outlined by the concentration of impurities along the wall. Sample 103-639A-10R-2, 108–112 cm; natural light.

3. Yellow internal detrital dolomite has a $^{m}Mg/^{m}Ca$ ratio that varies between 0.90 and 0.70. The internal sediment also contains SiO_2 (up to 3.4%); the matrix, which is dark under transmitted light, shows traces of Fe (up to 1300 ppm), Al, K, Na, and Cr.

In these dolomites, some occurrences of the dirty nuclei are more calcic and the clean crystal borders are more magnesian, whereas in other crystals the dirty nuclei are more magnesian and the saddle overgrowths more calcic. The $^{m}Mg/^{m}Ca$ ratio varies across the border of one large, transparent saddle crystal. However, most of the transparent overgrowths of dirty crystals is more calcic than the dirty nuclei; most of the saddle dolomite is more calcic than the earlier formed dirty dolomite of the same facies. Although the translucent crystal silts have the same composition as the mother dolomite, the internal yellow sediment, which is the most recent filling of the cavities, is the most calcic. The later-formed dolomite in a given texture is generally more calcic.

DISCUSSION

Chronology of Textures, Fractures, and Phases of Dolomitization in the Dolomite Unit

The four crystalline dolomite textures (indexed 1 to 4) and their variants are present in all of the recovered dolomites. The dirty textures (1a and 1b), clean saddle overgrowth (2a), and final xenotopic saddle texture (2c) belong to the host rock. The saddle cement texture (2b) fringes fractures, pores (often exhibiting a residual void), and larger cavities. The saddle crystals of texture 2b cement grew in syntaxial manner with the dirty and generally baroque crystals of the host rock. The detrital dolomite (4) lies unconformably over the other textures.

Fracturing is the most important characteristic, generally indicating extensional tectonics. Seven types of fissures, F(a) through F(g), were observed in the dolomite. The F(f) and F(g) fissures were the last to form, thereby creating a network for the supply of internal sediment throughout the formation, as well as for cavities within the host rock. Between the formation of the first, type F(a), fissures and the F(f) and F(g) fissures, an imprecise chronology of several types of fissures was formed. At least three sets of fissures can be established:

F_I = F(a) + F(b). Formed prior to development of textures 1a and 1b, this fracturing may have affected the limestone precursor or dolomitic limestones.

F_{II} = F(c) + F(d). This fracture set is intercalated between the first generation of baroque dolomite (texture 2a) and the generation of large saddle dolomite (2b and 2c).

F_{III} = F(e) + F(f) + F(g). This fracture set formed prior to the detrital textures (4).

The fracturing of the dolomites clearly altered the rock and modified crystalline textures. This alteration led to the opening of an important secondary porosity, the formation of cavities of different sizes, and the draining of dolomitizing fluids (Cros, 1977). This process enabled both the mechanical and chemical production of detrital material (crystalline and lithic) of all sizes, including fine silt. Simultaneous development of cement took place along the walls of the pores, and later, within fractures, at the same time as recrystallization of the host rock. Final diagenesis resulted in a dominantly saddle-shaped texture (2c). A fringe of saddle dolomite cement (texture 2b) closed the cavity.

The internal sediments infiltrated the last network of fractures and pores, collecting the disintegration products of the crystalline fringes and the host rock. Several periods of deposition can be distinguished, as evidenced by the textures and the colors of the sedimentary fillings. The existence of lamination evidences that deposition proceeded in a discontinuous fashion.

The dolomitization of the dolomite unit was polyphased, becoming progressively less magnesian with time. A diagenetic diagram (Fig. 26) summarizes the different textures of the final paragenesis and the timing of their growth. The first dolomitization phase affected the precursor limestone and produced a hypidiotopic dolomite texture, as suggested by the euhedral to subhedral phantoms of dirty nuclei. A first fracturing event affected the limestone or the dolomitic limestone.

A second, pervasive dolomitization phase (including several crystal growth phases) produced (1) aggrading baroque dolomite from the first dolomite, (2) recrystallization of the first do-

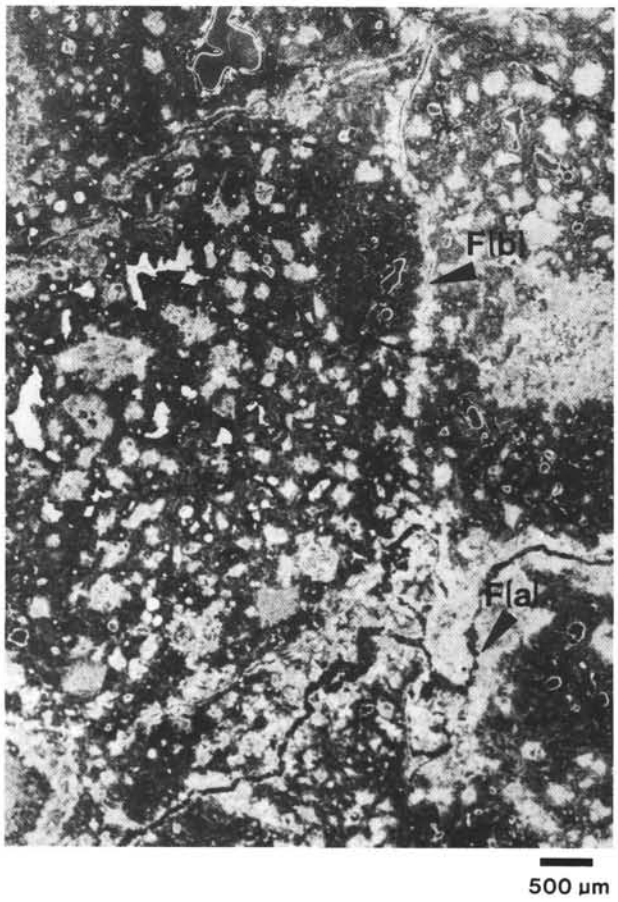

Figure 19. Negative print of a thin section showing two sets of fissures in dolomite, types F(a) and F(b). Type F(a) is as described in Figures 17 and 18. The F(b) fissure undulates slightly and exhibits a serrated distribution of dark impurities in the wall crystals outlining euhedral phantoms of rhombs. Islets of dirty dolomite are white; the network of saddle dolomite with residual pores is in black. Sample 103-639A-9R-1, 94–98 cm.

lomite into xenotopic saddle texture, and (3) direct saddle cement precipitation within a network of fissures and voids. These phases are clearly linked to fracturing. The resulting dolomite is diagenetic and structural.

A third dolomitization phase is linked both to fracturing and to an erosional event recorded as a vadose detrital silt dolomite deposit and other successive internal microbreccia and laminated sediments. Most significantly, these last-formed internal sediments are distinctive in terms of color, $\delta^{18}O$ values, and Mg/Ca content.

Final, later dolomitization occurs as black cathodoluminescent overgrowths of saddle cements and detrital crystals within Valanginian marls and stylolites.

Age of Dolomitization and Correlation with Limestone Diagenesis

Detrital internal dolomite is sealed with Valanginian deposits; therefore, all of the preceding diagenetic phases are pre-Valanginian. Of course, we cannot exclude that part of the F(c) and F(d) fissures may be Valanginian or later (cf. 5 in Fig. 27), but all F(a), F(b), F(e), F(f), and F(g) type fissures are necessarily pre-Valanginian. Likewise, other minor transformations, such as the overgrowth of crystal borders (which are black under cathodoluminescence), may have occurred later. There is idiotopic to hypidiotopic dolomite in Valanginian deposits and dolomite within later and poorly dated stylolites of the limestone unit. But major dolomitization of the Tithonian carbonates took place before the Valanginian.

Fissures are relative chronologic markers that we can tentatively use for correlations of tectonic events and diagenetic stages within the limestone and dolomite units. We suggest that the three sets of pre-Valanginian fractures occurring within the dolomite unit of Hole 639A are not far from being equivalent with the fracture sets observed in the Hole 639D limestones (cf. 1 through 5 in Fig. 27).

1. Both the F(a) fissures in the dolomite and F1a fissures in the limestones are the first-formed fissure sets and they have the same outline, strongly suggesting that they can be correlated. Thus, F1a fissures in the limestones are pre-Valanginian.
2. F(b) fissures in the dolomites are rarely observed. They are similar to the F(a) fissures in that both sets are fissure phantoms, mostly undulating, and clearly outlined with dark impuri-

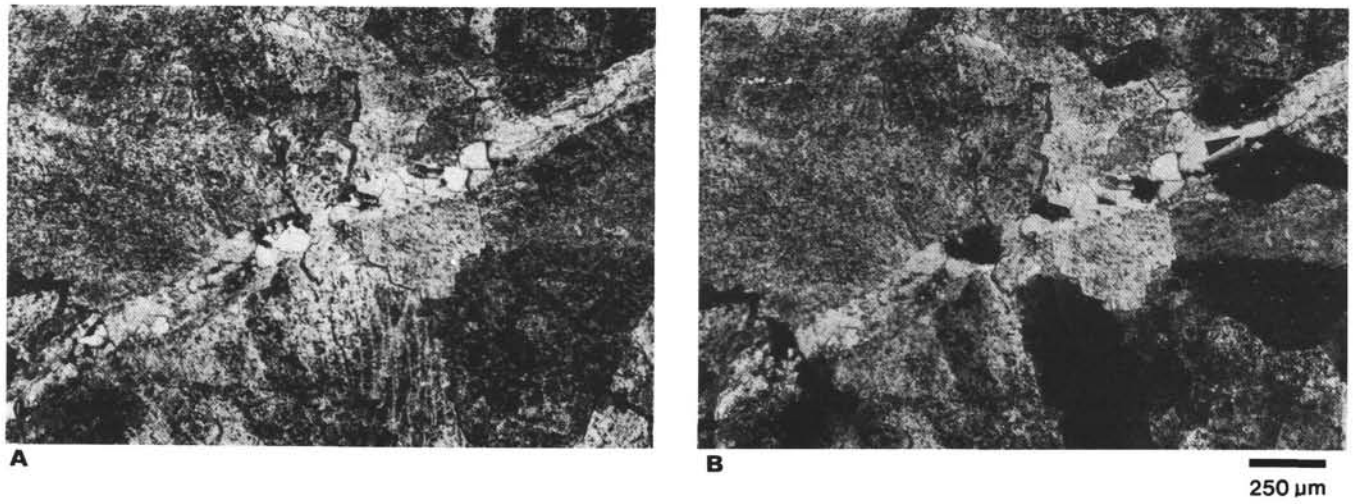

Figure 20. Fissure type F(c) in the dolomite unit. The fissure is filled with clean dolomite crystals, most of which are in syntaxial growth relative to the wall. The compromise boundary is approximately in the middle of the fissure. Sample 103-639A-10R-1, 13–14 cm. **A.** Natural light. **B.** Polarized analyzed light.

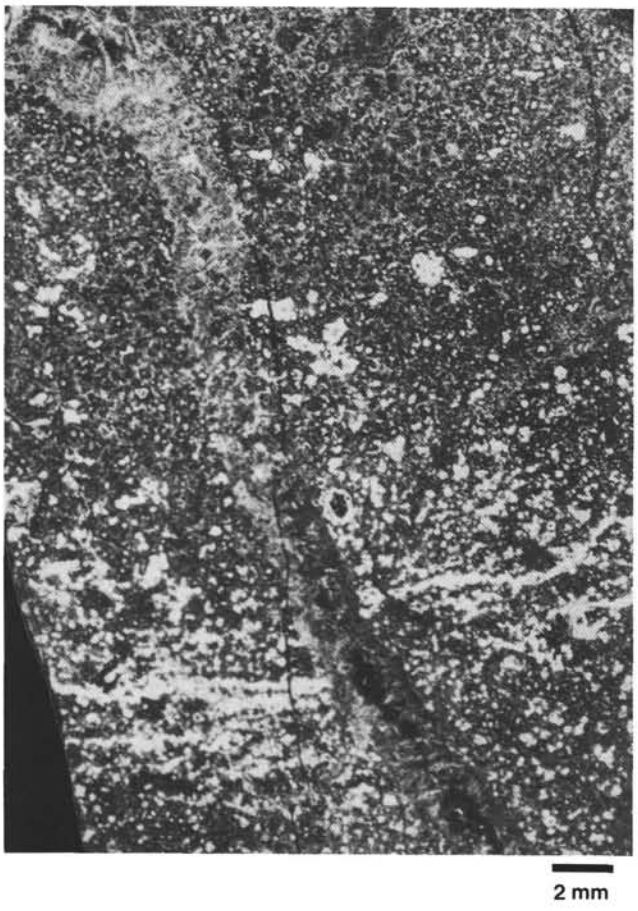

Figure 21. Negative print of a thin section showing fissure type F(d) in the dolomite unit. The mostly undulating fissure is filled with saddle dolomite has a compromise boundary near the center. Sample 103-639A-9R-1, 67–71 cm.

ties. F(b) may therefore be correlated with the F1 fissures of the limestones like F(a). Alternatively, these dark impurities outline serrated edges similar to the F2 fissures of the limestones, and F(b) may correlate with the variant F2a of the F2 set.

3. It is realistic to expect that the tectonics that produced fissure sets II and III in the dolomite also produced some fracturing in the limestones, at least the fissures of the F2 set. F2 fissures in the limestones and their associated diagenesis are most probably pre-Valanginian.

4. F3 fissures in the limestones (and possibly reactivation of F2 fissures) cannot be clearly correlated with a set of dolomite fissures nor can they be dated.

5. Some fractures similar to F1c and F2 fissure activation, but without intersections with other fissures, remain uncertain as to chronology and timing. They could be of Early Cretaceous age, but the main conclusions remain valid and are summarized as follows: (1) like the dolomite fissures, most of the fissures and associated diagenesis within the Hole 639D limestones is also pre-Valanginian, and (2) these fissures are probably related to the fracturing and faulting linked to the extensional tectonics prior to the tilting of the fault blocks, which places the timing of the beginning of rifting earlier than previously determined. Of course, fissures without intersections are in the dolomite as well as in the limestone section, and these could have occurred later (with special uncertainty for the timing of F3 fissures in the Hole 639D limestones) (Fig. 27). They could be the equivalent of a fissure set present in the Valanginian-Hauterivian deposits of Holes 638B and 638C (i.e., syn-rift; see Boillot, Winterer, et al., 1987).

Diagenesis of Limestones: Main Features and Chronology

The main evidence for limestone diagenesis in Hole 639D can be summarized as follows:

1. Bioturbation during sedimentation caused various textures of different mineralogical types and porosities and led to differential diagenesis on a small scale.
2. Slight synsedimentary lithification has unevenly affected the microfacies.
3. Dolomitization played an important role in several subunits, with one part of the dolomite remaining as relics whereas the remainder recrystallized into calcite.
4. Diagenesis was marked by some events producing distensive fissuring of the strata.

Under discussion is the original mineralogical nature of the micrites, the relation between the slight and uneven early lithification and the relatively early and partial dolomitization, and the chronology of the diagenesis and the dolomitization in the fractures.

Original Mineralogy of Micrites

Comparison of the diagenesis of the original aragonitic elements and of the micritic matrix immediately in contact with them leads to the conclusion that the original mud was not aragonitic like equivalent Recent sediments (Loreau, 1982). For instance, the contact between the coral skeleton (classically recrystallized into a sparitic mosaic) and the external micrite or the micrite filling the coralites is clear (Fig. 3), preserving the delicate morphology of the septae. This means that the micritic mold of the coral was mineralogically more stable than the skeleton, which dissolved or recrystallized; therefore, the mud was most probably calcite. Such micrite can be considered as a good sample of marine mud least modified after minor diagenesis. The $\delta^{18}O$ value of about $-1.50‰$ is in good agreement with the usual values given for precipitate in normal sea water between 20° and 25°C (Veizer, 1983).

Of course, all of the matrices could not have been exclusively calcitic. For instance, a micropackstone matrix rich in finely fragmented aragonitic allochems and replaced by microspar suggests that the muddy fraction also contained aragonite. Furthermore, this type of matrix was more commonly effected by partial dolomitization.

Dolomitization

Early dolomitization irregularly effected the micrite within the micropackstone matrix and also partly effected the micrite rich in very small aragonitic fragments. Almost all of the fissure cements are dolomite. Some aragonitic bioclasts, especially the small ones, and a large part of the fissure walls were dolomitized.

Oncoids, pellets, calcitic bioclasts, and tuberoids and most of the large aragonitic bioclasts (corals and pelecypods) and siliceous sponge spicules associated with the micrite were not dolomitized. Early dolomitization does not appear to have effected the slightly argillaceous homogeneous muds and whatever had been lithified in the environment of deposition. The dolomitization as a whole is most important in the upper unit of limestone that is nearest to the overlying dolomite formation. But at the same time, dolomitization is associated with a maximum of fracturing, which probably signifies a fault. It is clear that the more porous areas of the matrix and the successive fissures re-

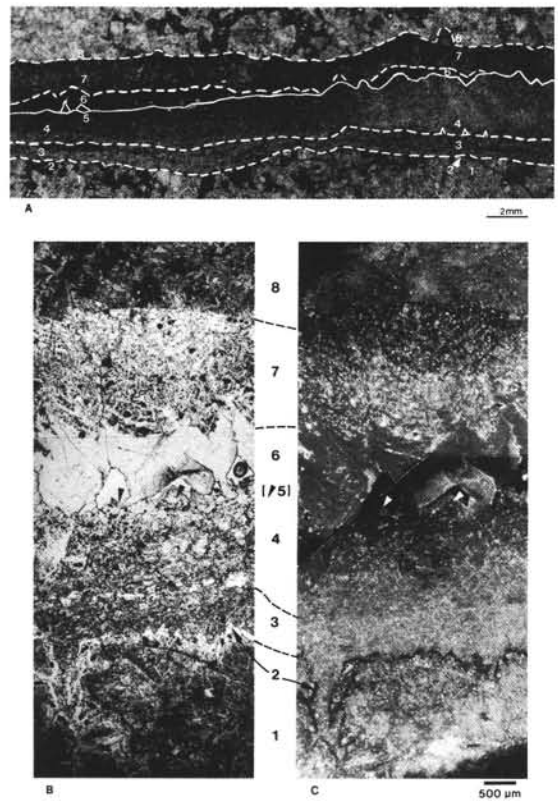

Figure 22. Fissure type F(e) in the dolomite unit. Sample 103-639A-10R-1, 15–18 cm. **A.** Negative print of the thin section showing a type F(e) fissure with an asymmetric polyphased filling. 1 = host rock; 2 = irregular, eroded and furrowed fissure floor covered by a clear baroque fringe that is very dark under cathodoluminescence; 3 = recrystallized silt; 4 = coarser recrystallized silt (under cathodoluminescence, the clear orange underlies the bedding, whereas the much larger saddle crystals that grew in alignment toward the top of the small beds show dark zones of crystalline growth, suggesting that they grew partly at the expense of the smaller surrounding crystals); 5 = transparent saddle crystals, which are redder and darker under cathodoluminescence, grew upward, partly at the expense of the underlying sediment filling part of the void; 6 = transparent saddle dolomite corresponding to the distal part of the crystals growing from the roof to the internal sediment; 7 = basal part of downward growing saddle crystals shows a slightly dirty and cleaved appearance (texture 2′); 8 = host rock with microfissured, cleaved texture of type 1′. **B.** Natural light; **C.** Detail of fissure shown in Figure 22A. Numbers as in Figure 22A. Cathodoluminescence.

newing the porosity have preferentially drained dolomitizing waters.

Comparative Chronology of Diagenetic Phases and Tectonic Events Recorded in the Limestones

The diagenetic diagrams in Figure 28 present a complete sequence of events for the development of the heterogeneous packstone units at the base of the series (Fig. 28B) and for the upper wackestone-floatstone unit that contains small corals and sponges (Fig. 28A). Fracturing phases F1, F2, F3, and F4 and stylolites schematically represent porosity variations and frame the relative chronology of the diagenetic stages:

1. Synsedimentary lithification of very low intensity
2. Early burial lithification of the rock, slight and heterogeneous
3. Recrystallization of selected aragonitic bioclasts + rare drusic cements + first differential dolomitization
4. F1 fracturing + differential dolomitization and fissure infilling
5. F2 fracturing + dolomitization (overgrowth of baroque dolomite, recrystallization of dolomite into saddle dolomite)
6. Reactivation of F2 fissures + same phenomena as preceding stage + partial dedolomitization
7. F3 fracturing + second phase of dolomitization, including the development only in the upper units (probably as a result of local faulting) of large, transparent saddle dolomite. This saddle dolomite cements calcite fragments that had partially replaced the preceding dolomite. A reactivation of F2 fissures in the lower units could be synchronous to F3
8. Stylolites and other compaction effects + precipitation of dolomite in the stylolites
9. F4 + calcitic cement
10. Poorly dated alteration of dolomite and dedolomitization.

In the fissures filled with dolomite or calcite after dolomite, aragonite or calcite cement does not seem to have served as a precursor to dolomite. In effect, fissure types F2a, F2b, and F2d show an evolutionary growth of dolomite from the initial precipitation in the center of the narrow capillary fissures. The growth outward from the center of baroque dolomite visible under cathodoluminescence predates the reactivation of the F2 fissures. The morphology of the fissure edges suggests a syntaxial growth of baroque dolomite, to the detriment of the wall.

Some dedolomitization (calcite replacing dolomite), seems to be contemporaneous with the reactivation of the F2 fissures. Other dedolomitization events occurred later and are poorly dated.

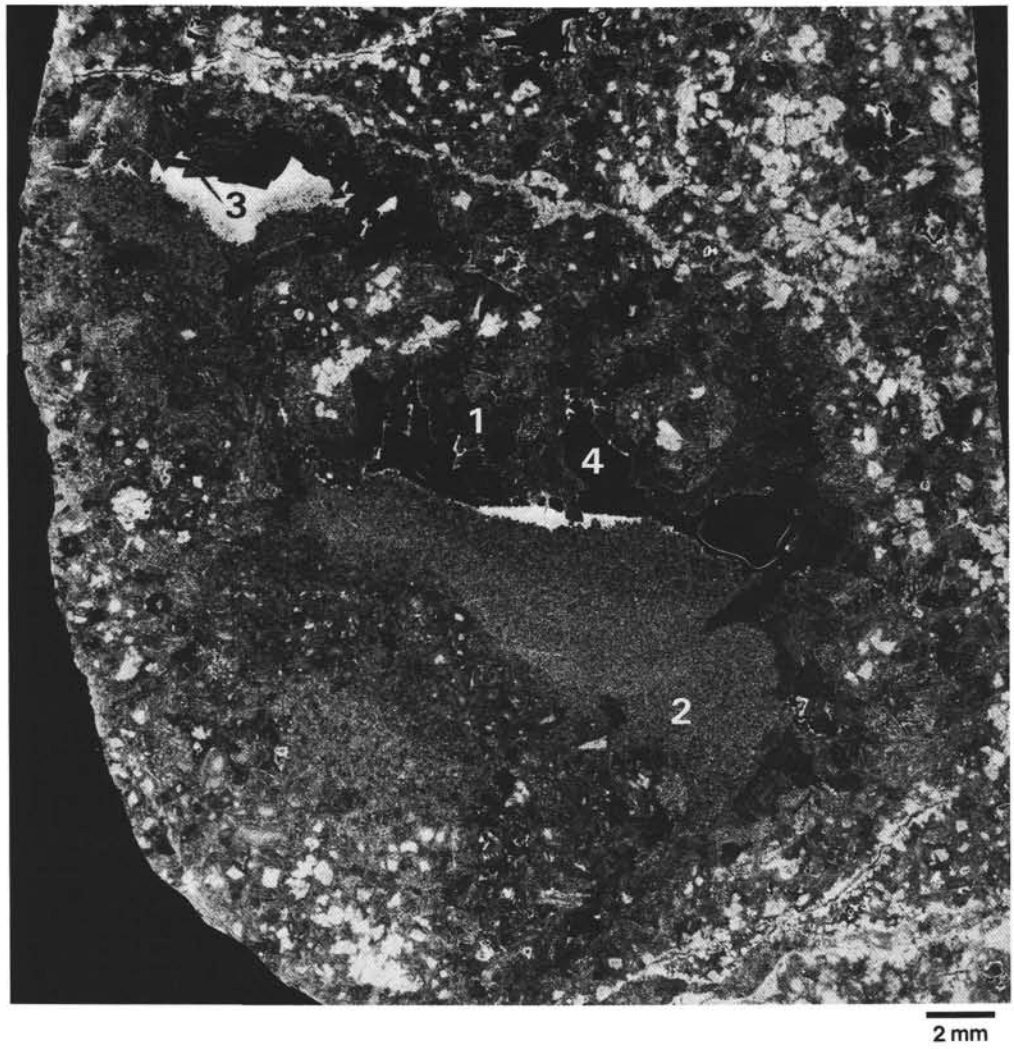

Figure 23. Negative print of a thin section showing coarse crystalline dolomite with fissures and a network of centimeter-size cavities filled with internal sediments. 1 = saddle dolomite fringing cavities, with the largest (several millimeters) crystals hanging from the roof; 2 = recrystallized "gray" internal silt; 3 = fine brown yellow silty mud (white on negative); 4 = residual pore. Sample 103-639A-10R-1, 35–38 cm.

Environments of Diagenesis

Indisputable indicators of the environments of diagenesis are rare; the petrographic characters and isotopic data can be interpreted in two ways.

Sparitization of Bioclasts and Precipitation of Drusy Calcite in Limestones: FreshWater Influence vs. Marine and/or Early Burial Diagenesis

Significant evidence of a freshwater influence is the sparitization of bioclasts and the precipitation of drusy calcite in the limestones. Early calcite that formed as cement or replaced aragonite bioclasts clearly resembles the drusy calcite or replacement mosaics that originate through freshwater diagenesis (Bathurst, 1975, 1983; Longman, 1980). Such an early—but not synsedimentary—diagenesis milieu supposes emersion of the top of the series (which was not recovered). However, other arguments have to be considered.

First, the direct precipitation of calcite cement or recrystallization of aragonite into calcite occurs in several environments. Submarine and late burial diagenesis mechanisms have been demonstrated recently (Freeman-Lynde et al., 1986; Saller, 1986), and the characteristics of the cements related to these environments are medium to coarse, crystalline, equant-spar calcite cements and radiaxial calcite, respectively. But these criteria are rarely observed in the Site 639 limestones (see the preceding discussion on the comparison of bioclast diagenesis with cements); thus, the freshwater origin of calcite remains valid. Second, the early calcite could have been directly precipitated in sea water (Sandberg, 1975, 1983; Loreau, 1978, 1979, 1982; Wilkinson, 1979; Wilkinson et al., 1985; Mackenzie and Pigott, 1981). It can be suggested that the micrite in the limestone matrices was originally calcite. These contentions that a freshwater influence is not necessary remain under debate; however, the arguments do not sufficiently constrain the viability of the two interpretations.

Dolomitization: Freshwater Influence and Mixing Zone Model vs. Hydrothermal Origin

Early dolomitization within the limestones was either simultaneous or closely linked to the development of sparite. This relationship suggests, for the origin of dolomite, one of the two previously discussed hypotheses, that of the influence of brackish ground water in the mixing zone (Hanshaw et al., 1971; Badiozamani, 1973; Folk and Land, 1975; Choquette and Steinen, 1980; Sibley, 1980).

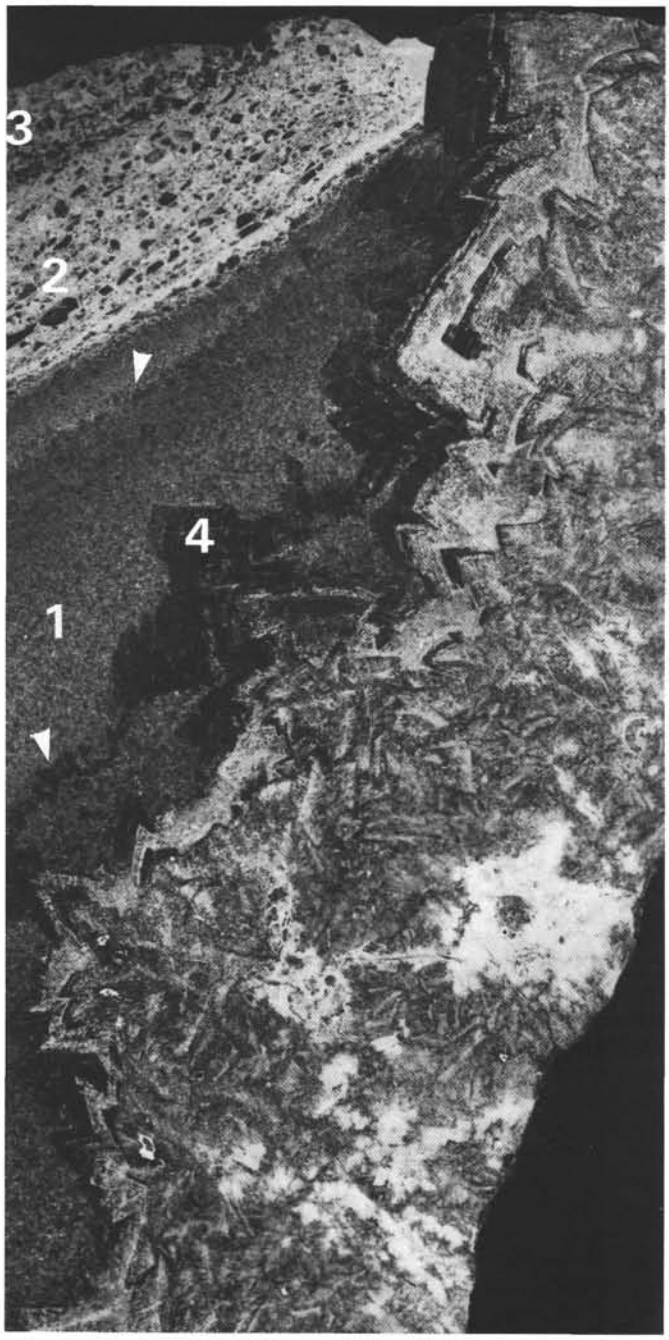

Figure 24. Negative print of a thin section showing a part of a cavity several centimeters in diameter, fringed by large, zoned saddle dolomite and filled by polyphased internal sedimentation. 1 = heterometric recrystallized translucent silt, with larger crystals growing at the tops of some beds (arrows); 2 = (yellow) mostly bedded sediment composed of a fine matrix and clear crystal debris (black on negative); 3 = second (yellow) heterometric grain-supported, nonbedded sediment; 4 = very clear saddle dolomite (black on negative) growing at the expense of internal sediments. Sample 103-639A-10R-2, 18–21 cm.

Subsequent dolomitization of the upper Tithonian section affected limestones that were already lithified and partially dolomitized; the earliest fissuring, type F(a), preceded the first baroque dolomite, which is consistent with the evidence of early diagenesis and dolomitization within the underlying limestones.

We will now discuss this second, pervasive, polyphased dolomitization, taking isotopic data and the significance of saddle dolomite in account.

The two main sets of $\delta^{13}C$ and $\delta^{18}O$ values for dolomite correspond to distinct dolomitization phases established by petrographic criteria. Interestingly, ^{18}O enrichment occurs with the latest (but pre-Valanginian) dolomitization phase indicated by diagenetic microstratigraphy. Confirmation for this coincident timing comes from a sample of host rock from the top of the Tithonian dolomites. Although only one value is available (point 9; Fig. 25), this value fits a latest pre-Valanginian dolomitization.

The $\delta^{13}C$ values do not indicate a significant organic matter influence during dolomitization. The negative signature of the $\delta^{18}O$ values can be explained in two ways, (1) as a temperature effect resulting from either deep-burial diagenesis or an initial hydrothermal influence or (2) from the influence of fresh water (Land, 1980; Veizer, 1983).

The freshwater influence explanation that recalls the mixing zone model previously discussed for the early dolomitization cannot be discarded because emersion is suggested by the petrographic characters (see the following). However, this currently favored model of dolomitization has been seriously questioned (see Hardie, 1987), and the pervasive saddle dolomite found in our examinations is a highly constraining feature.

Saddle dolomite has been interpreted as a diagenetic product formed in hypersaline carbonate deposits (Folk, 1977; Friedman, 1980). But burial dolomitization is also well known for producing this texture (Mattes and Mountjoy, 1980). Furthermore, field and petrographic observations, considerations of crystal growth theory (Radke and Mathis, 1980; Gregg and Sibley, 1984), and experiments (Gregg and Sibley, 1984) strongly link saddle dolomite to elevated temperatures. Radke and Mathis (1980) found that saddle dolomite is a potential geothermometer, because it is indicative of 60°–150°C temperatures. Gregg and Sibley (1984) reported xenotopic saddle dolomite replacing limestone during the migration of hot (>50°C) fluids along fracture systems in the Ordovician Trenton Limestone of Michigan. In turn, we will now discuss development of saddle dolomite in the Site 639 Tithonian carbonates as an effect of hot fluids.

Stratigraphic observations suggest the dismissal of deep-burial diagenesis because it is difficult to envision a sufficient depth of burial for the Tithonian carbonates before the Valanginian. In addition, the isotopic data revealed the $\delta^{18}O$ values of the coburial limestones to be much less negative than would be expected in comparison to dolomite $\delta^{18}O$ values for deep burial. Consequently, the circulation of hydrothermal fluids, mainly through successive fracture sets and a significantly renewed porosity, could explain the dolomitization of upper unit and fissure filling within the limestones underneath.

Evidence of Emersion Suggested by Vadose Silt

The detrital dolomite filling various fractures and vugs could be the most significant indicators of the diagenetic milieu. One of the internal sediments is very similar to vadose silt described and interpreted by Dunham (1969). Whereas they have a similar detrital nature (Cros, 1977), this silt is not a synsedimentary internal sediment. It originated as a crystal silt resulting from the alteration and destruction of both the previous saddle dolomite and the host rock, as shown by the identical $^{m}Mg/^{m}Ca$ ratios and the same $\delta^{13}C$ and $\delta^{18}O$ values. Its origin was not strictly local because the vug was already cemented and fringed by saddle dolomite. Silt and various detrital resedimented dolomite must have come from the upper part or from the surface of the sedimentary sequence. Alteration, erosion, and transport suppose a vadose origin of the crystal silt and thus, an emersion. The last yellow internal sediment is characterized by another set of $\delta^{13}C$

Table 4. Stable carbon and oxygen isotope values of separated dolomite phases from ODP Site 639 (N = sample number in Fig. 25).

Sample	N	Description	$\delta^{13}C$	$\delta^{18}O$
Hole 639A:				
8R, CC (13–16 cm)	9	Slightly yellow fine crystalline dolomite	+2.47	−2.76
10R-1, 15–17 cm	14	Clear saddle dolomite	+1.68	−8.99
	15	"Gray" translucent silt infilling	+1.65	−9.48
	16	Host rock (textures 1a, b, and 2a)	+1.68	−8.28
10R-1, 35–38 cm	1	"Gray" translucent silt infilling	+1.58	−7.14
	2	Clear saddle dolomite	+1.75	−6.94
	3	Host rock (textures 1a, b, and 2a)	+1.64	−10.30
10R-1, 40–44 cm	10	Yellow laminated sediment	+3.11	+2.52
	11	Host rock (textures 1a, b, and 2a)	+1.55	−10.25
10R-2, 18–21 cm	4	Yellow internal sediment	+2.46	−3.96
	7	Clear saddle dolomite	+1.68	−10.10
	8	Host rock (textures 1a, b, and 2a)	+1.92	−9.57
10R-2, 45–47 cm	17	Yellow internal sediment	+3.47	+3.08
Hole 639B:				
4R-1, 7–9 cm	12	Yellow internal microbreccia	+2.25	−4.16
	13	Host rock (textures 1a, and 2a)	+1.63	−9.58

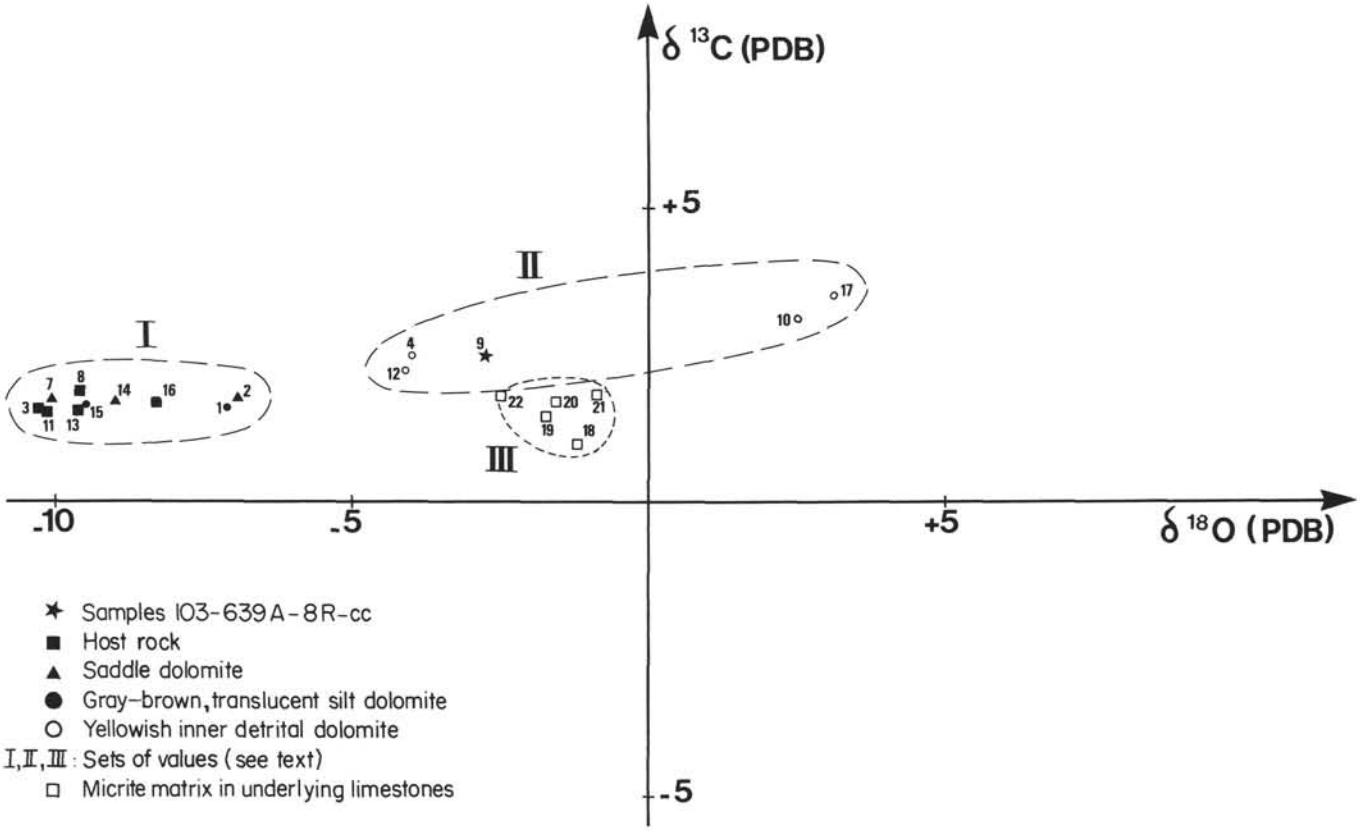

Figure 25. Carbon and oxygen composition of separated dolomites and micrite matrices.

and $\delta^{18}O$ values that are either positive or tend toward positive. This might suggest a different diagenetic environment for the top of the section, at near-hypersaline conditions.

The dolomitization is clearly related to fracturing. The geometry of the fissures suggests that the fracturing occurred under extension. The top of the dolomitized Tithonian carbonates experienced an erosional phase. The evidence of moved blocks and resedimented detrital dolomite agrees with the seismic profile interpretation suggesting erosion (Mauffret and Montadert, 1987). The vadose silt and various equivalent internal sediments strongly suggest emersion of the section. These events correspond to the eustatic sea-level lowering at the Berriasian/Valanginian boundary (Vail et al., 1977). They also correspond to extensional tectonics, which probably occurred at the beginning of the rifting of the Iberian margin, prior to block tilting.

CONCLUSIONS

1. Induration of the Hole 639D limestone began within an infratidal synsedimentary environment and included an early

Table 5. Stable carbon and oxygen isotope values of separated micrite matrices from Hole 639D limestones (N = sample number in Fig. 25).

Sample	N	Description	$\delta^{13}C$	$\delta^{18}O$
5R-1, 25–29 cm	20	Micrite matrix within floatstone	+1.77	−1.60
5R-2, 18–20 cm	19	Homogeneous micrite (mudstone)	+1.46	−1.81
5R-2, 94–97 cm	18	Micrite matrix within wackestone	+0.99	−1.24
6R-1, 141–143 cm	21	Micropackstone matrix rich in fine bioclasts	+1.81	−0.98
10R-1, 38–41 cm	22	Micrite matrix poor in fine bioclasts	+1.97	−2.69

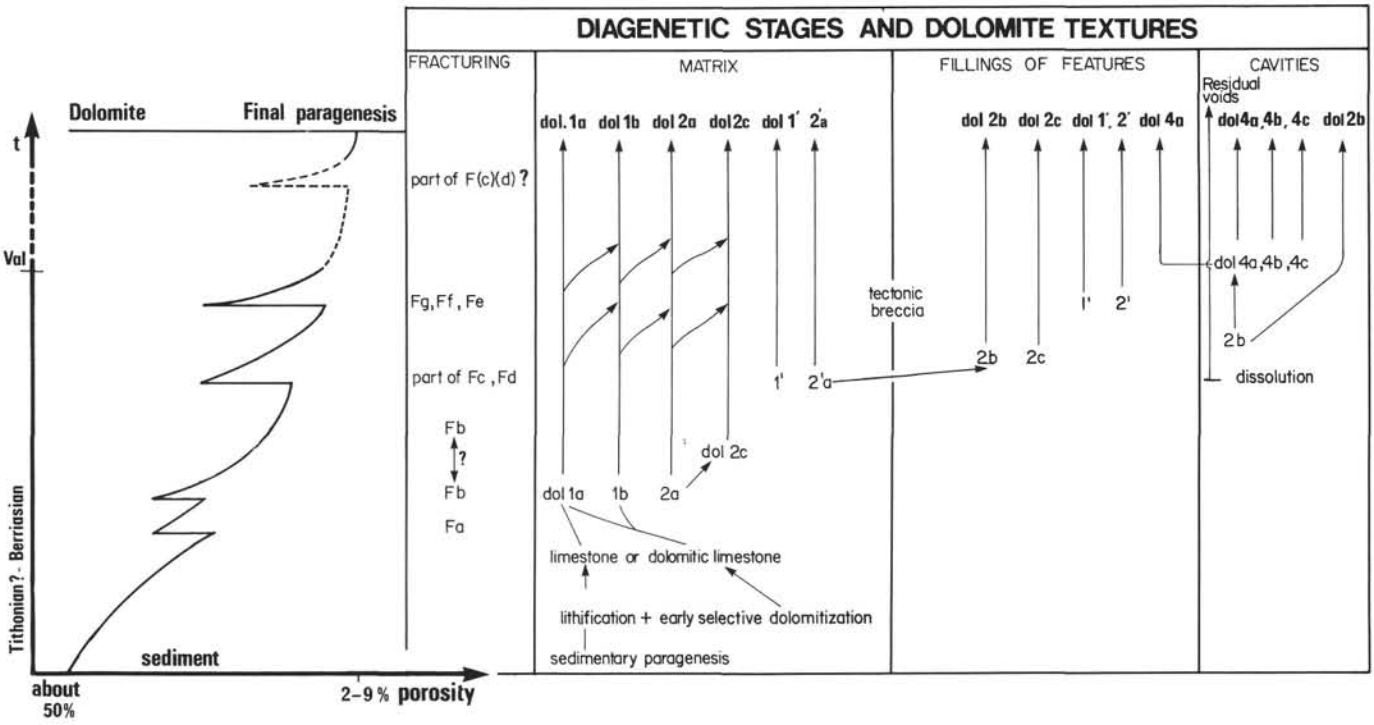

Figure 26. Summary of diagenetic structural and mineralogical transformations in Hole 639A dolomite. The Berriasian/Valanginian boundary is positioned following the sealing by Valanginian marls or fissures filled with resedimented detrital dolomite. The Tithonian/Berriasian boundary could not be identified by fissure chronology. The initial porosity of the Tithonian sediment is estimated, whereas the porosity of the recovered dolomites was measured aboard ship (Boillot, Winterer, et al., 1987, p. 435). See Tables 2 and 3 for dolomite and fissure types, respectively.

partial dolomitization. The dolomite was later recrystallized into calcite.

2. Dolomitization of the upper unit affected limestone that was already lithified and partially dolomitized. This dolomitization was polyphased, causing a progressive increase in xenotopic saddle texture and an accompanying decrease of magnesium content. These phases are clearly linked to fracturing.

3. The last-formed fissures and voids in the dolomite unit were filled by crystal silt and other detrital dolomite. They were sealed with deposits of Valanginian age. Therefore, most of dolomitization can be dated as pre-Valanginian. The fissures are used as chronologic markers to tentatively correlate the dolomite and limestone diagenesis and thereby determine the age of the limestone diagenesis.

4. The petrographic characteristics of the limestone and dolomite and the negative $\delta^{18}O$ values of the dolomite may be interpreted in two ways to explain the dolomitization. Early sparite replacing aragonitic bioclasts, early drusy sparite cement, and rather strongly negative $\delta^{18}O$ values of dolomite all suggest a freshwater influence and a mixing zone model. On the other hand, the significance of the saddle dolomite and the same negative $\delta^{18}O$ values suggest a temperature effect. We have effectively dismissed deep burial; therefore, hydrothermal dolomite is the most probable explanation.

5. Crystal silts, internal dolomite microbreccia, and various laminated detrital dolomites within fissures and vugs are indicators of alteration, erosion, and transport in vadose conditions, even if the internal sediments were deposited in the phreatic zone. Whatever the dolomitization processes were, these types of deposits suggest emersion.

6. The strongly differing—and even positive—$\delta^{18}O$ values of the last-formed internal yellow sediment suggest that the top of the sequence could have been dolomitized under saline to hypersaline conditions.

7. Fracture-renewed porosity that drained dolomitizing fluids was linked to extensional tectonics that occurred prior to block tilting; this is an earlier timing than expected for the beginning of the rifting of the Iberian margin.

8. Dolomitization, emersion, and erosion correspond to the eustatic lowering of sea level at the Berriasian/Valanginian boundary. Diagenesis, rather than sedimentation, principally marks this event and records the regional tectonic history.

ACKNOWLEDGMENTS

J.-P. Loreau wishes to thank the Ocean Drilling Program for inviting him to participate on Leg 103 aboard *JOIDES Resolution*. This work was supported by French CNRS grants "ATP Géologie Géophysique des Océans" no. 981051 and "ASP ODP France". The authors are

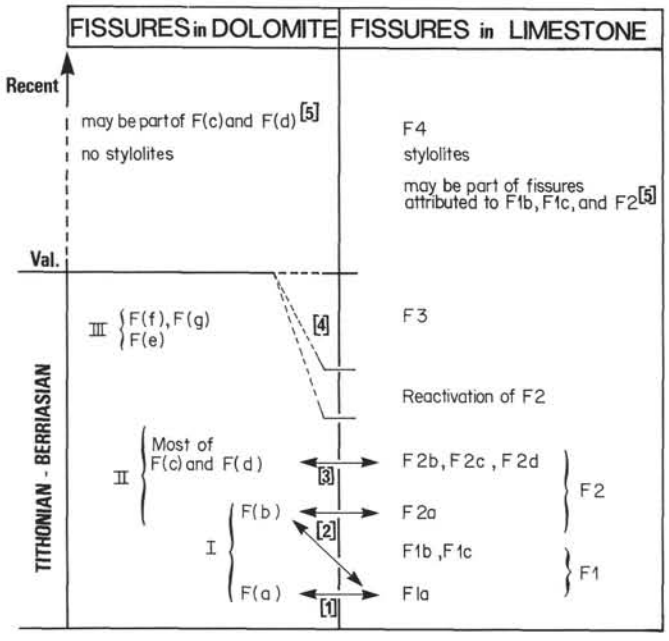

Figure 27. Tentative correlation between fissures in Hole 639A dolomite and in Hole 639D limestone. Numbers 1–5 are explained in the text.

grateful for stimulating discussions with D. Aissaoui, G. Boillot, M. C. Comas, J. Malod, M. Moullade, and J. Girardeau. They express special thanks to J. H. Schroeder and A. W. Meyer for useful comments on the manuscript. They are indebted to S. Clauser for isotopic analysis and thank M. Destarac, O. Faille, L. Ganon, J. Bernard, G. Tortel, S. Loreau, N. Loreau, E. Cambreleng, O. Sancini, M. Barandon, and J. P. Gely for their assistance and help.

REFERENCES

Amieux, P., 1982. La cathodoluminescence: méthode d'étude sédimentologique des carbonates. *Bull. Cent. Rech. Explor. Prod. Elf Aquitaine*, 6:437–483.

Badiozamani, K., 1973. The Dorag dolomitization model: application to the middle Ordovician of Wisconsin. *J. Sediment. Petrol.*, 43: 965–984.

Bathurst, R.G.C., 1966. Boring algae, micrite envelopes and lithification of molluscan biosparites. *Liverpool Manchester Geol. J.*, 5:25–32.

_____, 1975. *Carbonate Sediments and their Diagenesis* (2nd ed.): Amsterdam (Elsevier).

_____, 1983. Neomorphic spar versus cement in some Jurassic grainstones: significance for evaluation of porosity evolution and compaction. *J. Geol. Soc. (London)*, 140:229–237.

Boillot, G., Winterer, E. L., et al., 1987. *Proc. ODP, Init. Repts.*, 103: College Station, TX (Ocear Drilling Program).

Choquette, P. W., and Steinen, R. P., 1980. Mississippian non-supratidal dolomite, Ste. Genevieve limestone, Illinois Basin: evidence for mixed-water dolomitization. *In* Zenger, D. H., Dunham, J. B., and Ethington, R. L. (Eds.), *Concepts and Models of Dolomitization*: Spec. Publ. Soc. Econ. Paleontol. Mineral., 28:163–196.

Cros, P. G., 1977. Données nouvelles sur la dolomitisation des carbonates triasiques des Dolomites italiennes. *Sci. Terre.*, 21:307–355.

Dunham, R. J., 1969. Early vadose silt in Townsend mound (reef), New Mexico. *In* Friedman, G. M. (Ed.), *Depositional Environments in Carbonate Rocks: A Symposium*: Spec. Publ. Soc. Econ. Paleontol. Mineral., 14:132–181.

Folk, R. L., 1977. Peculiar forms of diagenetic carbonate from hypersaline and cave deposits, ancient to Recent. *West Tex. Geol. Soc. Newsl.*, Nov.: 11.

Folk, R. L., and Land, L. S., 1975. Mg/Ca ratio and salinity: two controls over crystallization of dolomite. *AAPG Bull.*, 59:60–68.

Freeman-Lynde, R. P., Fulker Whitley, K., and Lohmann, K. C., 1986. Deep-marine origin of equant spar cements in Bahama escarpment limestone. *J. Sediment. Petrol.*, 56:799–811.

Friedman, G. M., 1965. Terminology of crystallization textures and fabrics in sedimentary rocks. *J. Sediment. Petrol.*, 35:643–655.

_____, 1980. Dolomite is an evaporite mineral: evidence from the rock record and from sea-marginal ponds of the Red Sea. *In* Zenger, D. H., Dunham, J. B., and Ethington, R. L. (Eds.), *Concepts and Models of Dolomitization*: Spec. Publ. Soc. Econ. Paleontol. Mineral., 28:69–80.

Fritz, G. K., 1958. Schwammstotzen, tuberolithe und schuttbrecien im weissen Jura der Schwäbischen Alb. *Arb. Inst. Geol. Palaeontol. Univ. Stuttgart*, 13:1–119.

Fürsich, F. T., 1979. Genesis, environment, and ecology of Jurassic hardgrounds. *Neues Jahrb. Mineral. Geol. Palaeonol., Abh., Abt. B*, 158:1–63.

Gaillard, C., 1982. Les biohermes à spongiaires et leur environnement dans l'Oxfordien du Jura meridional. *Doc. Lab. Geol. Fac. Sci. Lyon*, 90:1–515.

Gregg, J. M., and Sibley, D. F., 1984. Epigenetic dolomitization and the origin of xenotopic dolomite texture. *J. Sediment. Petrol.*, 54:908–931.

Hanshaw, B. B., Back, W., and Deike, R. G., 1971. A geochemical hypothesis for dolomitization by groundwater. *Econ. Geol.*, 66:710–724.

Hardie, L. A., 1987. Dolomitization: a critical view of some current views. *J. Sediment. Petrol.*, 57:166–183.

Juignet, P., and Kennedy, W. J., 1974. Structures sédimentaires et mode d'accumulation de la craie du Turonien supérieur et du Sénonien du Pays de Caux. *Bull. Bur. Rech. Geol. Min., Sec. 4 (Fr.)*, 2:19–47.

Land, L. S., 1980. The isotopic and trace element geochemistry of dolomite: the state of the art. *In* Zenger, D. H., Dunham, J. B., and Ethington, R. L. (Eds.), *Concepts and Models of Dolomitization*: Spec. Publ. Soc. Econ. Paleontol. Mineral., 28:87–110.

Longman, M. W., 1980. Carbonate diagenetic textures from near surface diagenetic environments. *AAPG Bull.*, 64:461–487.

Loreau, J. P., 1978. Initial calcitic mineralogy and diagenesis of marine Jurassic ooids and associated sediments. *Congr. Int. Assoc. Sedimentol. Abst., 10th (Jerusalem)*, 1:394–395.

_____, 1979. Nature calcitique initiale et diagenèse des oolithes jurassiques du Bassin de Paris. *In Symposium Sédimentation Jurassique W. Européen*: Spec. Publ. A.S.F., 1:417–429.

_____, 1982. Sédiments aragonitiques et leur genèse. *Mem. Mus. Nat. Hist. Nat. Ser. C (Paris)*, 47.

Mackenzie, F. T., and Pigott, J. D., 1981. Tectonic controls of Phanerozoic sedimentary rock cycling. *J. Geol. Soc. (London)*, 138:183–196.

Mattes, B. W., and Mountjoy, E. W., 1980. Burial dolomitization of the Upper Devonian Miette Buildup, Jasper National Park, Alberta. *In* Zenger, D. H., Dunham, J. B., and Ethington, R. L. (Eds.), *Concepts and Models of Dolomitization*: Spec. Publ. Soc. Econ. Paleontol. Mineral., 28:259–297.

Mauffret, A., and Montadert, L., 1987. Rift tectonics on the passive continental margin off Galicia (Spain). *Mar. Pet. Geol.*, 4:49–70.

Pierson, B. J., 1981. The control of cathodoluminescence in dolomite by iron and manganese. *Sedimentology*, 28:601–610.

Radke, B., and Mathis, R. L., 1980. On the formation and occurrence of saddle dolomite. *J. Sediment. Petrol.*, 50:1149–1168.

Saller, A. H., 1986. Radiaxial calcite in lower Miocene strata, subsurface - Eniwetok Atoll. *J. Sediment. Petrol.*, 56:743–762.

Sandberg, P. A., 1975. New interpretation of Great Salt Lake ooids and of ancient non-skeletal carbonate mineralogy. *Sedimentology*, 25: 673–702.

_____, 1983. An oscillating trend in Phanerozoic non-skeletal carbonate mineralogy. *Nature*, 305:19–22.

Sander, B., 1936. Beitrage zur kenntniss der anlagerungsgefuge (rhythmische kalke und dolomite aus der Trias). *Tschermaks Mineral. Petrogr. Mitt.*, 48:27–209.

Sibley, D. F., 1980. Climatic control of dolomitization, Serve Domi Formation (Pliocene), Bonaire, N.A. *In* Zenger, D. H., Dunham, J. B., and Ethington, R. L. (Eds.), *Concepts and Models of Dolomitization*: Spec. Publ. Soc. Econ. Paleontol. Mineral., 28:247–258.

Vail, P. R., Mitchum, J. R., and Thompson, S., 1977. Seismic stratigraphy and global changes of sea level from coastal onlap. *AAPG Bull.*, 26:63–97.

Veizer, J., 1983. Trace elements and isotopes in sedimentary carbonates. *Rev. Mineral.*, 11:265–299.

Wanless, H. R., 1981. Burial diagenesis in limestones. *In* Parker, A., and Sellwood, B. W. (Eds.), *Sediment Diagenesis*: Dordrecht (Reidel), 379–417.

Wilkinson, B. H., 1979. Biomineralization, paleoceanography, and the evolution of calcareous marine organisms. *Geology*, 7:524–527.

Wilkinson, B. H., Owen, R. M., and Carroll, A. R., 1985. Submarine hydrothermal weathering, global eustasy, and carbonate polymorphism in Phanerozoic oolites. *J. Sediment. Petrol.*, 55:171–183.

Date of initial receipt: 24 April 1987
Date of acceptance: 2 February 1988
Ms 103B-125

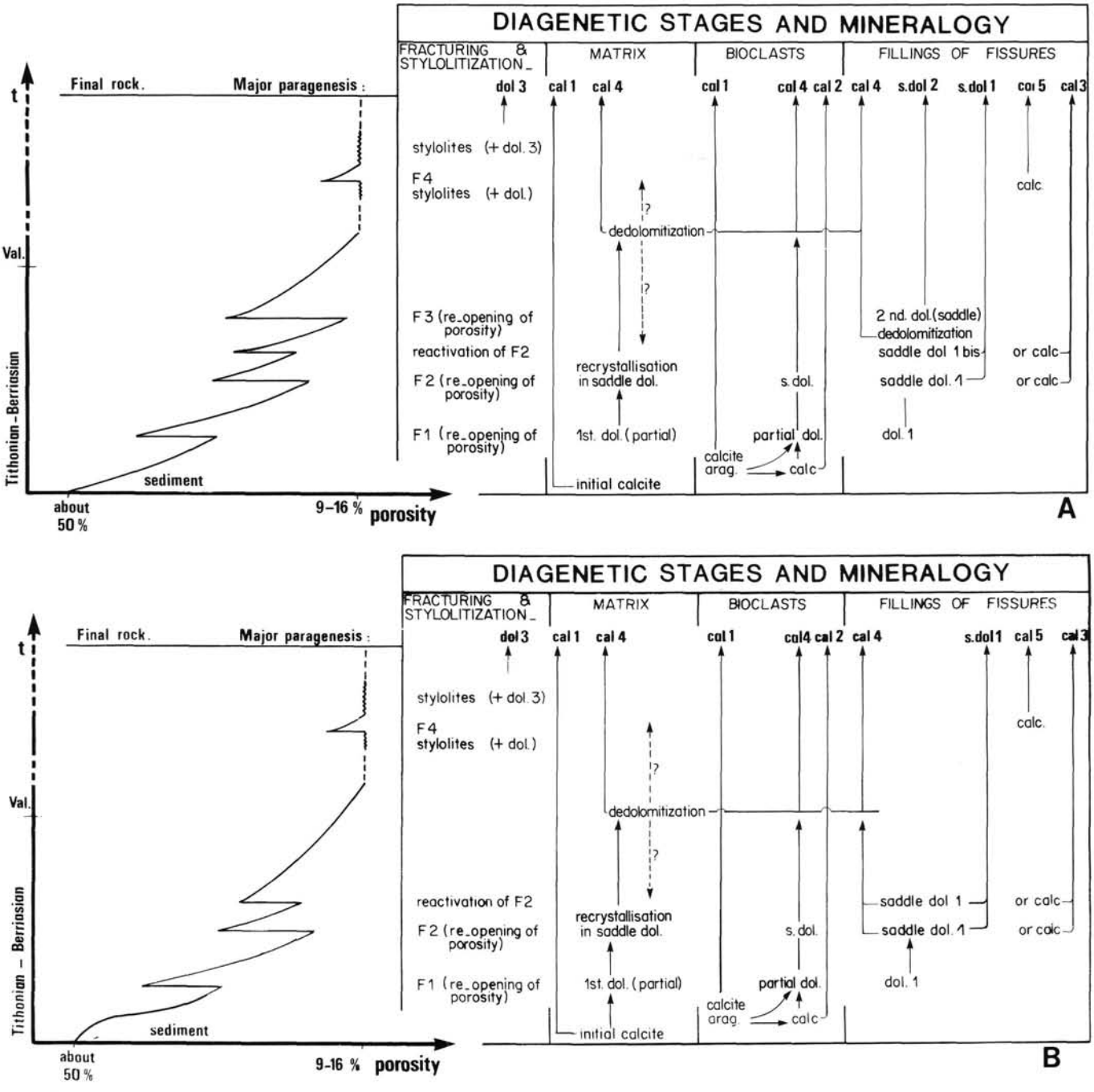

Figure 28. Summary of diagenetic structural and mineralogical transformations in Hole 639D limestones through time. Fissures (Table 2) occurring within the dolomite unit of Hole 639A can be dated as pre-Valanginian in age. Correlations with fissures occurring in the limestones of Hole 639D (cf. Fig. 27) suggest that these fissures are also pre-Valanginian. The Berriasian/Valanginian boundary has been positioned approximately after F3. The Tithonian/Berriasian boundary could not be identified by fissure chronology. The initial porosity of the Tithonian sediment is estimated, whereas the porosity of the recovered limestones was measured aboard ship (Boillot, Winterer, et al., 1987, p. 435). Paragenesis: cal 1 = initial calcite; cal 2 = calcite replacing aragonite and opal; cal 3 = calcite filling F2; cal 4 = calcite recrystallization of dolomite; cal 5 = late sparite filling fissures F4 and voids; dol 1 = dolomite of first dolomitization; s. dol 1 = saddle dolomite from recrystallization of dol 1; s. dol 2 = saddle dolomite of second dolomitization; dol 3 = dolomite in stylolites. **A.** Diagenetic diagram of upper limestone unit (wackestones and floatstones with small corals and sponges) in Cores 103-639D-4R and 103-639D-5R. **B.** Diagenetic diagram of lower limestone units (heterometric packstones with oncoids) in Cores 103-639D-11R through 103-639D-13R.

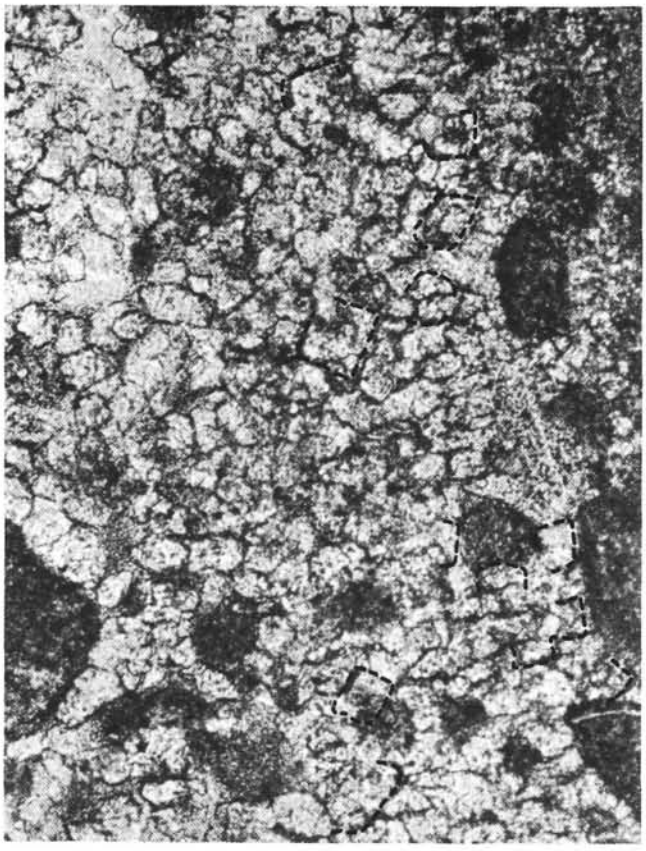

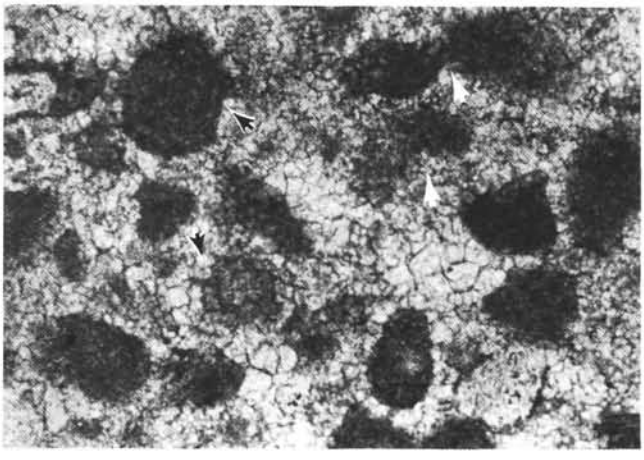

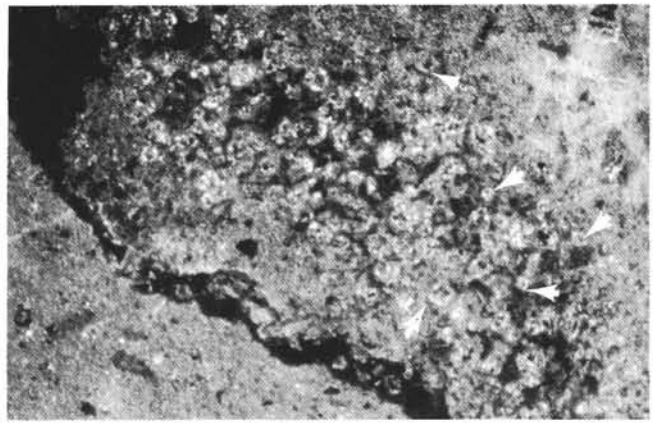

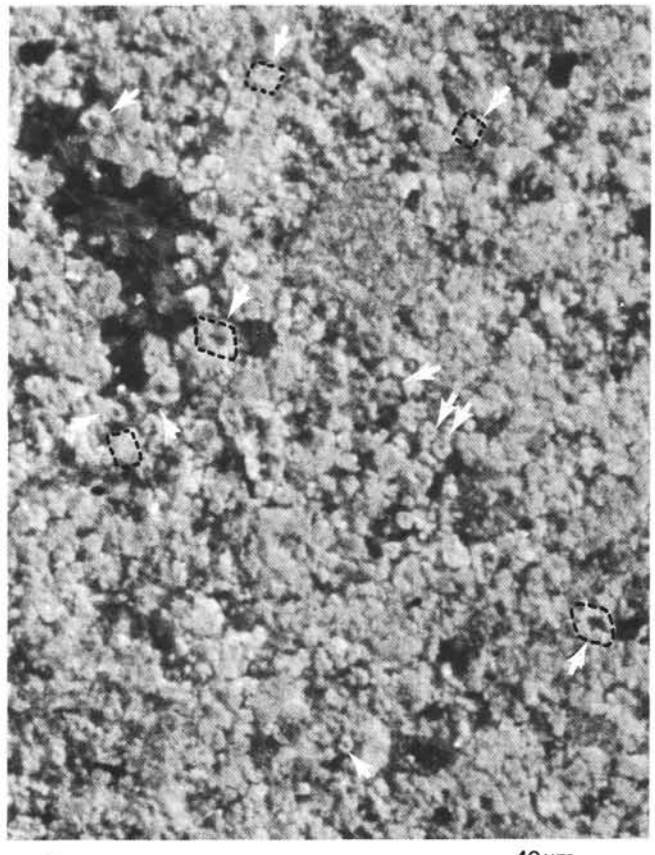

Plate 1. Evidence for dolomitization and dedolomitization of matrix. **1.** Clotted structure showing floating relics (micrite patches and pellets) entirely surrounded by neomorphic microspar. The xenomorphic fabric with mono- and polycrystalline pseudomorphs of rhombs suggests dolomitization followed by replacement of dolomite by calcite microspar. Sample 103-639D-13R-1, 77–80 cm; natural light. **2.** Polygonal aspect of pellets within dedolomitized matrix. This morphology (arrows) corresponds to the ends of original dolomitic rhombs within the matrix along the border of the pellets. Sample 103-639D-11R-2, 45–48 cm; natural light. **3.** Dedolomitized matrix with zoned rhombohedral phantoms (arrows). Sample 103-639D-10R-1, 17–21 cm; under cathodoluminescence. **4.** Fabric of dedolomitized matrix showing phantoms of the former microrhombs (arrows). Sample 103-639D-5R-1, 55–57 cm; under cathodoluminescence.

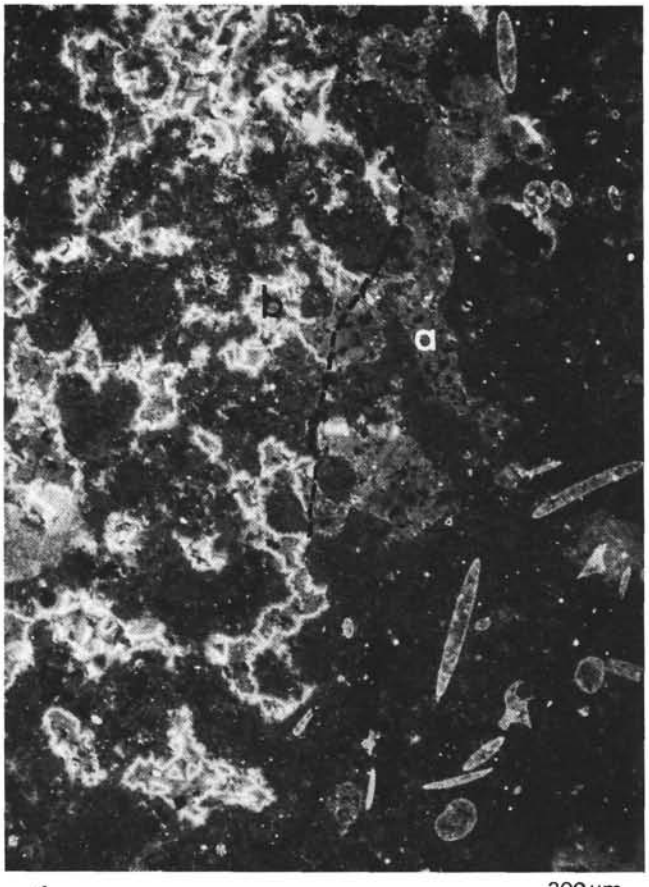

1 200 µm

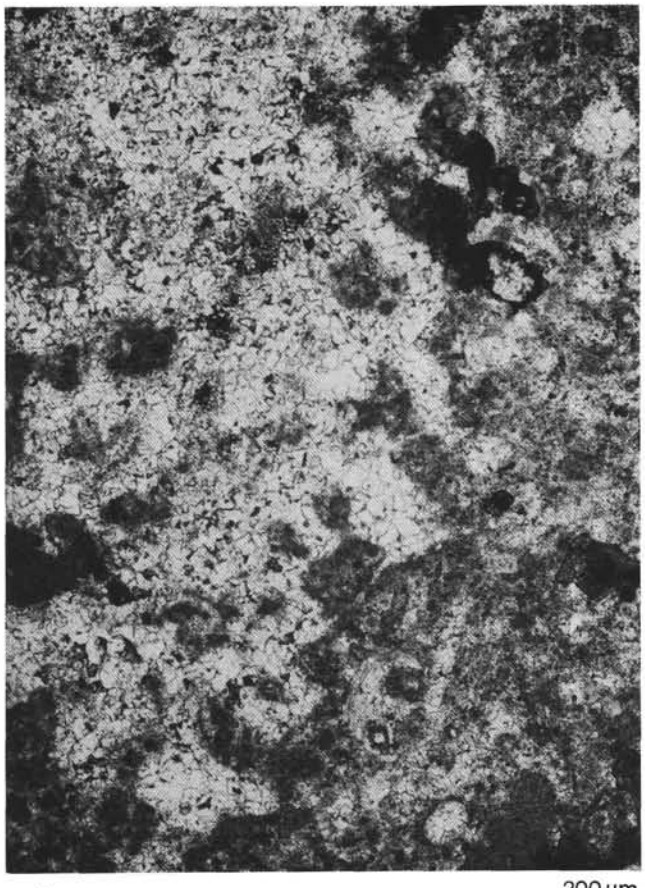

2 200 µm

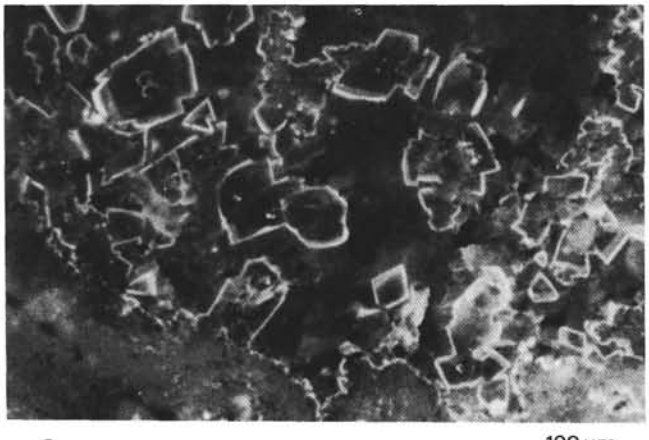

3 100 µm

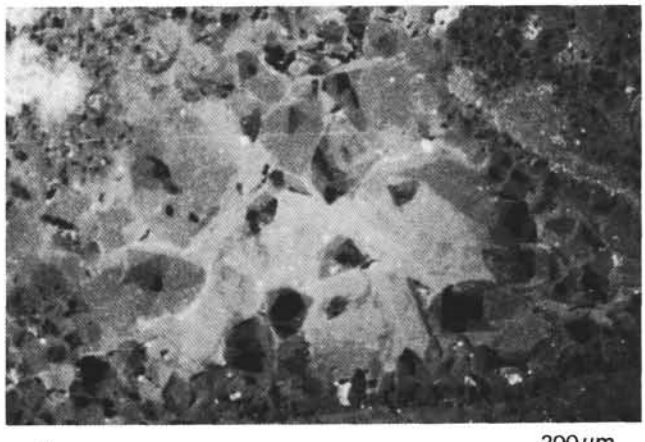

4 200 µm

Plate 2. Calcite replacing aragonite and opal, calcite cement, and calcite from dedolomitization. **1.** Cathodoluminescence. **2.** Natural light. Differential diagenesis of a coral skeleton within a micritic matrix with a clotted structure and rich in sponge spicules. Figure 1 shows two fields in the pseudosparitized coral: a = mosaic aspect of calcite after aragonite; b = mosaic aspect of the same calcite with an additional bright (yellow) serrated rim (see Fig. 3). Calcite replacing the sponge spicule opal is also outlined by a bright (yellow) rim (see the text). Sample 103-639D-4R-1, 26–28 cm. **3.** Detail of a coral skeleton showing two calcite phases. The first calcite has a dull cathodoluminescence with dark patches giving a mosaic appearance. The cathodoluminescence reveals bright phantoms of faintly zoned crystals with curved faces. These phantoms are dolomite crystals recrystallized into a second calcite. Sample 103-639D-5R-3, 39–41 cm; under cathodoluminescence. **4.** Void filled with an early drusy calcite without dolomitization and dedolomitization. Sample 103-639D-5R-2, 95–97 cm; under cathodoluminescence.

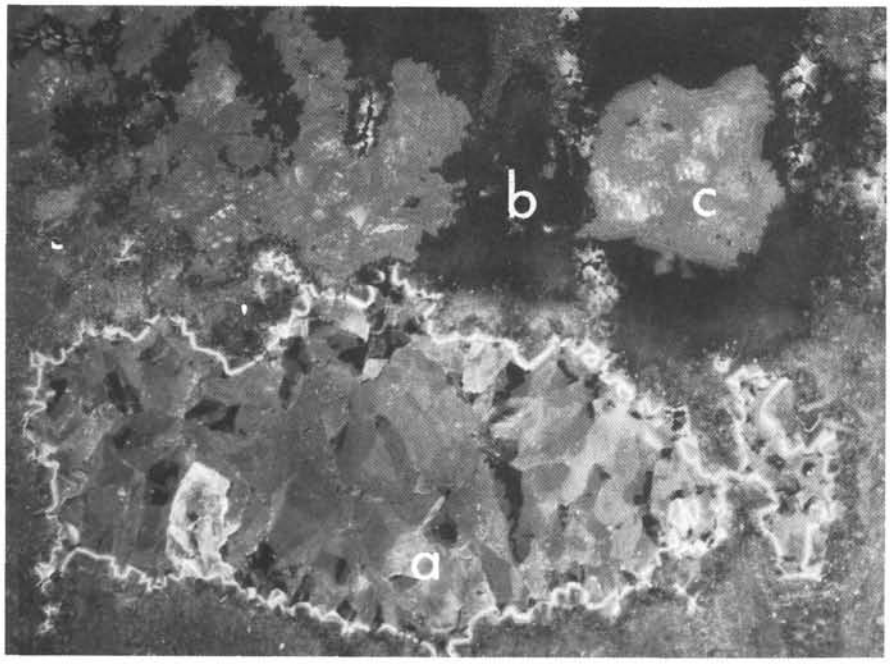

1

200 µm

3

250 µm

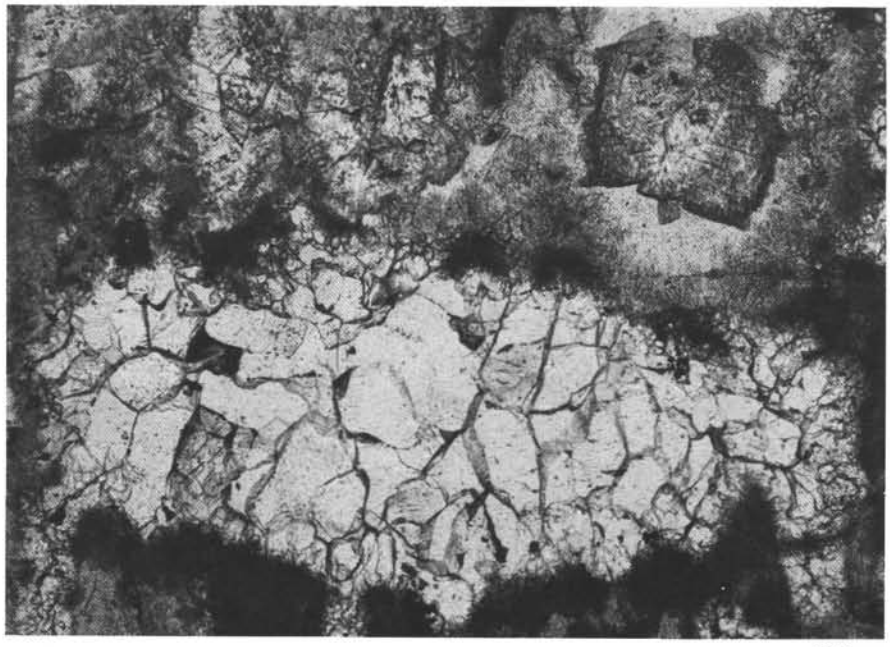

2

200 µm

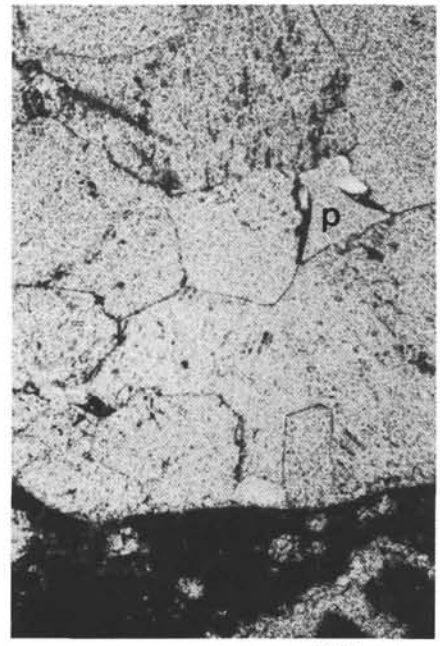

4

250 µm

Plate 3. Early calcite cement, calcite from dedolomitization, and late calcite cement. **1.** Cathodoluminescence. **2.** Natural light. An early diagenetic void filling (a) within a chaetetid, silicification (b) of the chaetetid skeleton, and partial replacement of silica by clear subhedral saddle dolomite (c). Under cathodoluminescence, the calcite drusy mosaic has a bright (yellow) serrated rim corresponding to the ends of the dolomitic phantoms along the original border of the cement. Sample 103-639D-5R-3, 39–41 cm. **3.** Cathodoluminescence. **4.** Natural light. Late diagenetic calcite filling a void with residual porosity (p). Under cathodoluminescence, calcite is clearly zoned. Equant morphology, coarse size, and the cathodoluminescence characteristics of these crystals are different from other calcites. Sample 103-639D-13R, CC (30–34 cm).

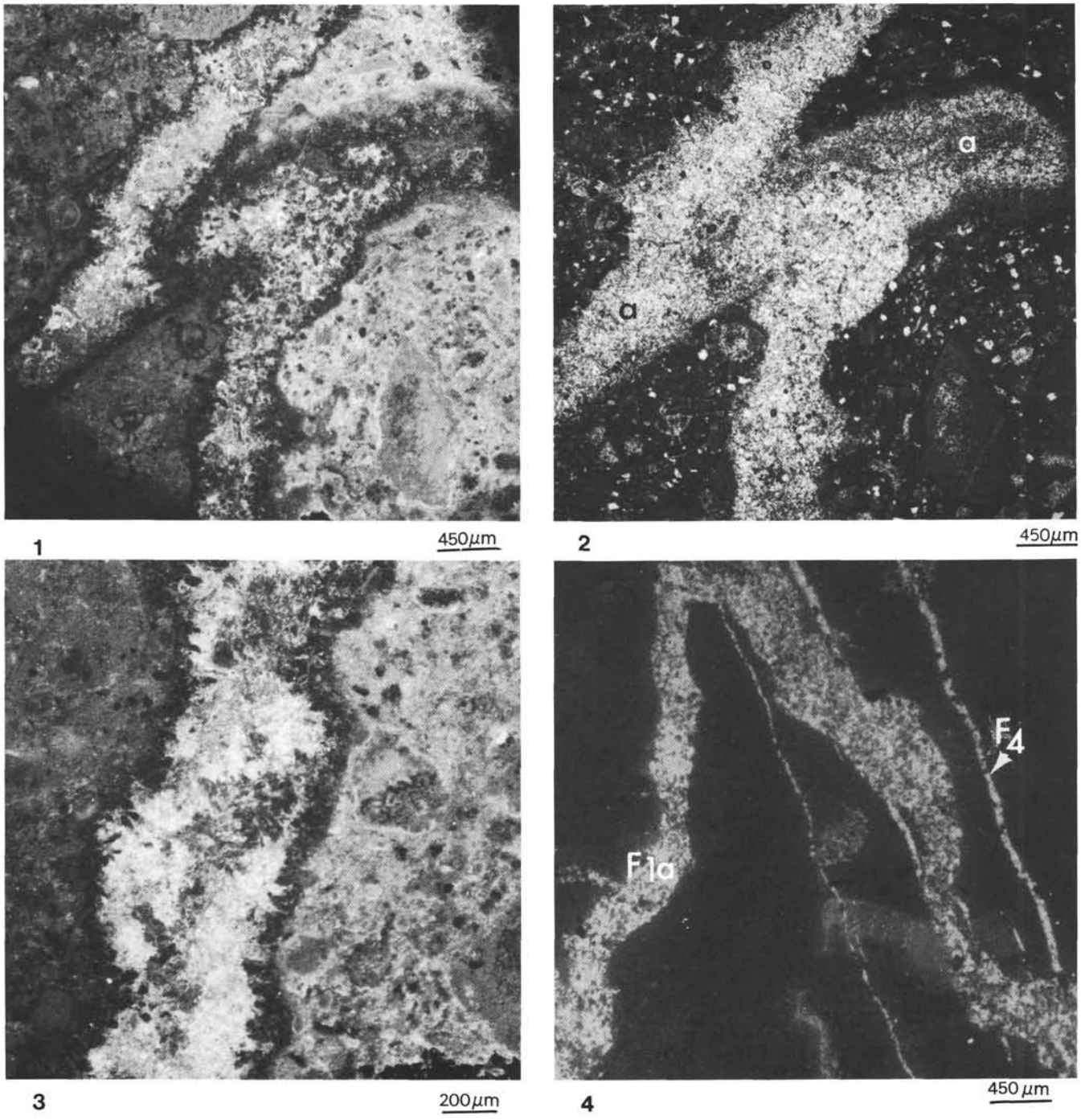

Plate 4. Fissure type F1 in limestone (see Table 1). **1.** and **2.** Cathodoluminescence. Fissure type F1a intersecting a pelecypod clast (a). The fissure is filled by anhedral calcite with a speckled appearence under cathodoluminescence. Sample 103-639D-8R-1, 19–23 cm. **3.** Detail of the calcitic filling with a contrasting cathodoluminescence that makes incomplete crystalline form ends appear toward the walls. Sample 103-639D-8R-1, 19–23 cm. **4.** Intersection of fissure type F1a with fissures of type F4. The two different sets are peculiarly homogenized by late iron hydroxides that mask the relative chronology of the fissures. Sample 103-639D-10R-1, 38–41 cm.

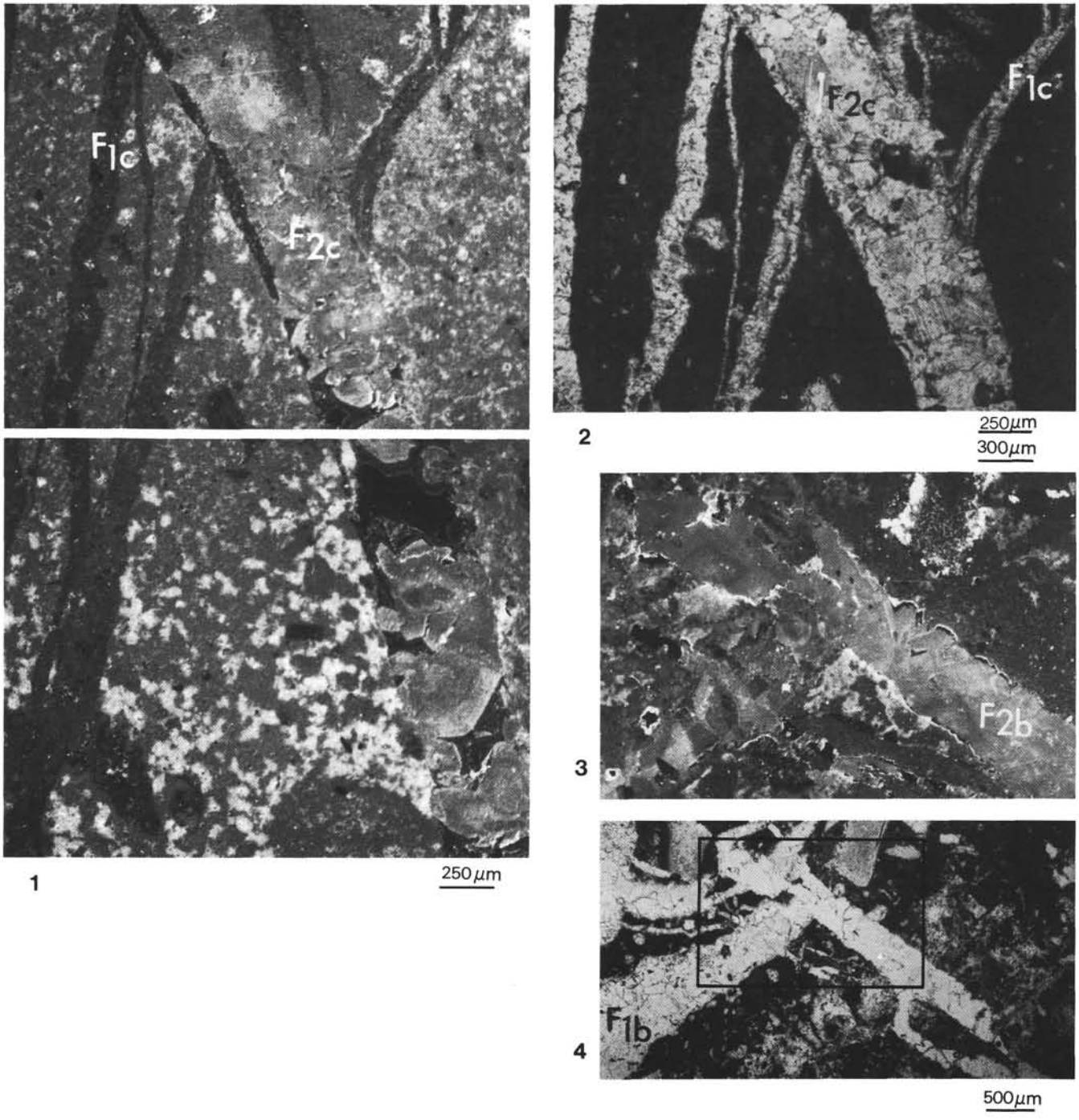

Plate 5. Type F2 fissures intersecting type F1 fissures in limestone. **1.** and **2.** Cathodoluminescence. Fissures F2c and F1c. The F1c set is filled with a dark cathodoluminescent calcite and displaced by the F2c fissure. This wider fissure is filled with larger, twinned crystals. Cathodoluminescence reveals faintly zoned dolomitic phantoms. Black cathodoluminescence corresponds to the last growth of the dolomite, now dedolomitized. Sample 103-639D-10R-1, 128–130 cm. **3.** Cathodoluminescence. **4.** Natural light. Fissures F2b and F1b in limestone. Fissure F1b is filled with xenotopic sparite showing an heterogeneous cathodoluminescence. Fissure F2b is filled with dolomite showing an homogeneous catholuminescence (but a very narrow zoned rim) and curved faces along the wall. Sample 103-639D-5R-2, 63–65 cm. □ in Figure 4 = location of Figure 3.

Plate 6. **1.** Negative print of a thin section showing three sets of fissures in limestone (F1, F2, and F3; see text). F1 is filled with calcite, F2 with saddle dolomite, and F3 with a second generation of saddle dolomite enclosing large sparite debris. Sample 103-639D-5R-2, 137–139 cm. Box shows location of Figures 2 and 3. **2.** Cathodoluminescence. **3.** Natural light. Detail showing the intersection of an F1b fissure filled with homogeneous, dull cathodoluminescence calcite and an F2d fissure filled with *zoned dolomite* (*cf. Figs.* 11A and 11B).

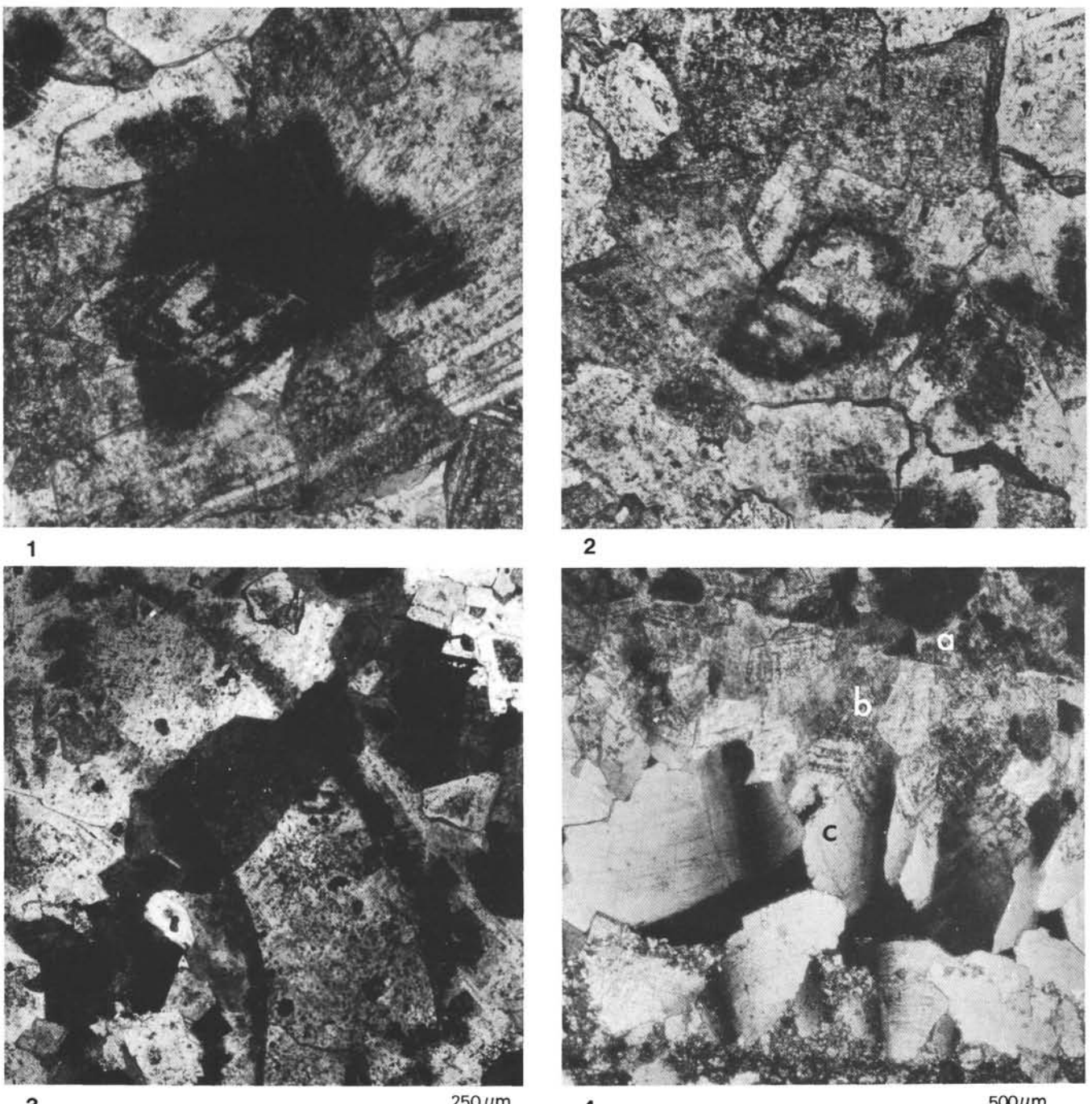

Plate 7. Type 2 dolomite textures of mostly clean saddle dolomite. **1.** Texture 2a showing zoned euhedral dolomite crystal, partially replaced by anhedral saddle dolomite well evidenced under polarized analyzed light. Sample 103-639A-10R-1, 35–38 cm. **2.** Texture 2a showing phantom of a foraminifer outlined by impurities. The phantom belongs to several baroque dolomite crystals, which shows that dolomite replaced a previous lithified limestone or dolomitic limestone. Sample 103-639A-10R-1, 35–38 cm; natural light. **3.** Texture 2a showing phantom of a mollusk fragment outlined by impurities that probably correspond to the initial micritic coating. The whole fragment is intersected by large saddle dolomite crystals. Sample 103-639A-10R-2, 52–56 cm; polarized analyzed light. **4.** Dolomite texture type 2b. Saddle dolomite cement with subhedral crystals showing curved faces and sweeping extinction. Detail of a fissure showing the wall (a) and cement filling. The basal part of the crystals is cleaved and slightly zoned by impurities (b); the distal part of the crystals is very pure and transparent (c); the compromise boundary is underlined with residual voids (black). Sample 103-639A-10R-1, 13–14 cm; polarized analyzed light.

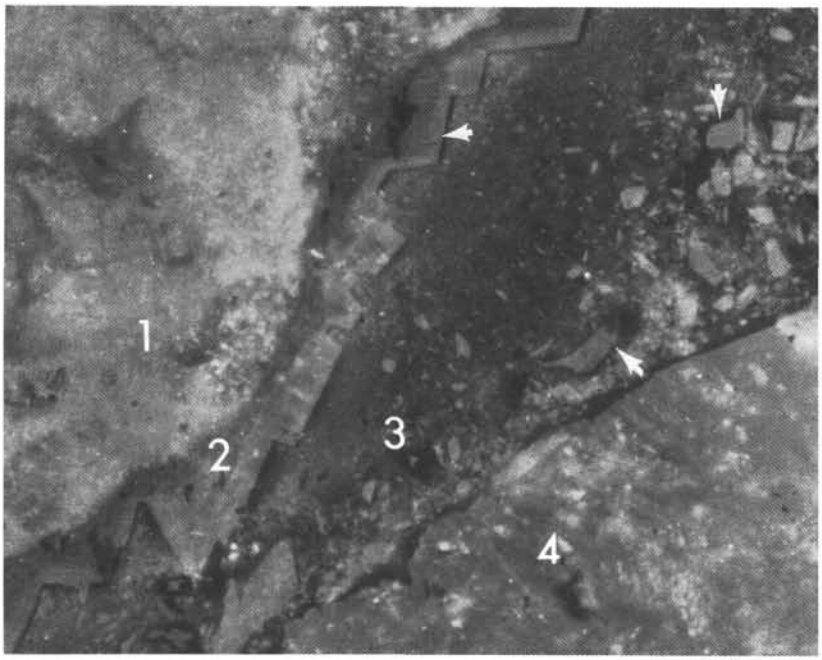

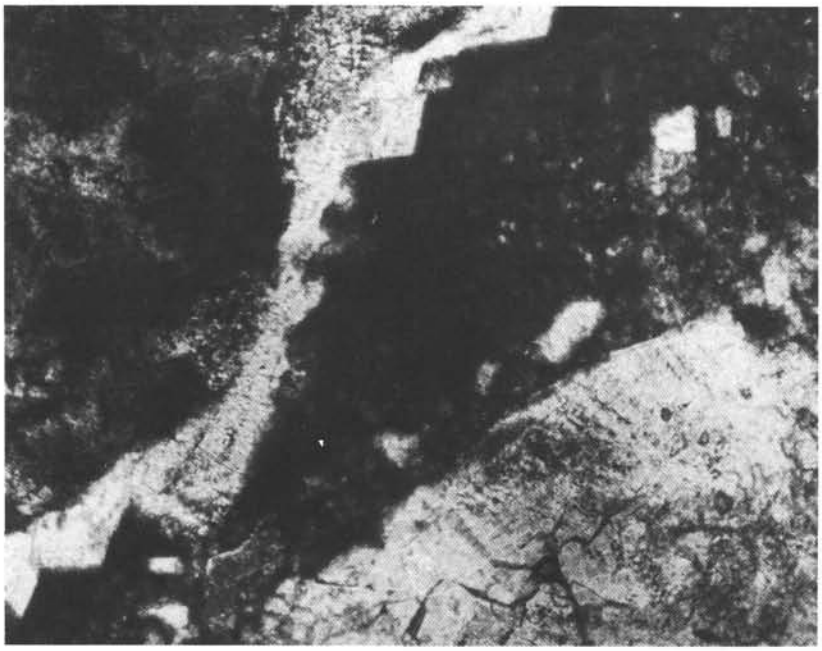

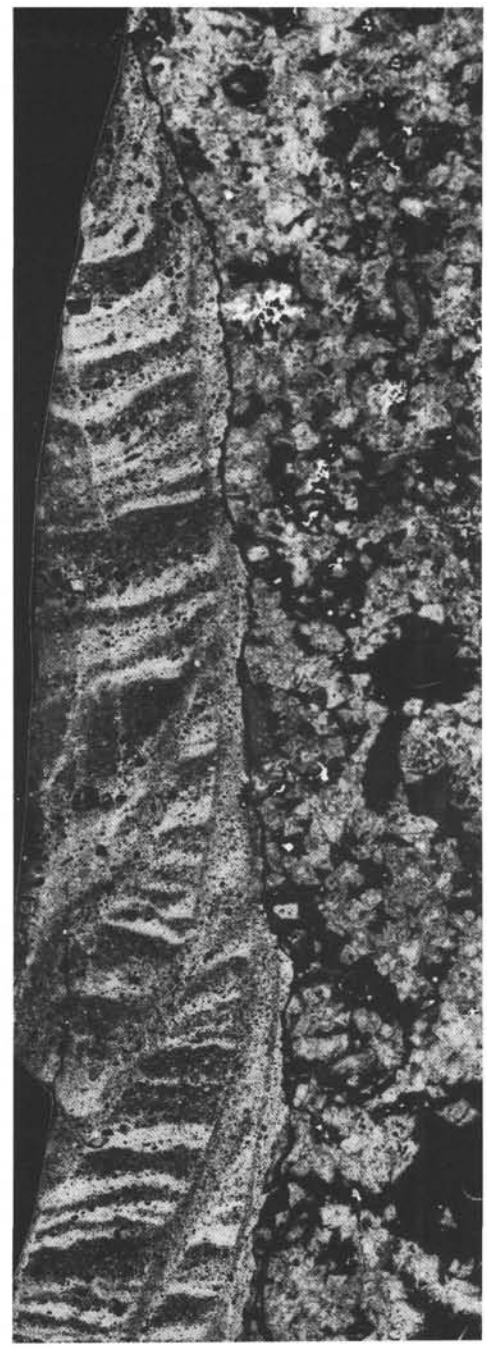

Plate 8. Detrital dolomite filling fissures and vugs. **1.** Cathodoluminescence. **2.** Natural light. Graded bedding, heterometric microbreccia filling a fracture in dolomite. 1 = host rock with a relatively clear cathodoluminescence corresponding to dirty texture; 2 = fringe of clean saddle dolomite exhibiting a dark cathodoluminescence along the roof of the fissure; 3 = internal sediment composed of a dark matrix (with a very dark to black cathodoluminescence) embedding clean crystalline and lithic debris (with a dark cathodoluminescence); 4 = large dolomite element of the internal breccia showing a truncated and eroded surface. The margin of saddle dolomite and all the sedimented crystals present a final thin black zonation under cathodoluminescence (arrows). Sample 103-639A-10R-1, 81–83 cm. **3.** Negative print of a thin section showing a laminated deposit partially coating the surface of a piece of dolomite. This coating appears to be an incompletely recovered filling of a large fissure. The boundary between the host rock and cavity intersects all recognized crystalline textures and is fringed by a transparent (black on negative) rim of baroque dolomite. The laminated sediment was affected by internal gliding planes and resedimentation, which evidence rapid lithification. Sample 103-639A-10R-1, 40–44 cm.

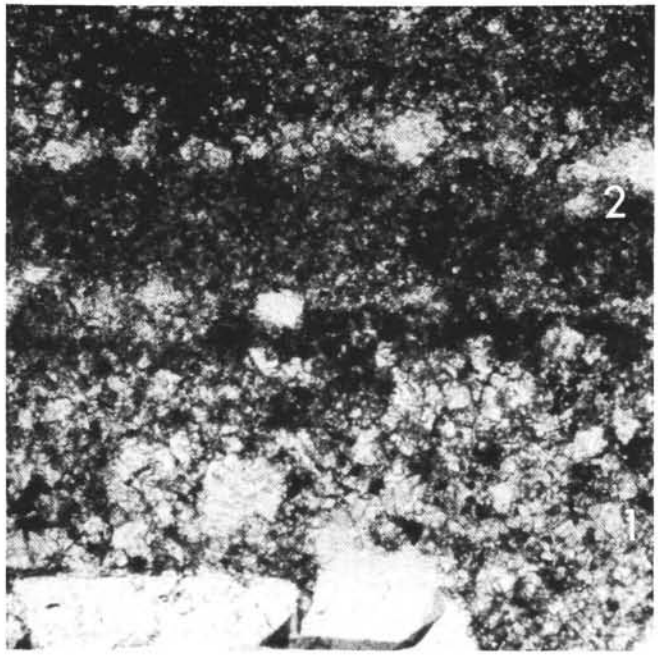

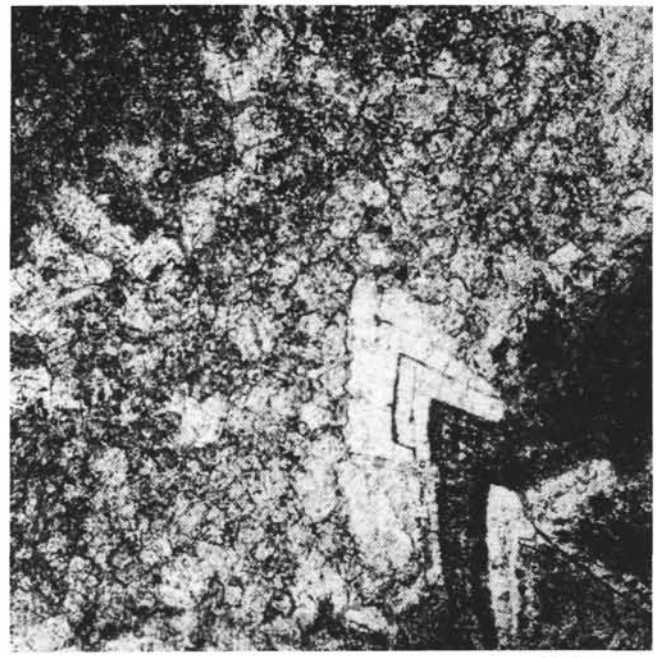

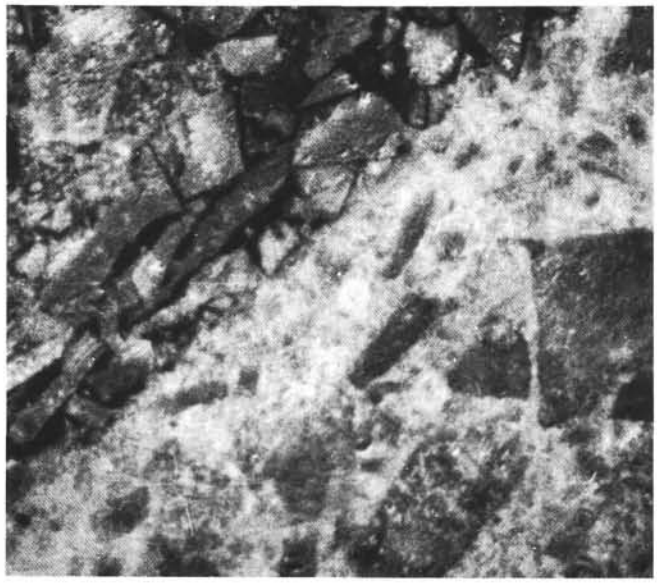

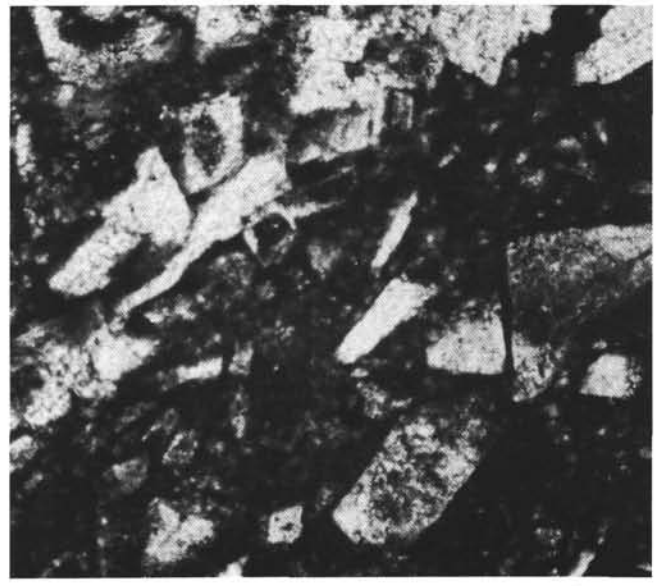

Plate 9. **1.** Two internal sediments superimposed within a cavity. 1 = translucent dolomitic crystal silt with some larger transparent crystal debris; 2 = darker laminated sediment. Detail showing recrystallizations (agrading neomorphism). Sample 103-639A-10R-2, 43–47 cm; natural light. **2.** Translucent dolomitic crystal silt composed of anhedral crystals, 50–100 μm and some larger, with jig-saw structure. Recrystallization at the contact of saddle dolomite fringe into transparent saddle dolomite grew at the expense of the silt. Sample 103-639A-10R-1, 15–18 cm; natural light. **3.** Cathodoluminescence. **4.** Natural light. Contrast between two recrystallized sediment laminae. The lower lamina has an abundant dark matrix (with light cathodoluminescence) and transparent elements (with dark cathodoluminescence) float in the matrix. The upper lamina has little dark matrix, and the clear crystalline and lithic debris are closely packed and visible under cathodoluminescence, with a black rim revealing a late and poorly dated overgrowth. Sample 103-639A-10R-2, 18–21 cm.

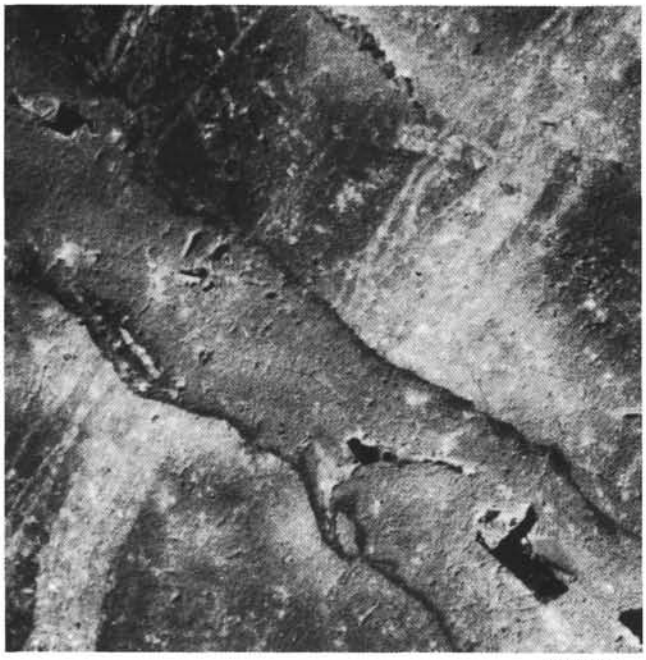

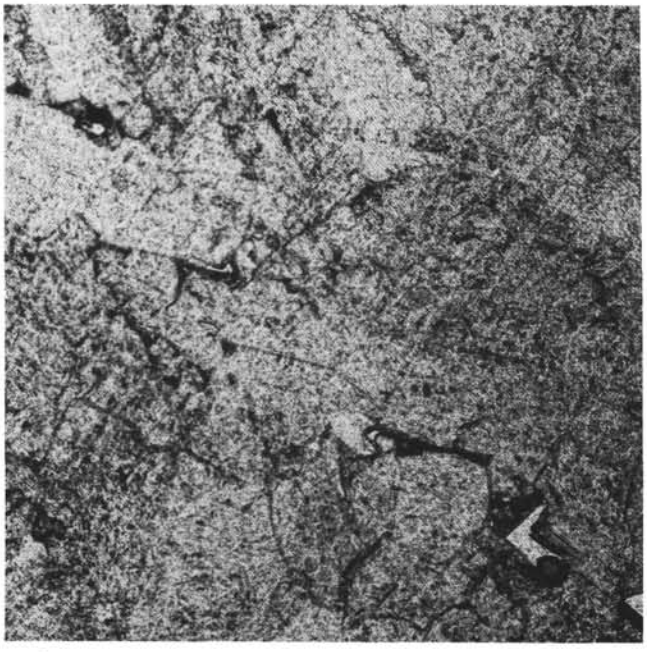

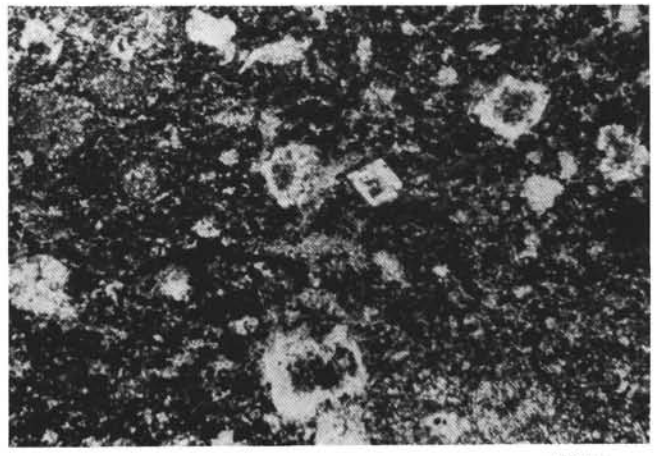

Plate 10. **1.** Cathodoluminescence. **2.** Natural light. Coarse, clear saddle dolomite affected by two sets of fractures that are visible only under cathodoluminescence. This texture is merely the result of successive fractures and their filling; the host rock was completely replaced. Sample 103-639B-3R-1, 88–91 cm. **3.** Negative print of a thin section showing fissures outlined by dirty dolomite (white on negative). The fissures are interrupted by an irregular network of clear, coarse saddle dolomite (black on negative) that probably resulted from another fracturing episode. Sample 103-639B-2R-1, 17–22 cm. **4.** Dolomitic rhombs within mudstones of Valanginian age, from near the contact of the Tithonian(?) dolomite unit. Sample 103-639A-8R-2, 37–40 cm; natural light.